Searches for electroweak production of supersymmetric particles with compressed mass spectra in $\sqrt{s} = 13$ TeV pp collisions with the ATLAS detector

G. Aad *et al.*[*]
(ATLAS Collaboration)

(Received 2 December 2019; accepted 30 January 2020; published 11 March 2020)

This paper presents results of searches for the electroweak production of supersymmetric particles in models with compressed mass spectra. The searches use 139 fb^{-1} of $\sqrt{s} = 13$ TeV proton-proton collision data collected by the ATLAS experiment at the Large Hadron Collider. Events with missing transverse momentum and two same-flavor, oppositely charged, low-transverse-momentum leptons are selected, and are further categorized by the presence of hadronic activity from initial-state radiation or a topology compatible with vector-boson fusion processes. The data are found to be consistent with predictions from the Standard Model. The results are interpreted using simplified models of R-parity-conserving supersymmetry in which the lightest supersymmetric partner is a neutralino with a mass similar to the lightest chargino, the second-to-lightest neutralino, or the slepton. Lower limits on the masses of charginos in different simplified models range from 193 to 240 GeV for moderate mass splittings, and extend down to mass splittings of 1.5 to 2.4 GeV at the LEP chargino bounds (92.4 GeV). Similar lower limits on degenerate light-flavor sleptons extend up to masses of 251 GeV and down to mass splittings of 550 MeV. Constraints on vector-boson fusion production of electroweak SUSY states are also presented.

DOI: 10.1103/PhysRevD.101.052005

I. INTRODUCTION

Extensions of the Standard Model (SM) that include new states with nearly degenerate masses can help to resolve open issues in particle physics while evading constraints from experiments at high-energy colliders. The mass spectra of such new states are referred to in this paper as "compressed." Supersymmetry (SUSY) [1–6] predicts new particles that have identical quantum numbers to their SM partners with the exception of spin, with SM fermions having bosonic partners and SM bosons having fermionic partners. The neutralinos $\tilde{\chi}^0_{1,2,3,4}$ and charginos $\tilde{\chi}^\pm_{1,2}$ are collectively referred to as electroweakinos, where the subscripts indicate increasing electroweakino mass. If the $\tilde{\chi}^0_1$ is stable, e.g., as the lightest SUSY partner (LSP) in R-parity-conserving SUSY models [7], then it is a viable dark-matter candidate [8,9]. In the compressed SUSY models considered in this paper, the $\tilde{\chi}^0_1$ is close in mass to a heavier SUSY partner such as a chargino ($\tilde{\chi}^\pm_1$), second-lightest neutralino ($\tilde{\chi}^0_2$), or slepton ($\tilde{\ell}$, the SM lepton partner).

This paper presents searches for physics beyond the SM in signatures sensitive to models with compressed mass spectra. Simplified SUSY models [10–12] are used to optimize the searches and interpret the results. The searches use 13 TeV pp collision data corresponding to 139 fb^{-1} of integrated luminosity, collected by the ATLAS experiment [13] from 2015 to 2018 at the CERN Large Hadron Collider (LHC).

All searches assume pair production of SUSY particles via electroweak interactions, with subsequent decays into the $\tilde{\chi}^0_1$ and SM particles. The electroweakino mass eigenstates are a mixture of wino, bino, and Higgsino fields,[1] which form the SUSY partners of the SM W, γ/Z, and Higgs fields, respectively. In the minimal supersymmetric extension of the SM (MSSM) [14,15], the masses of the bino, wino, and Higgsino states are parametrized in terms of M_1, M_2, and μ, respectively. For large values of $\tan(\beta)$, these three parameters drive the phenomenology of the electroweakinos.

Four SUSY scenarios are considered in the interpretation of the searches. In the first scenario, the lightest SUSY partners are assumed to be a triplet of Higgsino-like states

[*]Full author list given at the end of the article.

[1]In the minimal supersymmetric extension of the SM, the Higgs sector is extended to contain two Higgs doublets, and $\tan(\beta)$ is the ratio of the vacuum expectation values of the two Higgs doublets.

$(\tilde{\chi}_1^0, \tilde{\chi}_1^\pm, \tilde{\chi}_2^0)$, in which the mass splitting between the states is partially determined by the magnitude of M_1 or M_2 relative to $|\mu|$. Such a scenario, referred to here as Higgsino models, is motivated by naturalness arguments [16,17], which suggest that $|\mu|$ should be near the weak scale [18–21], while M_1 and/or M_2 can be larger.

The second scenario features a similar particle spectrum to the first, except with $|M_1| < |M_2| \ll |\mu|$, so that the produced electroweakinos have a wino and/or bino nature. In such wino/bino scenarios, the LSP can be a thermal-relic dark-matter candidate that was depleted in the early Universe through coannihilation processes to match the observed dark-matter density [22,23]. The production cross section in such scenarios is typically larger than in the first scenario. They are also poorly constrained by dark-matter direct-detection experiments, and collider searches constitute the only direct probe for $|\mu| > 800$ GeV [24]. Diagrams representing the production mode for the first two scenarios are shown in Fig. 1(a). A $\tilde{\chi}_2^0$ produced in either scenario can decay into a dilepton pair via an off-shell Z boson (Z^*), such that the dilepton invariant mass $m_{\ell\ell}$ is kinematically restricted to be smaller than the mass splitting between the $\tilde{\chi}_2^0$ and $\tilde{\chi}_1^0$. Hadronic initial-state radiation (ISR) is also required to boost the system as a way of enhancing the sensitivity of the search.

The third scenario is similar to the previous two, but it instead assumes that the pair production of the electroweakinos proceeds via vector-boson fusion (VBF) processes, in which SM weak bosons exchange an electroweakino in a t-channel process to produce two electroweakinos and a pair of forward jets. Such scenarios typically have very low cross sections, but they can complement the sensitivity of $q\bar{q}$ annihilation modes that dominate the inclusive Higgsino and wino/bino cross sections, especially for LSP masses above a few hundred GeV [25]. An example of such a process is illustrated in Fig. 1(b). The kinematic cutoff of the $m_{\ell\ell}$ distribution is also used as the primary discriminant in this scenario, along with the presence of two forward jets consistent with a VBF production mode.

The fourth scenario assumes the presence of scalar partners of the SM leptons (sleptons, $\tilde{\ell}$) that are slightly heavier than a bino-like LSP. Such models can explain dark-matter thermal-relic densities through coannihilation channels, as well as the muon $g-2$ anomaly [26,27]. This process is illustrated in Fig. 1(c). This scenario exploits the relationship between the lepton momenta and the missing transverse momentum through the stransverse mass, m_{T2} [28,29], which exhibits a kinematic end point similar to that for $m_{\ell\ell}$ in electroweakino decays.

Events with two same-flavor opposite-charge leptons (electrons or muons), significant missing transverse momentum of size $E_{\mathrm{T}}^{\mathrm{miss}}$, and hadronic activity are selected for all scenarios. Signal regions (SRs) are defined by placing additional requirements on a number of kinematic variables. The dominant SM backgrounds are either estimated with *in situ* techniques or constrained using data control regions (CRs) that enter into a simultaneous likelihood fit with the SRs. The fit is performed in bins of either the $m_{\ell\ell}$ distribution (for electroweakinos) or the m_{T2} distribution (for sleptons).

Constraints on these compressed scenarios were first established at LEP [30–40]. The lower bounds on direct chargino production from these results correspond to $m(\tilde{\chi}_1^\pm) > 103.5$ GeV for $\Delta m(\tilde{\chi}_1^\pm, \tilde{\chi}_1^0) > 3$ GeV and $m(\tilde{\chi}_1^\pm) > 92.4$ GeV for smaller mass differences, although the lower bound on the chargino mass weakens to around 75 GeV for models with additional new scalars and Higgsino-like cross sections [41]. For sleptons, conservative lower limits on the mass of the scalar partner of the right-handed muon, denoted $\tilde{\mu}_R$, are approximately $m(\tilde{\mu}_R) \gtrsim 94.6$ GeV for mass splittings down to $m(\tilde{\mu}_R) - m(\tilde{\chi}_1^0) \gtrsim 2$ GeV. For the scalar partner of the right-handed electron, denoted $\tilde{e}_R$, LEP established a universal lower bound of $m(\tilde{e}_R) \gtrsim 73$ GeV that is independent of $\Delta m(\tilde{e}_R, \tilde{\chi}_1^0)$ [34]. Recent papers from the CMS [42–44] and ATLAS [45] Collaborations have extended the LEP limits for a range of mass splittings.

This paper extends previous LHC results by increasing the integrated luminosity, extending the search with additional channels, and exploiting improvements in detector calibration and performance. The dedicated search for production via VBF is also added, and the event selection is reoptimized and uses techniques based on recursive jigsaw reconstruction [46], which improve the separation of the SUSY signal from the SM backgrounds.

II. ATLAS DETECTOR

The ATLAS experiment is a general-purpose particle detector that surrounds the interaction point with nearly 4π solid angle coverage.[2] It comprises an inner detector, calorimeter systems, and a muon spectrometer. The inner detector provides precision tracking of charged particles in the pseudorapidity region $|\eta| < 2.5$, consisting of pixel and microstrip silicon subsystems within a transition radiation tracker. The innermost pixel detector layer, the insertable B-layer [47,48], was added for $\sqrt{s} = 13$ TeV data-taking to improve tracking performance. The inner detector is immersed in a 2 T axial magnetic field provided by a superconducting solenoid. High-granularity lead/liquid-argon

[2]ATLAS uses a right-handed coordinate system with its origin at the nominal interaction point (IP) in the center of the detector and the z axis along the beam pipe. The x axis points from the IP to the center of the LHC ring, and the y axis points upwards. Cylindrical coordinates (r, ϕ) are used in the transverse plane, ϕ being the azimuthal angle around the z axis. The pseudorapidity is defined in terms of the polar angle θ as $\eta = -\ln\tan(\theta/2)$. Angular distance is measured in units of $\Delta R \equiv \sqrt{(\Delta\eta)^2 + (\Delta\phi)^2}$. Rapidity is defined by $y = \frac{1}{2}\ln[(E + p_z)/(E - p_z)]$, where E is the energy and p_z is the longitudinal component of the momentum along the beam direction.

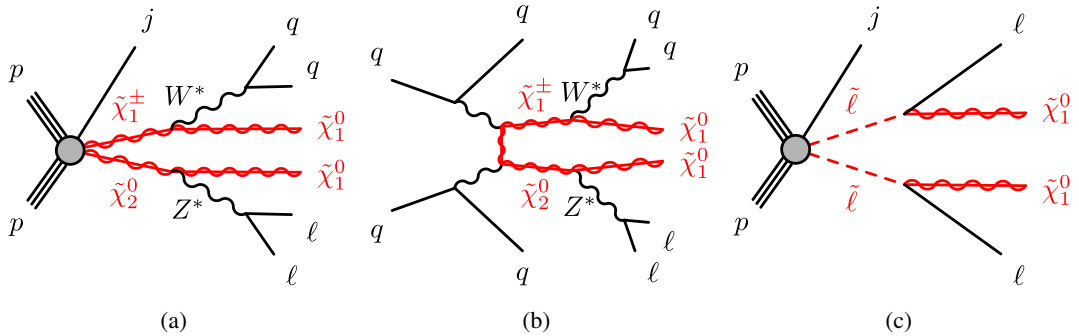

FIG. 1. Diagrams representing the two-lepton final state of (a) the production of electroweakinos $\tilde{\chi}_2^0\tilde{\chi}_1^\pm$ with initial-state radiation (j), (b) the VBF production of electroweakinos $\tilde{\chi}_2^0\tilde{\chi}_1^\pm$, and (c) slepton pair ($\tilde{\ell}\tilde{\ell}$) production in association with initial-state radiation (j). The Higgsino simplified model also considers $\tilde{\chi}_2^0\tilde{\chi}_1^0$ and $\tilde{\chi}_1^+\tilde{\chi}_1^-$ production.

electromagnetic sampling calorimeters are used for $|\eta| < 3.2$. Hadronic energy deposits are measured in a steel/scintillator tile barrel calorimeter in the $|\eta| < 1.7$ region. Forward calorimeters cover the region $3.2 < |\eta| < 4.9$ for both electromagnetic and hadronic measurements. The muon spectrometer comprises trigger and high-precision tracking chambers spanning $|\eta| < 2.4$ and $|\eta| < 2.7$, respectively, with a magnetic field provided by three large superconducting toroidal magnets. Events of interest are selected using a two-level trigger system [49], consisting of a first-level trigger implemented in hardware, which is followed by a software-based high-level trigger.

III. DATA AND SIMULATED EVENT SAMPLES

Events were selected with a $E_{\mathrm{T}}^{\mathrm{miss}}$ trigger, employing varied trigger thresholds as a function of the data-taking periods. The trigger is >95% efficient for offline $E_{\mathrm{T}}^{\mathrm{miss}}$ values above 200 GeV for all periods. The dataset used corresponds to 139 fb^{-1} of $\sqrt{s} = 13$ TeV pp collision data, where the uncertainty in the integrated luminosity is 1.7% [50], obtained using the LUCID-2 detector [51] for the primary luminosity measurements. The average number of interactions per bunch crossing was 33.7.

Samples of Monte Carlo (MC) simulated events are used to estimate the signal yields, and for estimating the background from processes with prompt leptons, as well as in the determination of systematic uncertainties.

For the first signal scenario introduced in Sec. I, samples were generated for a simplified model of Higgsino LSPs, including the production of $\tilde{\chi}_1^-\tilde{\chi}_1^+$, $\tilde{\chi}_2^0\tilde{\chi}_1^\pm$, and $\tilde{\chi}_2^0\tilde{\chi}_1^0$. The masses of the neutralinos ($\tilde{\chi}_{1,2}^0$) were varied, while the chargino mass was set to $\tilde{\chi}_1^\pm = \frac{1}{2}[m(\tilde{\chi}_1^0) + m(\tilde{\chi}_2^0)]$. Mass splittings in the case of pure Higgsinos are generated by radiative corrections, and are of the order of hundreds of MeV [52]. Mass splittings of the order of tens of GeV can be obtained by introducing mixing with wino or bino states. In this simplified model, mass differences ranging from 1 to 60 GeV are considered, but the calculated cross sections assume electroweakino mixing matrices corresponding to pure Higgsino $\tilde{\chi}_2^0$, $\tilde{\chi}_1^\pm$, and $\tilde{\chi}_1^0$ states, and all other SUSY particles are decoupled. Typical values of cross sections for $m(\tilde{\chi}_2^0) = 110$ GeV and $m(\tilde{\chi}_1^0) = 100$ GeV are 4.3 ± 0.1 pb for $\tilde{\chi}_2^0\tilde{\chi}_1^\pm$ production, 2.73 ± 0.07 pb for $\tilde{\chi}_2^0\tilde{\chi}_1^0$ production, and 2.52 ± 0.08 pb for $\tilde{\chi}_1^+\tilde{\chi}_1^-$ production. The samples were generated at leading order (LO) with MG5_aMC@NLO2.6.1 [53] using the NNPDF23LO [54] parton distribution function (PDF) set and included up to two extra partons in the matrix element (ME). The electroweakinos were decayed with MADSPIN [55]. The events were then interfaced with PYTHIA8.212 [56] to model the parton shower (PS), hadronization, and underlying event (UE) using the A14 set of tuned parameters (tune) [57]. The ME-PS matching was performed using the CKKW-L scheme [58] with the merging scale set to 15 GeV. To enforce an ISR topology, at least one parton in the final state was required to have a transverse momentum (p_{T}) greater than 50 GeV. Possible diagrams including colored SUSY particles were excluded from the generation.

In the wino/bino scenario, the generated process is $pp \to \tilde{\chi}_2^0\tilde{\chi}_1^\pm$. The $\tilde{\chi}_1^0$ is a pure bino state, with the $\tilde{\chi}_2^0$ and $\tilde{\chi}_1^\pm$ states forming degenerate pure wino states. The generator configurations are consistent with those used for the Higgsino samples. A typical value of the $\tilde{\chi}_2^0\tilde{\chi}_1^\pm$ production cross section is 16.0 ± 0.5 pb for $m(\tilde{\chi}_2^0) = m(\tilde{\chi}_1^\pm) = 110$ GeV.

Additional samples were generated for the third scenario of pair production of electroweakinos produced via VBF. These were generated with the same decay, PS, hadronization, and UE configuration as the Higgsino simplified model samples. The ME generation was the same as in the Higgsino case, but it used an updated version of MG5_aMC@NLO (version 2.6.2). In order to select uniquely the VBF topologies, the number of QCD vertices was set to zero. An additional filter was applied to select events with exactly two parton emissions in the ME. The invariant mass of the two partons is required to be at least 200 GeV, while the minimum transverse momentum of each parton is 12 GeV. Typical values of LO cross sections with these requirements for $m(\tilde{\chi}_2^0) = 100$ GeV and $m(\tilde{\chi}_1^0) = 90$ GeV

are 16 ± 1 fb and 47 ± 4 fb, for the Higgsino and wino/bino models, respectively. For Higgsino masses smaller than half of the Higgs boson mass, the cross sections include contributions from VBF Higgs production with decays $h \to \tilde{\chi}_2^0 \tilde{\chi}_1^0$.

The electroweakino searches exploit the kinematic endpoint in the dilepton invariant mass spectrum from the decay chain $\tilde{\chi}_2^0 \to Z^* \tilde{\chi}_1^0, Z^* \to \ell\ell$. Therefore, processes that involve the production of a $\tilde{\chi}_2^0$ neutralino dominate the sensitivity of the search. The branching ratios for the processes $\tilde{\chi}_2^0 \to Z^* \tilde{\chi}_1^0$ and $\tilde{\chi}_1^\pm \to W^* \tilde{\chi}_1^0$ were fixed to 100% for all the scenarios given above. The branching ratios of $Z^* \to \ell\ell$ and $W^{\pm *} \to \ell\nu$ depend on the invariant mass of the off-shell vector boson. For both the Higgsino and wino/bino models, the branching ratios were computed with SUSY-HIT1.5a [59], which accounts for finite b-quark and τ-lepton masses. At $\Delta m(\tilde{\chi}_2^0, \tilde{\chi}_1^0) = 40$ GeV, the $Z^* \to \ell\ell$ branching ratio to electrons or muons is 3.5%. This increases to 5.3% and 5.0%, respectively, at $\Delta m(\tilde{\chi}_2^0, \tilde{\chi}_1^0) = 1$ GeV, as decays into heavier quarks or τ leptons become kinematically inaccessible. Similarly, for $W^* \to \ell\nu$, the branching ratios to electrons or muons are both 11% at a mass splitting of 40 GeV, but they increase to 20% and 17%, respectively, for $\Delta m(\tilde{\chi}_2^0, \tilde{\chi}_1^0) = 1$ GeV.

The distribution of the dilepton invariant mass from the decay of the virtual Z^* [60] depends on the relative sign of the $\tilde{\chi}_1^0$ and $\tilde{\chi}_2^0$ mass parameters. In a pure Higgsino model, the product of the signed mass eigenvalues $(m(\tilde{\chi}_2^0) \times m(\tilde{\chi}_1^0))$ can only be negative, while for the wino/bino case either positive or negative products are allowed.[3] The generated wino/bino process assumes the product of the signed mass eigenvalues is positive, and the analytical description of the expected line shape is used to reweight the $m_{\ell\ell}$ distribution to the case of the product being negative. The difference between wino/bino and Higgsino line shapes, as well as the level of agreement between the reweighted distribution and the expected line shape, is shown in Fig. 2. The two possible wino/bino $m_{\ell\ell}$ distributions are used to provide two separate model-dependent interpretations of the results. With the exception of the signal modeling, the interpretations for Higgsino and both wino/bino samples are otherwise conducted identically and use the same search regions as defined in Sec. V.

For the fourth scenario, samples with direct production of selectrons $\tilde{e}_{L,R}$ or smuons $\tilde{\mu}_{L,R}$ were generated. The L, R subscripts denote left- or right-handed chirality of the corresponding SM lepton partners. All slepton flavors and chirality contributions are assumed to be degenerate

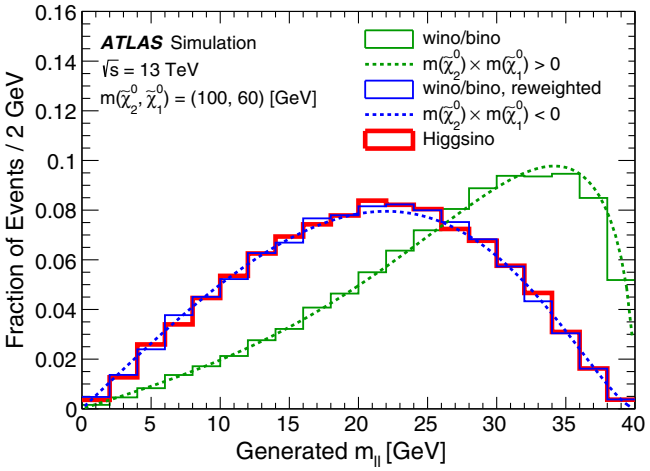

FIG. 2. Dilepton invariant mass for Higgsino and wino/bino simplified models. The end point of the distribution is determined by the difference between the masses of the $\tilde{\chi}_2^0$ and $\tilde{\chi}_1^0$. The results from simulation (histograms) are compared with analytic calculations of the expected line shape (dashed lines) presented in Ref. [60]. The product of the signed mass eigenvalues $(m(\tilde{\chi}_2^0) \times m(\tilde{\chi}_1^0))$ is negative for the Higgsino model and can be either negative or positive for wino/bino scenarios.

in mass. A typical value of the slepton production cross section is 0.55 ± 0.01 pb for $m(\tilde{e}_{L,R}) = 110$ GeV. These particles decay with a 100% branching ratio into their corresponding SM partner lepton and a pure bino neutralino, $\tilde{\chi}_1^0$. The slepton samples were generated with MG5_aMC@NLO2.6.1 and interfaced with PYTHIA8.230. The PDF set used was NNPDF23LO with the A14 tune. Similarly to the Higgsino and wino/bino samples, CKKW-L merging [58] was used for the ME-PS matching, with the merging scale set to a quarter of the slepton mass.

Cross sections for all but the VBF signal scenarios are calculated with RESUMMINO2.0.1 at NLO + NLL precision [63–70]. The VBF cross sections are computed at LO precision with MG5_aMC@NLO2.6.2. The evaluation of the cross sections and corresponding uncertainty are taken from an envelope of cross-section predictions using different PDF sets, and varied factorization and renormalization scales. This procedure is described in Ref. [71] and is the same procedure as used in the previous search [45].

The SM background processes are estimated from a combination of MC simulation as well as data-driven approaches. The latter are described in Sec. VI. The programs SHERPA2.2.1 and SHERPA2.2.2 [72] were used to model the V + jets ($V = W, Z, \gamma^*$) samples involving leptonically decaying vector bosons, as well as diboson (WW, ZZ, and WZ, collectively referred to as VV) and fully leptonic triboson processes. The $Z^{(*)}/\gamma^*$ + jets and VV samples provide coverage of dilepton invariant masses down to 0.5 GeV for $Z^{(*)}/\gamma^* \to e^+e^-/\mu^+\mu^-$, and 3.8 GeV for $Z^{(*)}/\gamma^* \to \tau^+\tau^-$. A separate set of $Z(\to \mu\mu)$ + jets

[3]The mixing matrix used to diagonalize the neutral electroweakino states is forced to be a real matrix in the SLHA2 format [61]. A consequence of this choice is a negative sign given to one or more mass eigenvalues, determined in part by the relative fractions of wino, bino, or Higgsino content of the physical states. For additional discussion of this, see Ref. [62].

samples were generated using MG5_aMC@NLO using the same configuration as for the signal samples described above in order to evaluate initial- and final-state radiation modeling in signal samples. Gluon-gluon fusion (ggF) and VBF single-Higgs production were generated with POWHEG-BOX [73], while Higgs production in association with a massive vector boson was generated with PYTHIA8.186, and $t\bar{t}h$ production was generated with MG5_aMC@NLO2.2.3. POWHEG-BOX was used to generate $t\bar{t}$ [73–76], single top [77], and top quarks produced in association with W bosons [78]. Rarer top-quark processes all used MG5_aMC@NLO (versions 2.2.2/2.3.3). Matrix elements, excluding those generated with PYTHIA or SHERPA, were then interfaced with PYTHIA8 using the ME + PS prescription. Further details on the configuration of the simulation of SM processes can be found in Refs. [79–83]. A summary of the generator configurations, including the PDF sets and the order of the cross-section calculations used for normalization, is given in Table I.

To simulate the effects of additional pp collisions, referred to as pileup, in the same and neighboring bunch crossings, additional interactions were generated using the soft QCD processes of PYTHIA8.186 with the A3 tune [96] and the MSTW2008LO PDF set [97], and were overlaid onto each simulated hard-scatter event. The MC events were reweighted to match the pileup distribution observed in the data.

Background and signal samples made use of EVTGEN1.6.0 and EVTGEN1.2.0 [98] to model the decay of bottom and charm quarks, with the exception of the background samples modeled with SHERPA. All MC-simulated samples were processed through the ATLAS simulation framework [99] in GEANT4 [100]. The samples for the signal scenarios made use of the ATLAS fast simulation, which parametrizes the response of the calorimeters.

IV. EVENT RECONSTRUCTION

Events are required to have at least one reconstructed pp interaction vertex with a minimum of two associated tracks with $p_{\mathrm{T}} > 500$ MeV. In events with multiple vertices, the primary vertex is defined as the one with the highest $\sum p_{\mathrm{T}}^2$ of associated tracks. To reject events with detector noise or noncollision backgrounds, a set of basic quality criteria [101] are applied.

Leptons, jets, and tracks are "preselected" using loose identification criteria, and must survive tighter "signal" identification requirements in order to be selected for the search regions. Preselected leptons and jets are used in fake/nonprompt (FNP) lepton background estimates, as well as in resolving ambiguities between tracks and clusters associated with multiple lepton and jet candidates.

Isolation criteria are used in the definition of signal leptons and are based on tracking information, calorimeter clusters, or both. Isolation energies are computed as a $\sum p_{\mathrm{T}}$ of nearby activity, excluding the contributions from nearby leptons, and are effective in reducing contributions from semileptonic heavy-flavor hadron decays and jets faking prompt leptons. The isolation requirements used in this analysis are based on those described in Refs. [102,103], with updates to improve their performance under the increased pileup conditions encountered in the 2017 and 2018 data samples.

Electrons are required to have $p_{\mathrm{T}} > 4.5$ GeV and $|\eta| < 2.47$. Preselected electrons are further required to

TABLE I. Simulated SM background processes. The PDF set refers to that used for the matrix element.

Process	Matrix element	Parton shower	PDF set	Cross section
V + jets	SHERPA2.2.1		NNPDF 3.0 NNLO [84]	NNLO [85]
VV	SHERPA2.2.1/2.2.2		NNPDF 3.0 NNLO	Generator NLO
Triboson	SHERPA2.2.1		NNPDF 3.0 NNLO	Generator LO, NLO
h (ggF)	POWHEG-BOX	PYTHIA8.212	NLO CTEQ6L1 [86]	N^{3}LO [87]
h (VBF)	POWHEG-BOX	PYTHIA8.186	NLO CTEQ6L1 [86]	NNLO + NLO [87]
$h + W/Z$	PYTHIA8.186		NNPDF 2.3 LO [54]	NNLO + NLO [87]
$h + t\bar{t}$	MG5_aMC@NLO2.2.3	PYTHIA8.210	NNPDF 2.3 LO	NLO [87]
$t\bar{t}$	POWHEG-BOX	PYTHIA8.230	NNPDF 2.3 LO	NNLO + NNLL [88–92]
t (s channel)	POWHEG-BOX	PYTHIA8.230	NNPDF 2.3 LO	NNLO + NNLL [93]
t (t channel)	POWHEG-BOX	PYTHIA8.230	NNPDF 2.3 LO	NNLO + NNLL [77,94]
$t + W$	POWHEG-BOX	PYTHIA8.230	NNPDF 2.3 LO	NNLO + NNLL [95]
$t + Z$	MG5_aMC@NLO2.3.3	PYTHIA8.212	NNPDF 2.3 LO	NLO [53]
$t\bar{t}WW$	MG5_aMC@NLO2.2.2	PYTHIA8.186	NNPDF 2.3 LO	NLO [53]
$t\bar{t} + Z/W/\gamma^*$	MG5_aMC@NLO2.3.3	PYTHIA8.210/8.212	NNPDF 2.3 LO	NLO [87]
$t + WZ$	MG5_aMC@NLO2.3.3	PYTHIA8.212	NNPDF 2.3 LO	NLO [53]
$t + t\bar{t}$	MG5_aMC@NLO2.2.2	PYTHIA8.186	NNPDF 2.3 LO	LO [53]
$tt\bar{t}\bar{t}$	MG5_aMC@NLO2.2.2	PYTHIA8.186	NNPDF 2.3 LO	NLO [53]

pass the calorimeter- and tracking-based *VeryLoose* likelihood identification [103], and to have a longitudinal impact parameter z_0 relative to the primary vertex that satisfies $|z_0 \sin\theta| < 0.5$ mm. Signal electrons must satisfy the *Medium* identification criterion [103], and be compatible with originating from the primary vertex, with the significance of the transverse impact parameter defined relative to the beam position satisfying $|d_0|/\sigma(d_0) < 5$. Signal electrons are further refined using the *Gradient* isolation working point [103], which uses both tracking and calorimeter information.

Muons are required to satisfy $p_{\mathrm{T}} > 3$ GeV and $|\eta| < 2.5$. Preselected muons are identified using the *LowPt* criterion [104], a reoptimized selection similar to those defined in Ref. [102] but with improved signal efficiency and background rejection for $p_{\mathrm{T}} < 10$ GeV muon candidates. The *LowPt* working point has improved efficiency for muons with $p_{\mathrm{T}} < 4$ GeV traversing the central detector region, which can lose enough energy in the calorimeters that they do not reach the second station of precision muon tracking chambers. The *LowPt* selection accepts candidates composed of track segments in the inner detector matched to track segments from a single station of the muon spectrometer. Misidentified muon candidates originating from in-flight hadron decays are rejected by requirements on the significance of a change in trajectory along the track, and by requiring that the momentum measurements in the inner tracker and in the muon spectrometer be compatible with each other. For prompt muons with $3 < p_{\mathrm{T}} < 6$ GeV, the *LowPt* criterion recovers approximately 20% of the identification efficiency in the $|\eta| < 1.2$ region, while maintaining an average misidentification probability comparable to the *Medium* selection described in Ref. [102].

Preselected muons must also satisfy $|z_0 \sin\theta| < 0.5$ mm. From the remaining preselected muons, signal muons must satisfy $|d_0|/\sigma(d_0) < 3$. Finally, signal muons are required to pass the *FCTightTrackOnly* isolation working point [102], which uses only tracking information.

Preselected jets are reconstructed from calorimeter topological energy clusters [105] in the region $|\eta| < 4.5$ using the anti-k_t algorithm [106,107] with radius parameter $R = 0.4$. The jets are required to have $p_{\mathrm{T}} > 20$ GeV after being calibrated in accord with Ref. [108] and having the expected energy contribution from pileup subtracted according to the jet area [109]. In order to suppress jets due to pileup, jets with $p_{\mathrm{T}} < 120$ GeV and $|\eta| < 2.5$ are required to satisfy the *Medium* working point of the jet vertex tagger [109], which uses information from the tracks associated with the jet. The *Loose* working point of the forward jet vertex tagger [110] is in turn used to suppress pileup in jets with $p_{\mathrm{T}} < 50$ GeV and $|\eta| > 2.5$. From the sample of preselected jets, signal jets are selected if they satisfy $p_{\mathrm{T}} > 30$ GeV and $|\eta| < 2.8$. The VBF search uses a modified version of signal jets, labeled VBF jets, satisfying $p_{\mathrm{T}} > 30$ GeV and $|\eta| < 4.5$.

Jets identified as containing b-hadron decays, referred to as b-tagged jets, are identified from preselected jets within $|\eta| < 2.5$ using the *MV2c10* algorithm [111]. The $p_{\mathrm{T}} > 20$ GeV requirement is maintained to maximize the rejection of the $t\bar{t}$ background. The b-tagging algorithm working point is chosen so that b-jets from simulated $t\bar{t}$ events are identified with an 85% efficiency, with rejection factors of 2.7 for charm-quark jets and 25 for light-quark and gluon jets.

The following procedure is used to resolve ambiguities between the reconstructed leptons and jets. It employs the distance measure $\Delta R_y = \sqrt{(\Delta y)^2 + (\Delta\phi)^2}$, where y is the rapidity. Electrons that share an inner detector track with a muon candidate are discarded to remove bremsstrahlung from muons followed by a photon conversion. Non-b-tagged jets that are separated from the remaining electrons by $\Delta R_y < 0.2$ are removed. Jets containing a muon candidate within $\Delta R_y < 0.4$ and with fewer than three tracks with $p_{\mathrm{T}} > 500$ MeV are removed to suppress muon bremsstrahlung. Electrons or muons with $\Delta R_y < 0.4$ from surviving jet candidates are removed to suppress bottom- and charm-hadron decays.

Signal regions based on a signal lepton and an isolated low-p_{T} track are used to increase the efficiency for electroweakino signals with the lowest mass splittings, where the lepton p_{T} can be very low. For these regions, the track is selected to be matched to a reconstructed electron or muon candidate with no identification requirements, including muons reconstructed with the *CaloTagged* and *SegmentTagged* algorithms described in Ref. [102]. Preselected tracks with $p_{\mathrm{T}} > 500$ MeV and $\eta < 2.5$ are selected using the *Tight-Primary* working point defined in Ref. [112]. Signal tracks are required to be within $\Delta R = 0.01$ of a reconstructed electron or muon candidate. Electron (muon) candidates can be reconstructed with transverse momenta as low as 1 (2) GeV, and are required to fail the signal lepton requirements defined above to avoid any overlap. Signal tracks with a p_{T} that differs from the transverse momentum of the matched lepton by more than 20% are rejected. The track–lepton matching allows the tracks to be identified as electron or muon tracks, reducing backgrounds from tracks not originating from the leptonic decay of a SUSY particle. Signal tracks must also satisfy dedicated isolation criteria: they are required to be separated from preselected jets by at least $\Delta R > 0.5$, and the $\sum p_{\mathrm{T}}$ of preselected tracks within $\Delta R = 0.3$ of signal tracks, excluding the contributions from nearby leptons, is required to be smaller than 0.5 GeV. Finally, signal tracks must satisfy $p_{\mathrm{T}} > 1$ GeV, $|z_0 \sin\theta| < 0.5$ mm, and $|d_0|/\sigma(d_0) < 3$.

The missing transverse momentum $\mathbf{p}_{\mathrm{T}}^{\mathrm{miss}}$, with magnitude $E_{\mathrm{T}}^{\mathrm{miss}}$, is defined as the negative vector sum of the transverse momenta of all preselected objects (electrons,

muons, jets, and photons [103]), and an additional soft term that is constructed from all tracks that are not associated with any lepton or jet, but that are associated with the primary vertex. A dedicated overlap removal procedure is used to resolve ambiguities between the reconstructed objects [113]. In this way, $E_{\mathrm{T}}^{\mathrm{miss}}$ is adjusted for the best calibration of jets and leptons, while maintaining pileup independence in the soft term [114].

Small scale factors are applied to the efficiencies of reconstructed electrons, muons, b-tagged jets, and tracks in the simulated samples to match the reconstruction efficiencies in data. The scale factors for b-tagged jets account for the differences between data and simulated samples in the identification efficiencies for jets, including b-hadron decays, as well as misidentification rates of jets initiated from charm quarks, light-flavor quarks, or gluons. The scale factors for low-momentum leptons are obtained from $J/\psi \to ee/\mu\mu$ events with the same tag-and-probe methods as used for higher-p_{T} electrons [103] and muons [102]. The scale factors used to account for track–lepton matching efficiency differences between data and simulation are derived from events with a J/ψ meson decaying into a low-p_{T} signal lepton and a preselected track. The track-isolation scale factors are measured using events with a Z boson decaying into a signal lepton and a track matched to a reconstructed lepton candidate. All track scale factors are found to be compatible with 1.

After all lepton selection criteria and efficiency scale factors are applied, the efficiency for reconstructing and identifying signal electrons within the detector acceptance in the Higgsino and slepton signal samples ranges from 20% for $p_{\mathrm{T}} = 4.5$ GeV to over 75% for $p_{\mathrm{T}} > 30$ GeV. The corresponding efficiency for signal muons ranges from approximately 50% at $p_{\mathrm{T}} = 3$ GeV to 90% for $p_{\mathrm{T}} > 30$ GeV. The efficiency of selecting signal tracks for electroweakino events peaks at 78% for tracks with $p_{\mathrm{T}} = 2.5$ GeV, with lower efficiencies at lower p_{T} due to track selection criteria and at higher p_{T} due to increasing electron and muon efficiencies. The efficiency for signal electrons, muons, and isolated tracks in a mix of slepton and Higgsino samples is shown in Fig. 3 as a function of lepton p_{T}.

Dedicated scale factors are also used to reweight MC events to properly model the trigger efficiency observed in data. These scale factors are measured in events selected with single-muon triggers, passing kinematic selections similar to the ones used to define the SRs. They are parametrized as a function of $E_{\mathrm{T}}^{\mathrm{miss}}$ and found to vary between 0.85 and 1 in the $E_{\mathrm{T}}^{\mathrm{miss}}$ range of interest. The uncertainty in the parametrization of the scale factors is negligible. An uncertainty of 5% is assigned to the scale factors to cover their dependence on other kinematic quantities of interest, such as $m_{\ell\ell}$ and m_{T2}. Additional uncertainties of at most 4% are assigned due to differences between the trigger efficiencies determined with MC events for the different signal and background processes.

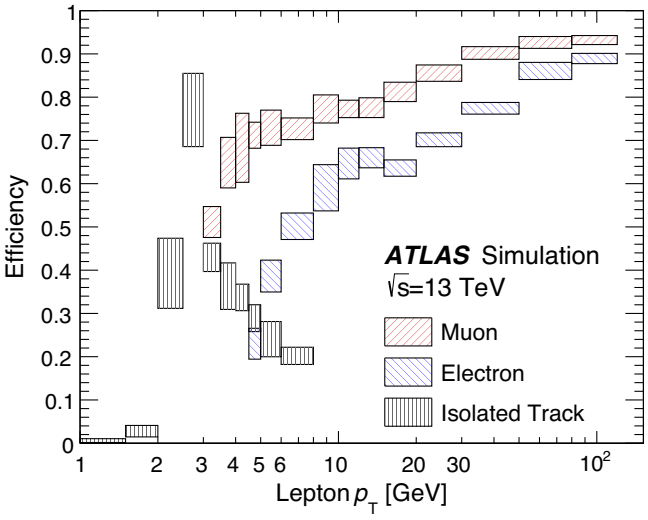

FIG. 3. Signal lepton efficiencies for electrons, muons, and isolated tracks in a mix of slepton and Higgsino samples. Combined reconstruction, identification, isolation, and vertex association efficiencies are shown for leptons within detector acceptance, and with lepton p_{T} within a factor of 3 of $\Delta m(\tilde{\ell},\tilde{\chi}_1^0)$ for sleptons or of $\Delta m(\tilde{\chi}_2^0,\tilde{\chi}_1^0)/2$ for Higgsinos. The efficiencies for isolated tracks include track reconstruction and vertex association efficiencies [112], as well as the efficiencies for track–lepton matching and track isolation, which are specific to this search. Scale factors are applied to match reconstruction efficiencies in data. The average number of interactions per crossing in the MC samples is 33.7; the number of pileup interactions match the distribution in data in spread and mean value. Uncertainty bands represent the range of efficiencies observed across all signal samples used for the given p_{T} bin.

V. SIGNAL REGIONS

Events entering into all SRs share a common preselection, with requirements listed in Table II. The 2ℓ channels require exactly two opposite-charge (OS) signal leptons of the same flavor, while the $1\ell 1T$ channel requires exactly one signal lepton and at least one OS signal track of the same flavor. In events where more than one OS same-flavor signal track is present, the candidate with the highest p_{T} is used to define the $1\ell 1T$ system. In regions with two leptons, the higher-p_{T} lepton is referred to as the "leading" lepton (ℓ_1), while the lower-p_{T} lepton is the "subleading" lepton (ℓ_2).

Preselection requirements are employed to reduce backgrounds and form a basis for SRs and CRs used in the simultaneous fit. The leading lepton is required to have $p_{\mathrm{T}} > 5$ GeV, which reduces backgrounds from FNP leptons. Pairs of muons are required to be separated by $\Delta R_{\mu\mu} > 0.05$, while pairs of electrons are required to be separated by $\Delta R_{ee} > 0.3$ to avoid reconstruction inefficiencies due to overlapping electron showers in the EM

TABLE II. Preselection requirements applied to all events entering into electroweakino, slepton, and VBF search regions. Requirements marked with † are not applied to VBF search regions. Requirements on jets are applied to VBF jets (satisfying $|\eta| < 4.5$) in the VBF channel.

	Preselection requirements	
Variable	2ℓ	$1\ell 1T$
Number of leptons (tracks)	=2 leptons	=1 lepton and ≥1 track
Lepton p_{T} [GeV]	$p_{\mathrm{T}}^{\ell_1} > 5$	$p_{\mathrm{T}}^{\ell} < 10$
$\Delta R_{\ell\ell}$	$\Delta R_{ee} > 0.30$, $\Delta R_{\mu\mu} > 0.05$, $\Delta R_{e\mu} > 0.2$	$0.05 < \Delta R_{\ell\mathrm{track}} < 1.5$
Lepton (track) charge and flavor	$e^{\pm}e^{\mp}$ or $\mu^{\pm}\mu^{\mp}$	$e^{\pm}e^{\mp}$ or $\mu^{\pm}\mu^{\mp}$
Lepton (track) invariant mass [GeV]	$3 < m_{ee} < 60$, $1 < m_{\mu\mu} < 60$	$0.5 < m_{\ell\mathrm{track}} < 5$
J/ψ invariant mass [GeV]	veto $3 < m_{\ell\ell} < 3.2$	veto $3 < m_{\ell\mathrm{track}} < 3.2$
$m_{\tau\tau}$ [GeV]	<0 or >160	no requirement
$E_{\mathrm{T}}^{\mathrm{miss}}$ [GeV]	>120	>120
Number of jets	≥1	≥1
Number of b-tagged jets	= 0	no requirement
Leading jet p_{T} [GeV]	≥100	≥100
$\min(\Delta\phi(\text{any jet}, \mathbf{p}_{\mathrm{T}}^{\mathrm{miss}}))$	>0.4	>0.4
$\Delta\phi(j_1, \mathbf{p}_{\mathrm{T}}^{\mathrm{miss}})^{\dagger}$	≥2.0	≥2.0

calorimeter. Electrons and muons are likewise required to be separated by $\Delta R_{e\mu} > 0.2$ to avoid energy deposits from muons spoiling electron shower shapes. An additional requirement that $m_{\ell\ell}$ be outside of [3.0, 3.2] GeV removes contributions from J/ψ decays, while requiring $m_{\ell\ell} <$ 60 GeV reduces contributions from on-shell Z-boson decays. Contributions from other hadronic resonances, e.g., Υ states, are expected to be negligible in the search regions and are not explicitly vetoed. Requirements on the minimum angular separation between the lepton candidates ($\Delta R_{\ell\ell}$) and invariant mass ($m_{\ell\ell}$) remove events in which an energetic photon produces collinear lepton pairs.

The $m_{\tau\tau}$ variable [115–117] approximates the invariant mass of a leptonically decaying τ-lepton pair if both τ leptons are sufficiently boosted so that the neutrinos from each τ decay are collinear with the visible lepton momentum. It is defined as $m_{\tau\tau} = \mathrm{sign}(m_{\tau\tau}^2)\sqrt{|m_{\tau\tau}^2|}$, which is the signed square root of $m_{\tau\tau}^2 \equiv 2p_{\ell_1} \cdot p_{\ell_2}(1+\xi_1)(1+\xi_2)$, where p_{ℓ_1} and p_{ℓ_2} are the lepton four-momenta, while the parameters ξ_1 and ξ_2 are determined by solving $\mathbf{p}_{\mathrm{T}}^{\mathrm{miss}} = \xi_1\mathbf{p}_{\mathrm{T}}^{\ell_1} + \xi_2\mathbf{p}_{\mathrm{T}}^{\ell_2}$. It can be less than zero in events where one of the lepton momenta has a smaller magnitude than the $E_{\mathrm{T}}^{\mathrm{miss}}$ and points in the hemisphere opposite to the $\mathbf{p}_{\mathrm{T}}^{\mathrm{miss}}$ vector. Events with $0 < m_{\tau\tau} < 160$ GeV are rejected, which reduces backgrounds from $Z \to \tau\tau$ and has an efficiency greater than 80% for the signals considered.

The reconstructed $E_{\mathrm{T}}^{\mathrm{miss}}$ is required to be greater than 120 GeV in preselection, with higher thresholds applied in some SRs. For SUSY events in which much of the invisible momentum is carried by the $\tilde{\chi}_1^0$ pair, these requirements on $E_{\mathrm{T}}^{\mathrm{miss}}$ suggest that the SUSY system is recoiling against additional hadronic activity, in the form of either ISR or the forward jets in VBF processes. All events are therefore required to have at least one jet with $p_{\mathrm{T}} > 100$ GeV. Additional jets in the event are also required to be separated from the $\mathbf{p}_{\mathrm{T}}^{\mathrm{miss}}$ by $\min(\Delta\phi(\text{any jet}, \mathbf{p}_{\mathrm{T}}^{\mathrm{miss}})) > 0.4$ in order to suppress the impact of jet energy mismeasurement on $E_{\mathrm{T}}^{\mathrm{miss}}$. For searches involving ISR, the leading jet is required to be separated from the $\mathbf{p}_{\mathrm{T}}^{\mathrm{miss}}$ by at least 2.0 radians in ϕ. In the 2ℓ channel, events with one or more b-tagged jets with $p_{\mathrm{T}} > 20$ GeV ($N_{b\text{-jet}}^{20}$) are vetoed to reduce backgrounds from $t\bar{t}$ production.

After applying the preselection requirements above, SRs are further optimized for specific SUSY scenarios. Three categories of SRs, labeled "SR-E," "SR-VBF," and "SR-S," are constructed: the first for electroweakinos recoiling against ISR (or simply electroweakinos), the second for electroweakinos produced through VBF, and the last targeting sleptons recoiling against ISR.

The SRs designed for optimal sensitivity to electroweakinos are defined in Table III. High-$E_{\mathrm{T}}^{\mathrm{miss}}$ regions, labeled "SR-E-high" and "SR-E-$1\ell 1T$," require $E_{\mathrm{T}}^{\mathrm{miss}} >$ 200 GeV, where the online $E_{\mathrm{T}}^{\mathrm{miss}}$ triggers are fully efficient for the SUSY signal. Low-$E_{\mathrm{T}}^{\mathrm{miss}}$ regions are constructed using events with 120 GeV $< E_{\mathrm{T}}^{\mathrm{miss}} <$ 200 GeV: "SR-E-med" targets electroweakinos with small mass splittings, and "SR-E-low" targets mass splittings larger than ∼10 GeV.

The p_{T} threshold for the subleading lepton is defined with sliding cuts that retain efficiency for soft leptons from low-Δm signals, while reducing backgrounds from FNP leptons in events with larger values of $m_{\ell\ell}$. The sliding requirement was optimized using a significance metric separately in each SR, considering signal models with a variety of masses and mass splittings. The significance was calculated following the profile likelihood method of

TABLE III. Requirements applied to events entering into the four signal regions used for electroweakino searches. The $1\ell 1T$ preselection requirements from Table II are implied for SR-E-$1\ell 1T$, while the 2ℓ ones are implied for the other SRs.

	Electroweakino SR requirements			
Variable	SR-E-low	SR-E-med	SR-E-high	SR-E-$1\ell 1T$
$E_{\mathrm{T}}^{\mathrm{miss}}$ [GeV]	[120, 200]	[120, 200]	>200	>200
$E_{\mathrm{T}}^{\mathrm{miss}}/H_{\mathrm{T}}^{\mathrm{lep}}$	<10	>10	···	>30
$\Delta\phi(\mathrm{lep}, \mathbf{p}_{\mathrm{T}}^{\mathrm{miss}})$	···	···	···	<1.0
Lepton or track p_{T} [GeV]	$p_{\mathrm{T}}^{\ell_2} > 5 + m_{\ell\ell}/4$	···	$p_{\mathrm{T}}^{\ell_2} > \min(10, 2 + m_{\ell\ell}/3)$	$p_{\mathrm{T}}^{\mathrm{track}} < 5$
$M_{\mathrm{T}}^{\mathrm{S}}$ [GeV]	···	<50	···	···
$m_{\mathrm{T}}^{\ell_1}$ [GeV]	[10, 60]	···	<60	···
R_{ISR}	[0.8, 1.0]	···	$[\max(0.85, 0.98 - 0.02 \times m_{\ell\ell}), 1.0]$	···

Ref. [118], under the assumption that the observation in each SR matches the expected number of signal plus background events.

The transverse mass of the leading lepton and $E_{\mathrm{T}}^{\mathrm{miss}}$ is defined as $m_{\mathrm{T}}^{\ell_1} = \sqrt{2(E_{\mathrm{T}}^{\ell_1} E_{\mathrm{T}}^{\mathrm{miss}} - \mathbf{p}_{\mathrm{T}}^{\ell_1} \cdot \mathbf{p}_{\mathrm{T}}^{\mathrm{miss}})}$ and is used in the SR-E-low and SR-E-high regions to reduce contributions from fake and nonprompt leptons.

In events with high-p_{T} ISR jets, the axis of maximum back-to-back p_{T}, referred to here as the thrust axis, approximates the direction of the recoil of the ISR activity against the sparticle pair. The recursive jigsaw reconstruction (RJR) technique [46] is used to divide each event into two hemispheres perpendicular to the thrust axis: a supersymmetric-particles hemisphere S, expected to contain the decay products of the electroweakinos or slepton pair and therefore the $E_{\mathrm{T}}^{\mathrm{miss}}$; and an ISR hemisphere, containing hadronic activity. This bisection allows the calculation of two discriminating variables that are useful in isolating events with ISR-induced $E_{\mathrm{T}}^{\mathrm{miss}}$ topologies: R_{ISR}, the ratio of the $E_{\mathrm{T}}^{\mathrm{miss}}$ to the transverse momentum of the ISR system, and $M_{\mathrm{T}}^{\mathrm{S}}$, the transverse mass of the S system. The R_{ISR} variable in particular is sensitive to the mass splitting, with values near 1.0 for the most compressed SUSY events. Figure 4 shows the relationship between R_{ISR} and $m_{\ell\ell}$ and m_{T2}^{100}, which is exploited in SR-E-high and SR-S-high (m_{T2}^{100} and SR-S-high are defined below) through sliding requirements on R_{ISR}.

The $E_{\mathrm{T}}^{\mathrm{miss}}/H_{\mathrm{T}}^{\mathrm{lep}}$ variable, where $H_{\mathrm{T}}^{\mathrm{lep}}$ is the scalar sum of the p_{T} of the two leptons, has been shown to be an effective discriminant for SUSY signals [45]. The two low-$E_{\mathrm{T}}^{\mathrm{miss}}$ electroweakino SRs are made orthogonal by requiring $E_{\mathrm{T}}^{\mathrm{miss}}/H_{\mathrm{T}}^{\mathrm{lep}} > 10$ for SR-E-med, where $H_{\mathrm{T}}^{\mathrm{lep}}$ is typically

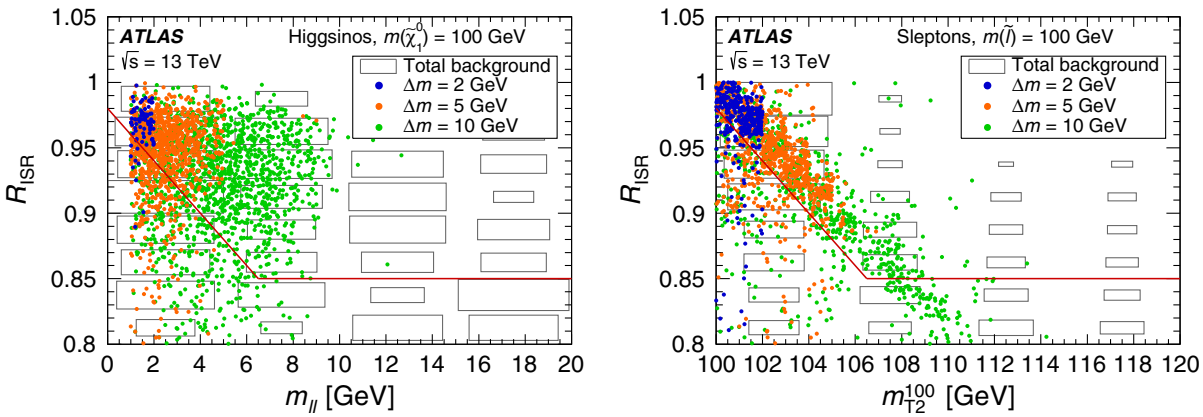

FIG. 4. Distributions of R_{ISR}, the ratio of the $E_{\mathrm{T}}^{\mathrm{miss}}$ to the transverse momentum of the hadronic ISR activity, for the electroweakino (left) and slepton (right) high-$E_{\mathrm{T}}^{\mathrm{miss}}$ SRs. Distributions are shown after applying all signal selection criteria except those on R_{ISR}. The solid red line indicates the requirement applied in the signal region; events in the region below the red line are rejected. Representative benchmark signals for the Higgsino (left) and slepton (right) simplified models are shown as circles. The gray rectangular boxes show the distribution of the total background prediction, which is primarily composed of top-like processes, diboson processes, and events with fake/nonprompt leptons. Regions at larger $m_{\ell\ell}$ and m_{T2} are not populated by the representative signals shown here, but are useful probes of less-compressed signal models.

TABLE IV. Requirements applied to all events entering into signal regions used for searches for electroweakinos produced through VBF. The 2ℓ preselection requirements from Table II are implied.

Variable	VBF SR requirements
$m_{\ell\ell}$ [GeV]	<40
Number of jets	≥2
$p_{\mathrm{T}}^{j_2}$ [GeV]	>40
$E_{\mathrm{T}}^{\mathrm{miss}}$ [GeV]	>150
$E_{\mathrm{T}}^{\mathrm{miss}}/H_{\mathrm{T}}^{\mathrm{lep}}$	>2
$p_{\mathrm{T}}^{\ell_2}$ [GeV]	$> \min(10, 2 + m_{\ell\ell}/3)$
$m_{\mathrm{T}}^{\ell_1}$ [GeV]	<60
R_{VBF}	$[\max(0.6, 0.92 - m_{\ell\ell}/60), 1.0]$
$\eta_{j_1} \cdot \eta_{j_2}$	<0
m_{jj} [GeV]	>400
$\Delta\eta_{jj}$	>2

	SR-VBF-low	SR-VBF-high
$\Delta\eta_{jj}$	<4	>4

smaller for the SUSY signal, and $E_{\mathrm{T}}^{\mathrm{miss}}/H_{\mathrm{T}}^{\mathrm{lep}} < 10$ for SR-E-low, where $H_{\mathrm{T}}^{\mathrm{lep}}$ increases due to the larger mass splitting.

The $1\ell 1T$ channel targets SUSY signals with especially low values of Δm, which produce decay products with very low momentum. The signal region "SR-E-$1\ell 1T$" therefore requires that the identified lepton have $p_{\mathrm{T}} < 10$ GeV and that the track have $p_{\mathrm{T}} < 5$ GeV. The lepton is also required to be within 1.0 radians of the $\mathbf{p}_{\mathrm{T}}^{\mathrm{miss}}$ in ϕ, to reduce backgrounds with tracks associated with nonprompt leptons or hadrons. Finally, the SR-E-$1\ell 1T$ region requires $E_{\mathrm{T}}^{\mathrm{miss}}/H_{\mathrm{T}}^{\mathrm{lep}} > 30$, where in this case $H_{\mathrm{T}}^{\mathrm{lep}}$ is the scalar sum of lepton and track p_{T}, again exploiting the low values of $H_{\mathrm{T}}^{\mathrm{lep}}$ expected for signal models with small mass splittings.

After all selection criteria are applied, the Higgsino model with $m(\tilde{\chi}_2^0) = 110$ GeV and $m(\tilde{\chi}_1^0) = 100$ GeV has an acceptance times efficiency of 1.1×10^{-4} in the union of all SR-E regions.

Signal regions designed for sensitivity to electroweakinos produced through VBF are defined in Table IV and denoted SR-VBF. VBF production is commonly characterized by the presence of two energetic jets with a large dijet invariant mass and large separation in pseudorapidity. Two regions are constructed, distinguished by the pseudorapidity gap between the two leading jets: events with $2 < \Delta\eta_{jj} < 4$ are tested in "SR-VBF-low," while events with $\Delta\eta_{jj} > 4$ are tested in "SR-VBF-high." The $E_{\mathrm{T}}^{\mathrm{miss}}$ is required to be greater than 150 GeV, which increases the acceptance relative to an $E_{\mathrm{T}}^{\mathrm{miss}} > 200$ GeV requirement while not introducing significant additional backgrounds. Additional requirements on $p_{\mathrm{T}}^{\ell_2}$, $m_{\mathrm{T}}^{\ell_1}$, and $E_{\mathrm{T}}^{\mathrm{miss}}/H_{\mathrm{T}}^{\mathrm{lep}}$ similarly reduce backgrounds for small losses in signal efficiency. The R_{VBF} variable is constructed similarly to R_{ISR}, with the vector sum of the two leading VBF jets in R_{VBF} taking the place of the ISR system in R_{ISR}. Additionally, in the case that an energetic jet is well separated from the two leading VBF jets, this jet is added to the decay tree. This forms an effective third-jet veto by altering the decay hemisphere, spoiling the back-to-back configuration in QCD-initiated events, while in signal events the central hadronic activity is expected to be suppressed. The R_{VBF} variable is also sensitive to the mass splitting, so sliding requirements on R_{VBF} are used in both VBF SRs. The acceptance times efficiency of Higgsinos with $m(\tilde{\chi}_2^0) = 100$ GeV and $m(\tilde{\chi}_1^0) = 95$ GeV produced through VBF in the SR-VBF is 2.9×10^{-4}.

The SRs designed to provide sensitivity for slepton production, denoted SR-S, are defined in Table V. The slepton search exploits the relationship between the mass splitting and the lepton and $E_{\mathrm{T}}^{\mathrm{miss}}$ kinematics via the stransverse mass (m_{T2}) variable [28,29]. The stransverse mass is defined as

$$m_{\mathrm{T2}}^{m_\chi}(\mathbf{p}_{\mathrm{T}}^{\ell_1}, \mathbf{p}_{\mathrm{T}}^{\ell_2}, \mathbf{p}_{\mathrm{T}}^{\mathrm{miss}}) = \min_{\mathbf{q}_{\mathrm{T}}}(\max[m_{\mathrm{T}}(\mathbf{p}_{\mathrm{T}}^{\ell_1}, \mathbf{q}_{\mathrm{T}}, m_\chi), m_{\mathrm{T}}(\mathbf{p}_{\mathrm{T}}^{\ell_2}, \mathbf{p}_{\mathrm{T}}^{\mathrm{miss}} - \mathbf{q}_{\mathrm{T}}, m_\chi)]),$$

where m_χ is the hypothesized mass of the invisible particles, and the transverse momentum vector $\mathbf{q}_{\mathrm{T}}$ with magnitude q_{T} is chosen to minimize the larger of the two transverse masses, defined by

TABLE V. Requirements applied to all events entering into signal regions used for slepton searches. The 2ℓ preselection requirements from Table II are implied.

	Slepton SR requirements	
Variable	SR-S-low	SR-S-high
$E_{\mathrm{T}}^{\mathrm{miss}}$ [GeV]	[150, 200]	>200
m_{T2}^{100} [GeV]	<140	<140
$p_{\mathrm{T}}^{\ell_2}$ [GeV]	$> \min(15, 7.5 + 0.75 \times (m_{\mathrm{T2}} - 100))$	$> \min(20, 2.5 + 2.5 \times (m_{\mathrm{T2}} - 100))$
R_{ISR}	[0.8, 1.0]	$[\max(0.85, 0.98 - 0.02 \times (m_{\mathrm{T2}} - 100)), 1.0]$

$$m_{\mathrm{T}}(\mathbf{p}_{\mathrm{T}}, \mathbf{q}_{\mathrm{T}}, m_{\chi}) = \sqrt{m_{\ell}^2 + m_{\chi}^2 + 2\left(\sqrt{p_{\mathrm{T}}^2 + m_{\ell}^2}\sqrt{q_{\mathrm{T}}^2 + m_{\chi}^2} - \mathbf{p}_{\mathrm{T}} \cdot \mathbf{q}_{\mathrm{T}}\right)}.$$

For signal events with slepton mass $m(\tilde{\ell})$ and LSP mass $m(\tilde{\chi}_1^0)$, the values of $m_{\mathrm{T2}}{}^{m_\chi}$ are bounded from above by $m(\tilde{\ell})$ when m_χ is equal to $m(\tilde{\chi}_1^0)$. The stransverse mass with $m_\chi = 100$ GeV, denoted m_{T2}^{100}, is used in this paper. The chosen value of 100 GeV is based on the expected LSP masses of the signals studied. The distribution of m_{T2}^{100} does not vary significantly for the signals considered in which $m(\tilde{\chi}_1^0) \neq 100$ GeV.

The "SR-S-low" slepton region requires events with $150\ \mathrm{GeV} < E_{\mathrm{T}}^{\mathrm{miss}} < 200\ \mathrm{GeV}$, while the "SR-S-high" region requires events with $E_{\mathrm{T}}^{\mathrm{miss}} > 200$ GeV. The SR-S-low region contributes most significantly for signals with $\Delta m \gtrsim 10$ GeV, where the leptons satisfy the p_{T} thresholds without needing a significant additional boost from ISR jets. Both regions are constructed with sliding requirements on $p_{\mathrm{T}}^{\ell_2}$, following the strategy for the electroweakino regions above. The requirements on R_{ISR} are looser in the SR-S-low region, targeting less compressed scenarios. The SR-S-high region uses a sliding requirement on R_{ISR} to maintain sensitivity to the most compressed scenarios while reducing backgrounds for events with larger m_{T2}^{100}. After all selection criteria are applied, the slepton model with $m(\tilde{\ell}) = 100$ GeV and $m(\tilde{\chi}_1^0) = 90$ GeV has an acceptance times efficiency of 2.5×10^{-3} when considering both SR-S regions. Acceptances and efficiencies for left- and right-handed sleptons are consistent with each other for all slepton scenarios under study.

After all selection requirements are applied, the SR-E and the SR-VBF regions are binned in $m_{\ell\ell}$, with bin boundaries at $m_{\ell\ell} = 1$, 2, 3, 5, 10, 20, 30, 40, and 60 GeV for the 2ℓ channels, and at $m_{\ell\mathrm{track}} = 0.5$, 1, 1.5, 2, 3, 4, and 5 GeV for the $1\ell 1T$ channel. Events in the SR-E-med region with $m_{\ell\ell} > 30$ GeV have minimal sensitivity to the electroweakino signals studied and are not considered. Similarly, events in the SR-E-$1\ell 1T$ region with $m_{\ell\mathrm{track}} > 5$ GeV are discarded. The slepton SR-S regions are instead binned in m_{T2}^{100}, with bin boundaries at $m_{\mathrm{T2}}^{100} = 100$, 100.5, 101, 102, 105, 110, 120, 130, and 140 GeV. Events with m_{T2}^{100} above 140 GeV have minimal sensitivity to compressed sleptons and are not considered in any of the regions. Events with $m_{\ell\ell}$ above 60 GeV are rejected in preselection for all channels.

The binned $m_{\ell\ell}$ and m_{T2}^{100} distributions are used in two different types of statistical tests. The first test is a search for excesses with minimal model dependence, in which any given fit considers a single inclusive SR. An inclusive electroweakino SR is constructed by merging all SR-E-high, SR-E-med, SR-E-low, and SR-E-$1\ell 1T$ bins below a $m_{\ell\ell}$ bin boundary listed above, with each 2ℓ electroweakino bin boundary corresponding to an inclusive SR. Similarly, the inclusive slepton regions are constructed by merging all SR-S-high and SR-S-low bins below the m_{T2}^{100} bin boundaries. The inclusive VBF SRs are also constructed by merging the SR-VBF-low and SR-VBF-high bins below the $m_{\ell\ell}$ boundaries. Additional inclusive VBF SRs are defined using events in SR-VBF-high only.

TABLE VI. Definition of control ("CR" prefix) and validation ("VR" prefix) regions used for background estimation in the electroweakino search, presented relative to the definitions of the corresponding signal regions SR-E-high, SR-E-med, and SR-E-low. The 2ℓ preselection criteria from Table II and selection criteria from Table III are implied, unless specified otherwise.

Region	SR orthogonality	Lepton flavor	Additional requirements
CRtop-E-high CRtop-E-low	$N_{b\text{-jet}}^{20} \geq 1$	$ee + \mu\mu + e\mu + \mu e$	$R_{\mathrm{ISR}} \in [0.7, 1.0]$, $m_{\mathrm{T}}^{\ell_1}$ removed $E_{\mathrm{T}}^{\mathrm{miss}}/H_{\mathrm{T}}^{\mathrm{lep}}$ and $m_{\mathrm{T}}^{\ell_1}$ removed
CRtau-E-high CRtau-E-low VRtau-E-med	$m_{\tau\tau} \in [60, 120]$ GeV	$ee + \mu\mu + e\mu + \mu e$	$R_{\mathrm{ISR}} \in [0.7, 1.0]$, $m_{\mathrm{T}}^{\ell_1}$ removed $R_{\mathrm{ISR}} \in [0.6, 1.0]$, $m_{\mathrm{T}}^{\ell_1}$ removed …
CRVV-E-high CRVV-E-low	$R_{\mathrm{ISR}} \in [0.7, 0.85]$ $R_{\mathrm{ISR}} \in [0.6, 0.8]$	$ee + \mu\mu + e\mu + \mu e$	$m_{\mathrm{T}}^{\ell_1}$ removed $m_{\mathrm{T}}^{\ell_1} > 30$ GeV, $N_{\mathrm{jets}} \in [1, 2]$, $E_{\mathrm{T}}^{\mathrm{miss}}/H_{\mathrm{T}}^{\mathrm{lep}}$ removed
VRSS-E-high VRSS–E–low VRSS-E-med	Same sign $\ell^{\pm}\ell^{\pm}$	$ee + \mu e, \mu\mu + e\mu$	$R_{\mathrm{ISR}} \in [0.7, 1.0]$, $m_{\mathrm{T}}^{\ell_1}$ and $p_{\mathrm{T}}^{\ell_2}$ removed $E_{\mathrm{T}}^{\mathrm{miss}}/H_{\mathrm{T}}^{\mathrm{lep}}$, $m_{\mathrm{T}}^{\ell_1}$ and $p_{\mathrm{T}}^{\ell_2}$ removed …
VRDF-E-high VRDF-E-low VRDF-E-med	$e\mu + \mu e$	$e\mu + \mu e$	… … …

TABLE VII. Definition of control ("CR" prefix) and validation ("VR" prefix) regions used for background estimation in the search for electroweakinos produced through VBF, presented relative to the definitions of the corresponding signal regions SR-VBF-high and SR-VBF-low. The 2ℓ preselection criteria from Table II and selection criteria from Table IV are implied, unless specified otherwise.

Region	SR orthogonality	Lepton flavor	Additional requirements
CRtop-VBF	$N_{b\text{-jet}}^{20} \geq 1$	$ee + \mu\mu + e\mu + \mu e$	R_{VBF} and $m_{\text{T}}^{\ell_1}$ removed
CRtau-VBF	$m_{\tau\tau} \in [60, 120]$ GeV	$ee + \mu\mu + e\mu + \mu e$	$E_{\text{T}}^{\text{miss}}/H_{\text{T}}^{\text{lep}} \in [2, 10]$, R_{VBF} and $m_{\text{T}}^{\ell_1}$ removed
VRSS-VBF	Same sign $\ell^{\pm}\ell^{\pm}$	$ee + \mu e, \mu\mu + e\mu$	R_{VBF}, $m_{\text{T}}^{\ell_1}$ and $p_{\text{T}}^{\ell_2}$ removed
VRDF-VBF-low	$e\mu + \mu e$	$e\mu + \mu e$	...
VRDF-VBF-high	$e\mu + \mu e$	$e\mu + \mu e$	...

The second type of test is referred to as an exclusion fit, which considers all relevant bins separately in the likelihood. Dielectron and dimuon events in the 2ℓ electroweakino SRs and in the slepton SRs are also fitted separately in the exclusion fits.

VI. BACKGROUND ESTIMATION

The sources of SM background in regions with two leptons can be subdivided into two categories: reducible backgrounds from events where at least one of the candidate leptons is FNP, and irreducible backgrounds from events that contain two prompt leptons.

Since MC simulation is not expected to model processes with FNP leptons accurately, a data-driven method, referred to as the fake factor method [119,120], is employed to estimate these backgrounds. The yields obtained from this procedure are cross-checked in validation regions (VRs), which are not used to constrain the fit and are orthogonal in selection to the CRs and SRs.

The dominant sources of irreducible background are $t\bar{t}/tW$, WW/WZ, and $Z^{(*)}/\gamma^*(\rightarrow \tau\tau) + \text{jets}$. These backgrounds are estimated using MC simulations normalized to data in dedicated CRs. Events originating from the production of a Drell-Yan lepton pair, a triboson, a Higgs boson, or top quarks in association with gauge bosons constitute a small fraction of the total background. Their contributions in the regions with two leptons are estimated using the MC samples listed in Table I. Additional VRs are used to validate the extrapolation of background in the fitting procedure within the same kinematic regime as the SRs.

The definitions of the CRs and VRs used in the electroweakino, VBF, and slepton searches are summarized in Tables VI, VII, and VIII, respectively. The VRSS regions are further described in Sec. VI A, in the context of the FNP background estimation, while the remaining CRs and VRs are explained in Sec. VI B.

The dominant source of background in the $1\ell 1T$ channel is combinatorial, from events containing one prompt lepton and one random track, and is collectively estimated using data, as described in Sec. VI C.

A. Reducible background in regions with two leptons

The FNP lepton background arises from jets misidentified as leptons, photon conversions, or semileptonic decays

TABLE VIII. Definition of control ("CR" prefix) and validation ("VR" prefix) regions used for background estimation in the slepton search, presented relative to the definitions of the corresponding signal regions SR-S-high and SR-S-low. The 2ℓ preselection criteria from Table II and selection criteria from Table V are implied, unless specified otherwise.

Region	SR orthogonality	Lepton flavor	Additional requirements
CRtop-S-high	$N_{b\text{-jet}}^{20} \geq 1$	$ee + \mu\mu + e\mu + \mu e$	$R_{\text{ISR}} \in [0.7, 1.0]$
CRtop-S-low			...
CRtau-S-high	$m_{\tau\tau} \in [60, 120]$ GeV	$ee + \mu\mu + e\mu + \mu e$	$R_{\text{ISR}} \in [0.7, 1.0]$
CRtau-S-low			$R_{\text{ISR}} \in [0.6, 1.0]$
CRVV-S-high	$R_{\text{ISR}} \in [0.7, 0.85]$	$ee + \mu\mu + e\mu + \mu e$	...
CRVV-S-low	$R_{\text{ISR}} \in [0.6, 0.8]$		$m_{\text{T}}^{\ell_1} > 30$, $N_{\text{jets}} \in [1, 2]$
VRSS-S-high	Same sign $\ell^{\pm}\ell^{\pm}$	$ee + \mu e, \mu\mu + e\mu$	$R_{\text{ISR}} \in [0.7, 1.0]$, $p_{\text{T}}^{\ell_2}$ removed
VRSS-S-low			$p_{\text{T}}^{\ell_2}$ removed
VRDF-S-high	$e\mu + \mu e$	$e\mu + \mu e$	...
VRDF-S-low			...

of heavy-flavor hadrons. Studies based on simulated samples indicate that the last is the dominant component in the SRs with two leptons. The contamination of the SRs by the FNP lepton background is large at low values of $m_{\ell\ell}$ and m_{T2}^{100}, and it decreases at the upper end of the distributions.

In the fake factor method, a two-lepton control sample is defined in data using leptons with modified signal lepton requirements. At least one of the leptons, labeled as "anti-ID," is required to fail one or more of the requirements applied to signal leptons, but is required to satisfy less restrictive requirements. The other lepton can either meet all signal lepton requirements, in which case it is labeled as ID, or satisfy the anti-ID requirements. This sample is enriched in FNP lepton backgrounds and is therefore referred to as the FNP control sample. The contributions from processes with two prompt leptons in the FNP control sample are subtracted using simulated samples. MC studies indicate that the leptons in the FNP control sample arise from processes similar to those for FNP leptons passing the SR selections. The FNP lepton background prediction in a given region is obtained by applying all selection requirements of that region to the FNP control sample and scaling each event by a weight assigned to each anti-ID lepton, referred to as the fake factor. Events in the FNP control sample containing a single anti-ID lepton have positive fake factors. Events with two anti-ID leptons receive a weight corresponding to the product of the weights for the two anti-ID leptons, and they enter with opposite sign to correct for events with two FNP leptons.

The fake factor is measured in a data sample collected with prescaled low-p_{T} single-lepton triggers. This sample is dominated by multijet events with FNP leptons and is referred to as the measurement sample. A selection of $m_{\mathrm{T}}^{\ell_1} < 40$ GeV is applied to reduce the contributions from processes with prompt leptons in the measurement sample. The contributions from these processes are subtracted using MC simulation, with negligible impact on the measured fake factors.

To enrich the sample in FNP leptons similar to those contaminating the SRs, the leading-jet p_{T} is required to be greater than 100 GeV. The fake factors are calculated as the ratio of ID to anti-ID leptons in the measurement sample, measured in bins of lepton p_{T}, separately for electrons and muons. The fake factors are also found to have a dependence on the number of b-tagged jets in the events. Different fake factors are therefore computed in events with and without b-tagged jets.

The yields predicted by the fake factor method are cross-checked in dedicated VRs enriched in FNP lepton backgrounds, labeled "VRSS." As summarized in Tables VI, VII, and VIII, a dedicated VRSS is constructed for each SR by selecting events with two leptons with the same electric charge. The kinematic requirements applied

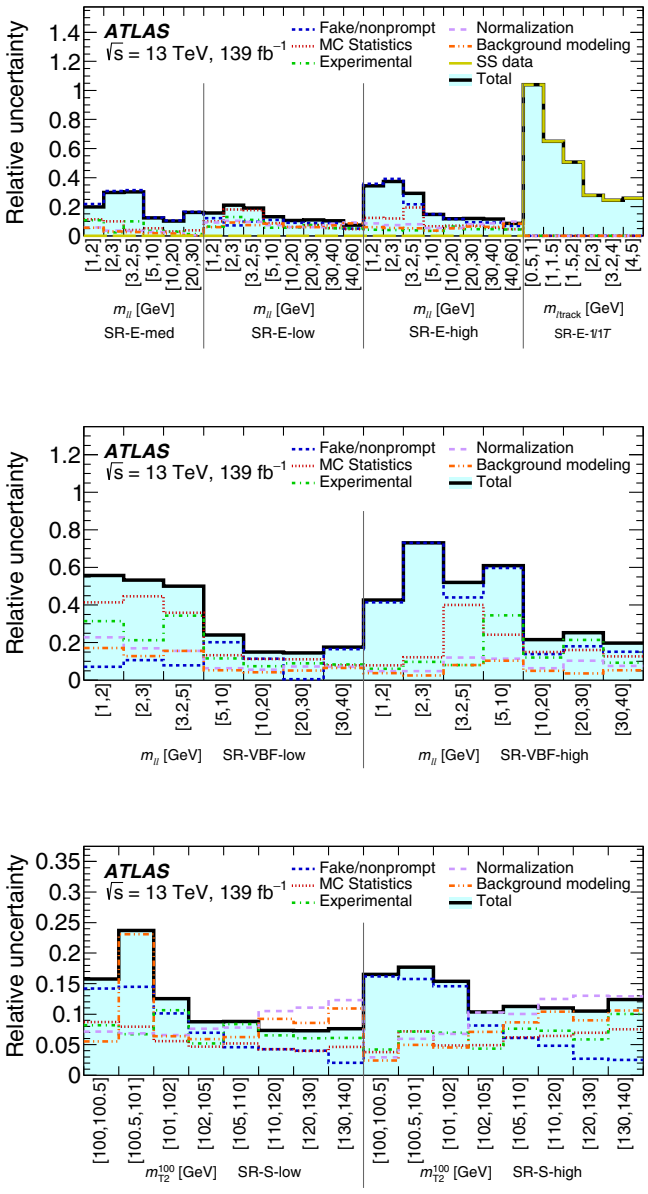

FIG. 5. The relative systematic uncertainties in the fitted SM background as obtained from CR + SR background-only fits for the electroweakino SRs (top), VBF SRs (middle), and slepton SRs (bottom). The uncertainty in the "SS data" includes a statistical component due to the size of the SS data sample used to estimate the background in the SR-E-1ℓ1T region, and a systematic component from the SS–OS extrapolation. The "MC Statistics" uncertainty originates from the limited size of the MC samples used to model the irreducible background contributions. The "Normalization" uncertainty arises from the use of CRs to normalize the contributions of $t\bar{t}/tW$, $Z^{(*)}/\gamma^*(\to \tau\tau)+$jets and WW/WZ backgrounds, while "Background modeling" includes the different sources of theoretical modeling uncertainties in the $m_{\ell\ell}$ or m_{T2}^{100} line shapes for the irreducible backgrounds. All sources of uncertainty affecting the FNP background estimate are included under "Fake/nonprompt." The uncertainties arising from the reconstruction and selection of signal leptons, jets, and $E_{\mathrm{T}}^{\mathrm{miss}}$ are included under the "Experimental" category. The individual uncertainties can be correlated and do not necessarily add up in quadrature to the total uncertainty.

to each VRSS are mostly the same as the ones used in the corresponding SR, ensuring that the FNP lepton processes are similar in the two regions. To guarantee high purity in FNP lepton background, the selection criteria designed to suppress these processes in the SRs, such as the sliding cut on the p_{T} threshold of the subleading lepton, are loosened or removed in each VRSS. The contribution of the FNP background in the VRSS regions is typically above 91%, with the remaining backgrounds originating from VV processes with two prompt leptons of the same electric charge. The signal contamination is at most 14%.

B. Irreducible background in regions with two leptons

Several CRs are defined for the electroweakino, VBF, and slepton searches and are used to normalize the MC simulations of $t\bar{t}/tW$ and $Z^{(*)}/\gamma^{*}(\rightarrow \tau\tau)+\text{jets}$ background processes to the data in a simultaneous fit also including the SRs, as described in Sec. VIII. In searches for electroweakinos and sleptons recoiling against ISR, CRs are also constructed to normalize the WW/WZ background. The event rates in the SRs are predicted by extrapolating from the CRs using the simulated MC distributions. This extrapolation is validated using events in dedicated VRs.

The CRs are designed to be statistically disjoint from the SRs, to be enriched in a particular background process, to have minimal contamination from the signals considered, and to exhibit kinematic properties similar to the SRs. The CRs labeled as "CRtop" are defined by selecting events with at least one b-tagged jet. The CRtop regions have purities ranging from 83% to 94% in processes with top quarks and are used to constrain the normalization of the $t\bar{t}$ and tW processes with dilepton final states. The "CRtau" regions, which are enriched in the $Z^{(*)}/\gamma^{*}(\rightarrow \tau\tau)+\text{jets}$ process with purities of at least 75%, are constructed by selecting events satisfying $m_{\tau\tau} \in [60, 120]$ GeV. Finally, the R_{ISR} selection used to define the SRs is modified to construct CRs enriched in WW and WZ processes, denoted "CRVV." In these CRs, 41%–45% of the events are VV events.

The $t\bar{t}/tW$, WW/WZ, and $Z^{(*)}/\gamma^{*}(\rightarrow \tau\tau)+\text{jets}$ processes containing two prompt leptons all yield same-flavor lepton pairs (ee and $\mu\mu$) at the same rate as for different-flavor pairs ($e\mu$ and μe, where the first lepton is the leading lepton). This feature is used to enhance the statistical constraining power of the CRs, by selecting events with all possible flavor assignments (ee, $\mu\mu$, $e\mu$, and μe). It is also used to define additional VRs, denoted "VRDF." One VRDF is defined for each 2ℓSR by requiring two different-flavor leptons ($e\mu$ and μe), but otherwise keeping the same kinematic selections as the corresponding SR. The relative fractions of each background process are similar in the SR and the corresponding VRDF. The signal contamination in the VRDF regions is at most 16%, originating from $\tilde{\chi}_1^+\tilde{\chi}_1^-$ or $\tilde{\chi}_2^0\tilde{\chi}_1^\pm$ Higgsino events decaying fully leptonically.

In the search for electroweakinos recoiling against ISR, six single-bin CRs are defined as summarized in Table VI. Three CRs, labeled "CR-E-high," employ a $E_{\mathrm{T}}^{\mathrm{miss}} > 200$ GeV selection and are used to constrain the normalization of $t\bar{t}/tW$, WW/WZ, and $Z^{(*)}/\gamma^{*}(\rightarrow \tau\tau)+\text{jets}$ backgrounds in SR-E-high. To minimize the impact of the mismodeling of the trigger efficiency in the simulation, three additional CRs, labeled "CR-E-low," are defined by selecting events with $E_{\mathrm{T}}^{\mathrm{miss}} \in [120, 200]$ GeV. These CRs are used to normalize the same background processes in SR-E-low. Events with FNP leptons entering the CRs are suppressed using the same sliding cut on $p_{\mathrm{T}}^{\ell_2}$ as the corresponding SRs.

The dominant source of irreducible background in the SR-E-med region is the $Z^{(*)}/\gamma^{*}(\rightarrow \tau\tau)+\text{jets}$ process. It is difficult to construct a dedicated CR with enough events to constrain the normalization of the $Z^{(*)}/\gamma^{*}(\rightarrow \tau\tau)+\text{jets}$ background in the SR-E-med region. The "CRtau-E-low" region is therefore used for this purpose. The extrapolation from CRtau-E-low to SR-E-med is tested in an additional VR, labeled "VRtau-E-med," defined by selecting events with $m_{\tau\tau} \in [60, 120]$ GeV, but otherwise applying the same kinematic selections as in the SR-E-med region, as summarized in Table VI.

TABLE IX. Normalization factors obtained from a background-only fit of the CRs defined for electroweakino, slepton, and VBF searches. The uncertainties include statistical and systematic contributions combined.

		Normalization parameters		
Backgrounds	$E_{\mathrm{T}}^{\mathrm{miss}}$ region	Electroweakino	Slepton	VBF
$t\bar{t}/Wt$	high	1.08 ± 0.20	1.05 ± 0.20	1.04 ± 0.04
	low	1.08 ± 0.18	1.09 ± 0.19	
$Z^{(*)}/\gamma^{*}(\rightarrow \tau\tau)+\text{jets}$	high	0.96 ± 0.14	0.80 ± 0.17	0.97 ± 0.13
	low	1.02 ± 0.15	1.08 ± 0.17	
VV	high	0.89 ± 0.27	0.85 ± 0.28	...
	low	0.69 ± 0.22	0.71 ± 0.23	

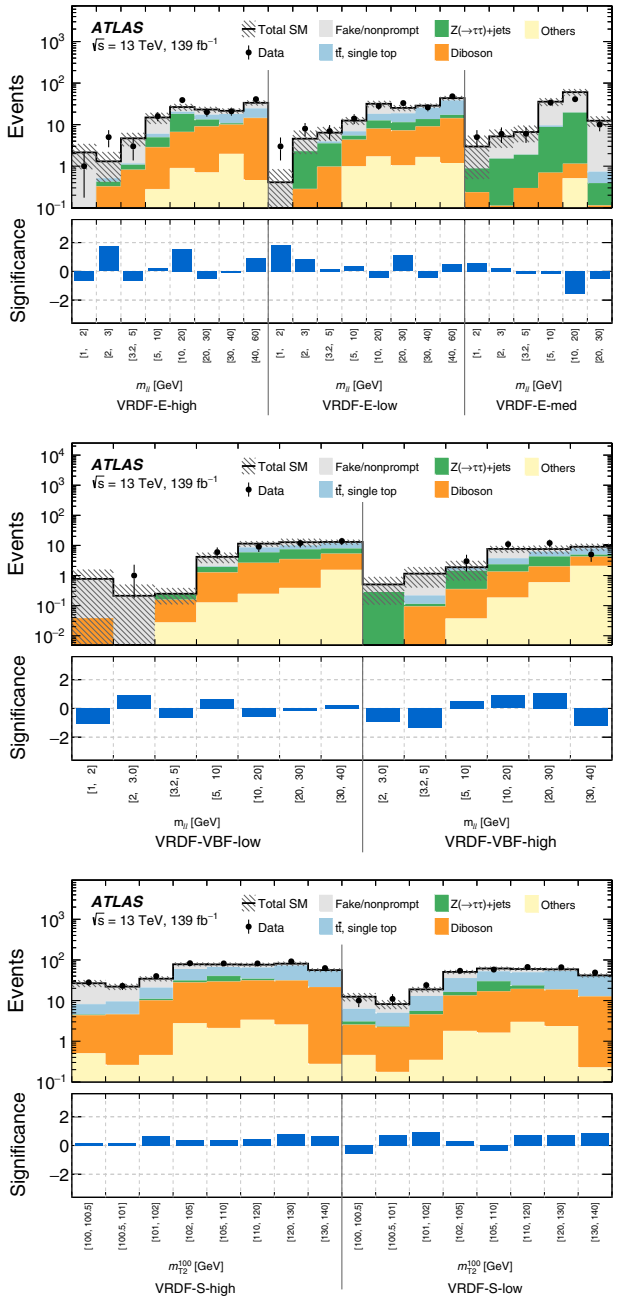

FIG. 6. Comparison of observed and expected event yields in the VRDF regions after a background-only fit of the CRs. The three VRDF-E regions are shown at the top, binned in $m_{\ell\ell}$ as the corresponding electroweakino SRs. The two VRDF-VBF regions are shown in the middle, also binned in $m_{\ell\ell}$. The bin 1 GeV $< m_{\ell\ell} <$ 2 GeV is omitted from the VRDF-VBF-high region because both the expected and observed event yields are zero. Finally, the two VRDF-S regions are shown at the bottom, binned in m_{T2}^{100} as the corresponding slepton SRs. Uncertainties in the background estimates include both the statistical and systematic uncertainties. The bottom panel in all three plots shows the significance of the difference between the expected and observed yields, computed following the profile likelihood method of Ref. [118] in the case where the observed yield exceeds the prediction, and using the same expression with an overall minus sign if the yield is below the prediction.

Two control regions are defined for the VBF search, as summarized in Table VII. The "CRtop-VBF" and the "CRtau-VBF" regions are designed with a $\Delta\eta_{jj} > 2$ requirement, and are used to constrain the normalizations of the $t\bar{t}/tW$ and $Z^{(*)}/\gamma^*(\to \tau\tau) +$ jets processes in both the SR-VBF-low and the SR-VBF-high regions. The number of events in the VBF CRs is increased by removing the $m_{\mathrm{T}}^{\ell_1}$ and R_{VBF} selections used in the SRs.

Six CRs are used to normalize the $t\bar{t}/tW$, WW/WZ, and $Z^{(*)}/\gamma^*(\to \tau\tau) +$ jets background processes entering the SR-S-low and SR-S-high regions, as summarized in Table VIII. The CRs used in the search for sleptons are designed similarly to the CRs used in the search for electroweakinos. One notable difference is the sliding cut on the $p_{\mathrm{T}}^{\ell_2}$ threshold, which is chosen to match the requirements used in the slepton SRs and therefore depends on m_{T2}^{100}.

C. Background in the $1\ell 1T$ signal region

The background in the SR-E-$1\ell 1T$ region is suppressed by requiring that the selected track be associated with a reconstructed lepton candidate. Simulation studies show that this background is dominated by events with one prompt lepton and one track from hadrons or nonprompt leptons. The MC samples used to model SM processes with two prompt leptons contribute negligibly in the $1\ell 1T$ SR.

The amount of background in the $1\ell 1T$ channel is estimated using a data-driven procedure. A control sample is defined in data with events that satisfy the same selection criteria as the SR-E-$1\ell 1T$ region. Instead of selecting OS events with one lepton and one track, the lepton and the track in the control sample are required to have the same electric charge (SS). The contamination of the SS control sample by signal is negligible. The data in the SS sample are directly used as the estimate of the background in SR-E-$1\ell 1T$. The background estimate assumes that the background events are produced with equal rates for OS and SS events. This is expected to be the case because the track is randomly selected and its electric charge is not correlated with the charge of the prompt lepton.

The assumption that OS and SS background events are produced with equal rates in the $1\ell 1T$ signal region is tested in simulation using $W +$ jets events. The ratio of OS to SS $W +$ jets events was found to be compatible with 1, with a statistical uncertainty of 12% determined by the size of the MC sample. A VR, denoted "VR-$1\ell 1T$," is constructed to test the assumption using data. The VR-$1\ell 1T$ is designed using the same kinematic selections as the $1\ell 1T$ SR, except that $\Delta\phi(\mathrm{lep}, \mathbf{p}_{\mathrm{T}}^{\mathrm{miss}}) > 1.5$ is required to ensure that the samples are disjoint. The upper bound on $\Delta R_{\ell\mathrm{track}}$ used in SR-E-$1\ell 1T$ is removed to reduce the signal contamination, and the $E_{\mathrm{T}}^{\mathrm{miss}}/H_{\mathrm{T}}^{\mathrm{lep}}$ requirement is loosened to $E_{\mathrm{T}}^{\mathrm{miss}}/H_{\mathrm{T}}^{\mathrm{lep}} > 15$ to increase the number of events in the

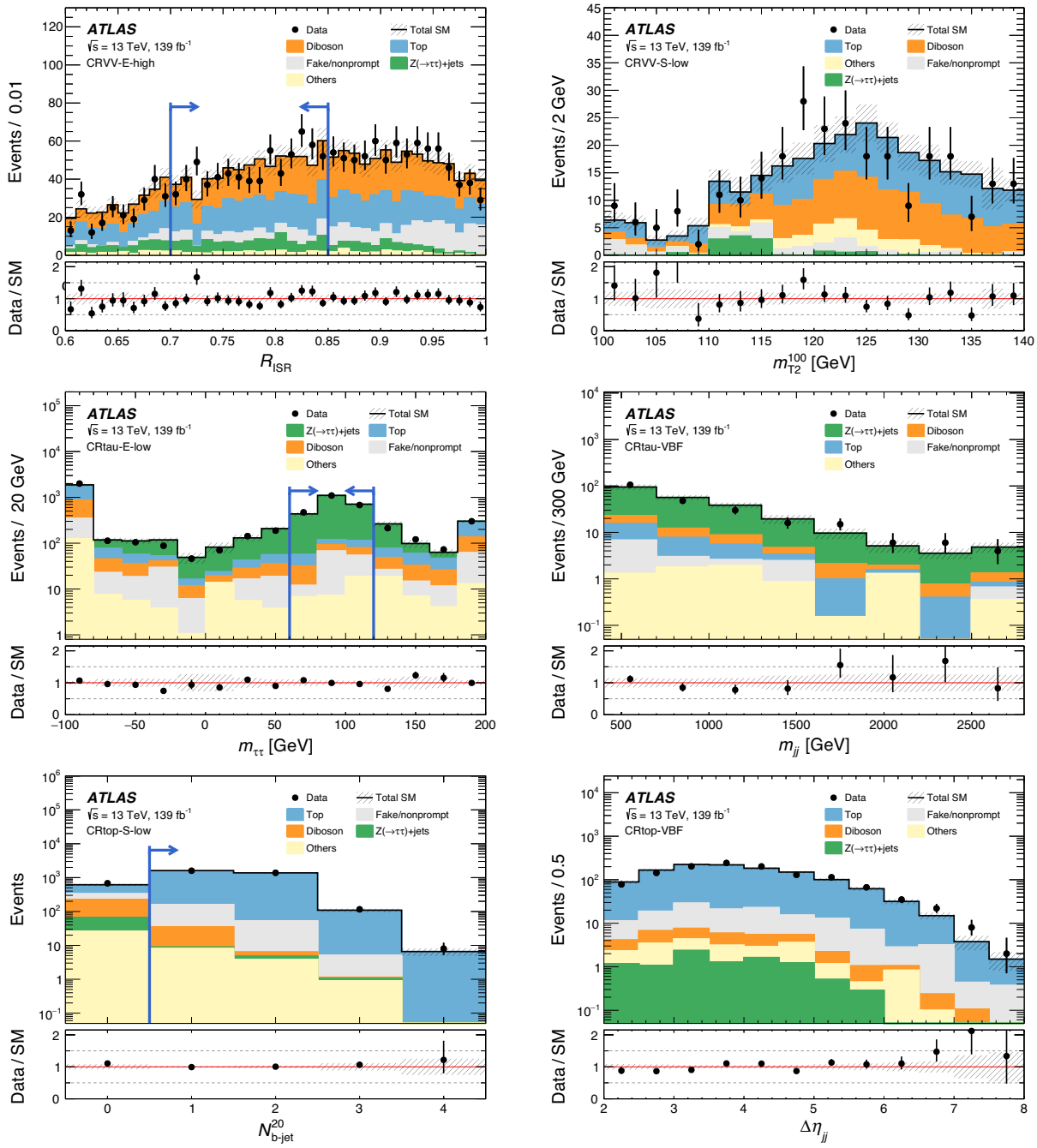

FIG. 7. Examples of kinematic distributions after the background-only fit of the CRs showing the data as well as the expected background in the control regions CRVV-E-high (top left), CRVV-S-low (top right), CRtau-E-low (middle left), CRtau-VBF (middle right), CRtop-S-low (bottom left), and CRtop-VBF (bottom right). The full event selection of the corresponding regions is applied, except for distributions showing blue arrows, where the requirement on the variable being plotted is removed and indicated by the arrows in the distributions instead. The first (last) bin includes underflow (overflow). The uncertainty bands plotted include all statistical and systematic uncertainties.

VR. The kinematic distributions of the SS and OS data events in the VR-1ℓ1T are compared and found to agree.

VII. SYSTEMATIC UNCERTAINTIES

Systematic uncertainties are evaluated for all background processes and signal samples. As the predictions for the main SM background processes modeled via MC simulation are normalized to data in dedicated control regions, the systematic uncertainties only affect the extrapolation to the signal regions in these cases.

Figure 5 illustrates the dominant classes of uncertainties in the expected background yields in the electroweakino, VBF, and slepton SRs. The main sources of experimental

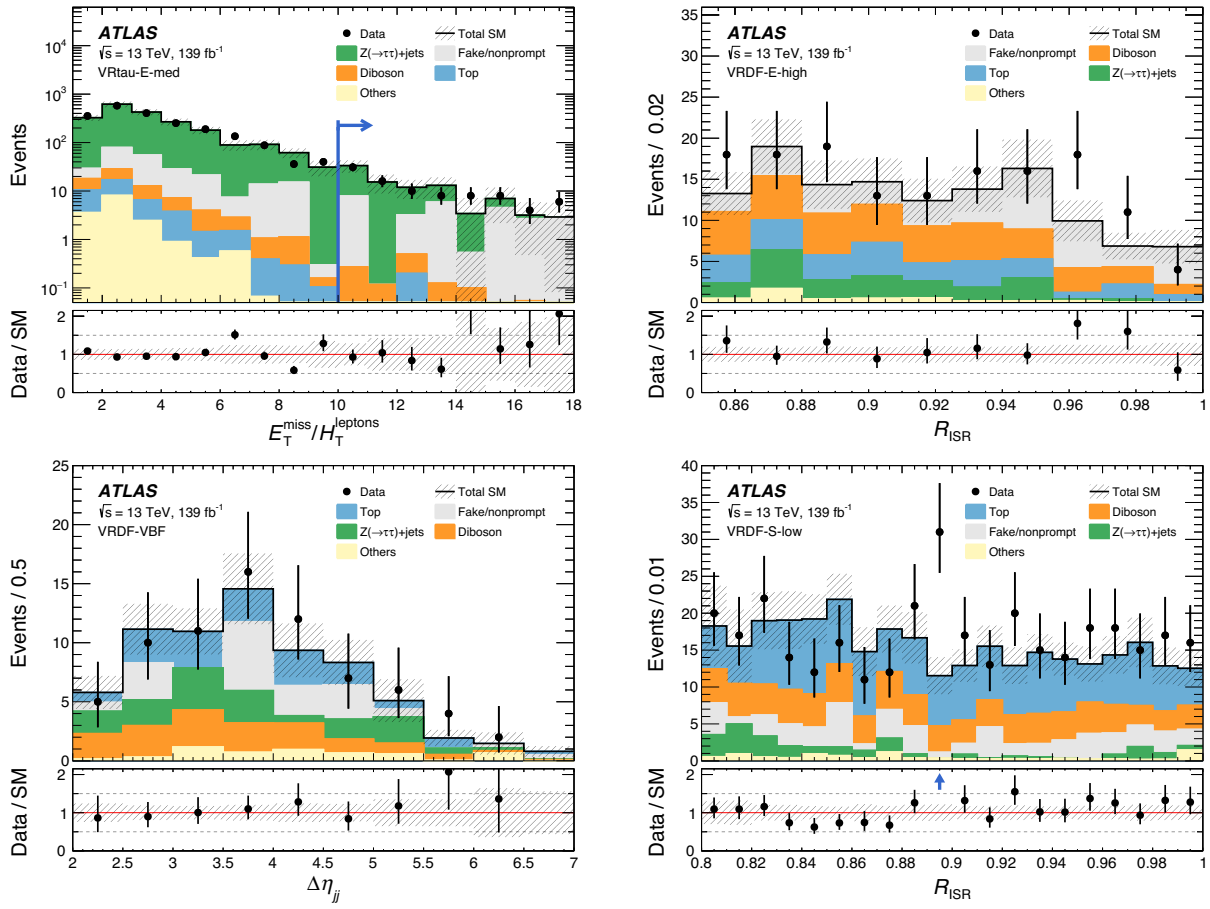

FIG. 8. Examples of kinematic distributions after the background-only fit of the CRs showing the data as well as the expected background in the validation regions VRtau-E-med (top left), VRDF-E-high (top right), VRDF-VBF, including both VRDF-VBF-high and VRDF-VBF-low (bottom left) and VRDF-S-low (bottom right). The full event selection of the corresponding regions is applied, except for distributions showing blue arrows, where the requirement on the variable being plotted is removed and indicated by the arrows in the distributions instead. The first (last) bin includes underflow (overflow). The uncertainty bands plotted include all statistical and systematic uncertainties.

uncertainty affect the FNP background predictions obtained with the fake factor method. These systematic uncertainties stem from the size of the FNP control samples, as well as from the size of the measurement sample used to compute the fake factors. The uncertainties associated with the subtraction of processes involving prompt leptons in the FNP control samples and in the measurement sample are estimated from simulation and found to be negligible. Uncertainties are also assigned to cover the differences in the event and lepton kinematics between the measurement region and the signal regions. Moreover, additional uncertainties are computed as the differences between the FNP background predictions and observed data in the VRSS regions.

Other sources of significant experimental systematic uncertainties are the jet energy scale (JES) and resolution (JER). The jet uncertainties are derived as a function of p_{T} and η of the jet, as well as of the pileup conditions and the jet flavor composition of the selected jet sample. They are determined using a combination of simulated samples and studies of data, such as measurements of the jet p_{T} balance in dijet, $Z+\mathrm{jet}$, and $\gamma+\mathrm{jet}$ events [108]. The systematic uncertainties related to the modeling of $E_{\mathrm{T}}^{\mathrm{miss}}$ in the simulation are estimated by propagating the uncertainties in the energy and momentum scale of each of the objects entering the calculation, as well as the uncertainties in the soft-term resolution and scale [113].

The reconstruction, identification, and isolation efficiencies for low-p_{T} leptons, as well as the momentum resolution and scale, are measured and calibrated following methods similar to those employed for higher-p_{T} electrons [103] and muons [102]. The associated systematic uncertainties are in general found to be small.

The MC samples simulating the dominant background processes, $t\bar{t}/tW$, $Z^{(*)}/\gamma^{*}(\rightarrow\tau\tau)+\mathrm{jets}$ and VV, are also affected by different sources of theoretical modeling uncertainty. The uncertainties related to the choice of QCD renormalization and factorization scales are assessed by varying the corresponding generator parameters up and

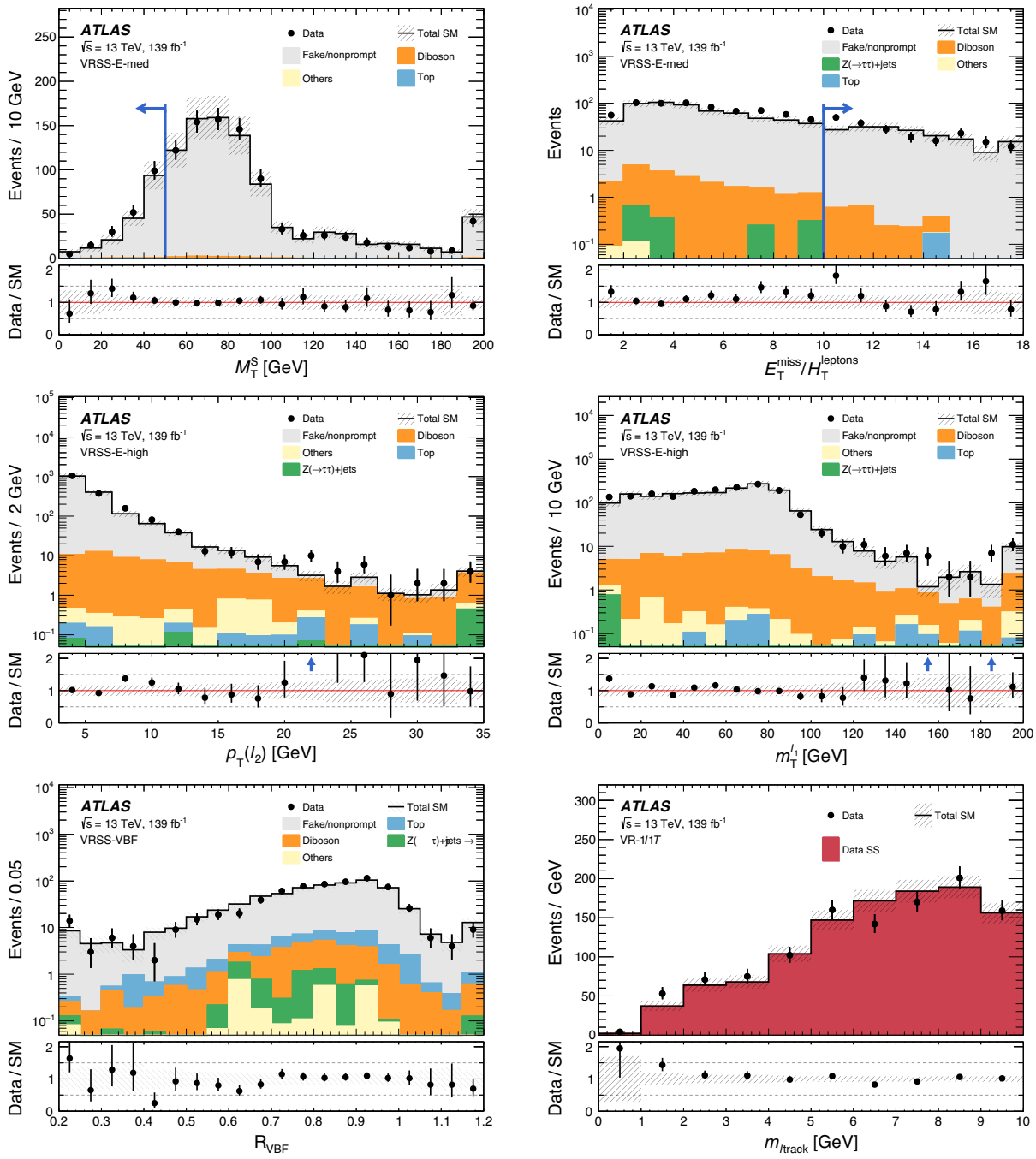

FIG. 9. Examples of kinematic distributions after the background-only fit of the CRs showing the data as well as the expected background in the validation regions VRSS-E-med (top), VRSS-E-high (middle), VRSS-VBF (bottom left), and VR-1ℓ1T (bottom right). The full event selection of the corresponding regions is applied, except for distributions showing blue arrows, where the requirement on the variable being plotted is removed and indicated by the arrows in the distributions instead. The first (last) bin includes underflow (overflow). The uncertainty bands plotted include all statistical and systematic uncertainties.

down by a factor of 2 around their nominal values. Uncertainties in the resummation scale and the matching scale between matrix elements and parton showers for the $Z^{(*)}/\gamma^*(\to \tau\tau) + \text{jets}$ samples are evaluated by varying up and down by a factor of 2 the corresponding parameters in SHERPA. The uncertainties associated with the choice of PDF set, NNPDF [54,84], and uncertainty in the strong coupling constant, α_s, are also considered.

As discussed in Sec. VI, the background predictions in the 1ℓ1T SR, selecting OS lepton–track pairs, are extracted from a SS data control sample. Two different types of

TABLE X. *Left to right:* The first column indicates the inclusive signal region under study, defined as the union of the individual SRs defined in Sec. V and by upper bounds on $m_{\ell\ell}$ or m_{T2}^{100} in GeV. The $m_{\ell\ell}$ regions include events in both the 2ℓ and $1\ell 1T$ channels, while the m_{T2}^{100} regions only include 2ℓ events. The next two columns present observed (N_{obs}) and expected (N_{exp}) event yields in the inclusive signal regions. The latter are obtained by the background-only fit of the CRs, and the errors include both the statistical and systematic uncertainties. The next two columns show the observed 95% C.L. upper limits on the visible cross section ($\langle\epsilon\sigma\rangle_{\mathrm{obs}}^{95}$) and on the number of signal events (S_{obs}^{95}). The next column (S_{exp}^{95}) shows the 95% C.L. upper limit on the number of signal events, given the expected number (and $\pm 1\sigma$ deviations from the expectation) of background events. The last column indicates the discovery p-value [$p(s=0)$].

	Signal region	N_{obs}	N_{exp}	$\langle\epsilon\sigma\rangle_{\mathrm{obs}}^{95}$ [fb]	S_{obs}^{95}	S_{exp}^{95}	$p(s=0)$
SR-E	$m_{\ell\ell} < 1$	0	1.0 ± 1.0	0.022	3.0	$3.0^{+1.3}_{-0.0}$	0.50
	$m_{\ell\ell} < 2$	46	44 ± 6.8	0.15	21	19^{+7}_{-5}	0.38
	$m_{\ell\ell} < 3$	90	77 ± 12	0.29	41	31^{+11}_{-9}	0.18
	$m_{\ell\ell} < 5$	151	138 ± 18	0.38	52	43^{+16}_{-11}	0.24
	$m_{\ell\ell} < 10$	244	200 ± 19	0.62	86	49^{+26}_{-13}	0.034
	$m_{\ell\ell} < 20$	383	301 ± 23	0.95	132	61^{+22}_{-16}	0.0034
	$m_{\ell\ell} < 30$	453	366 ± 27	1.04	144	70^{+26}_{-20}	0.0065
	$m_{\ell\ell} < 40$	492	420 ± 30	0.96	134	74^{+29}_{-20}	0.027
	$m_{\ell\ell} < 60$	583	520 ± 35	0.97	135	84^{+32}_{-23}	0.063
SR-VBF	$m_{\ell\ell} < 2$	0	2.8 ± 1.6	0.022	3.0	$3.9^{+1.6}_{-0.9}$	0.50
	$m_{\ell\ell} < 3$	1	3.1 ± 1.7	0.030	3.6	$4.4^{+2.0}_{-1.0}$	0.50
	$m_{\ell\ell} < 5$	2	3.3 ± 1.7	0.035	4.8	$5.2^{+2.1}_{-1.1}$	0.50
	$m_{\ell\ell} < 10$	9	8.4 ± 2.7	0.068	9.5	$8.8^{+3.2}_{-2.2}$	0.43
	$m_{\ell\ell} < 20$	36	32 ± 5	0.14	20	16^{+6}_{-4}	0.27
	$m_{\ell\ell} < 30$	58	52 ± 7	0.19	26	21^{+8}_{-6}	0.28
	$m_{\ell\ell} < 40$	82	74 ± 10	0.24	33	27^{+10}_{-7}	0.27
SR-VBF-high	$m_{\ell\ell} < 2$	0	2.4 ± 1.1	0.022	3.0	$4.0^{+1.6}_{-0.9}$	0.50
	$m_{\ell\ell} < 3$	1	3.0 ± 1.4	0.025	3.5	$4.6^{+1.8}_{-1.2}$	0.50
	$m_{\ell\ell} < 5$	2	3.0 ± 1.4	0.034	4.7	$5.1^{+2.0}_{-1.3}$	0.50
	$m_{\ell\ell} < 10$	3	3.8 ± 1.7	0.041	5.6	$5.8^{+2.1}_{-1.3}$	0.50
	$m_{\ell\ell} < 20$	9	11.7 ± 2.8	0.055	8	$9^{+4}_{-2.3}$	0.50
	$m_{\ell\ell} < 30$	17	20 ± 5	0.079	11	$13^{+5}_{-3.2}$	0.50
	$m_{\ell\ell} < 40$	26	28 ± 6	0.10	14	15^{+6}_{-4}	0.50
SR-S	$m_{\mathrm{T2}}^{100} < 100.5$	24	27 ± 4.8	0.09	13	14^{+5}_{-4}	0.50
	$m_{\mathrm{T2}}^{100} < 101$	41	46 ± 6.5	0.11	16	18^{+7}_{-5}	0.50
	$m_{\mathrm{T2}}^{100} < 102$	91	82 ± 10	0.25	35	28^{+10}_{-8}	0.25
	$m_{\mathrm{T2}}^{100} < 105$	158	158 ± 17	0.30	41	41^{+16}_{-11}	0.50
	$m_{\mathrm{T2}}^{100} < 110$	243	242 ± 21	0.38	52	52^{+19}_{-14}	0.36
	$m_{\mathrm{T2}}^{100} < 120$	328	312 ± 24	0.51	71	60^{+22}_{-17}	0.26
	$m_{\mathrm{T2}}^{100} < 130$	419	388 ± 28	0.66	92	68^{+27}_{-18}	0.17
	$m_{\mathrm{T2}}^{100} < 140$	472	443 ± 31	0.69	95	74^{+28}_{-21}	0.19

systematic uncertainty are associated with the OS–SS extrapolation. For $m_{\ell\mathrm{track}} < 2$ GeV, low-mass resonances can cause higher production rates for OS events than for SS events. A 30% uncertainty is assigned, based on an exponential fit to the OS/SS ratio as a function of $E_{\mathrm{T}}^{\mathrm{miss}}$ in the $\Delta\phi(\mathrm{lep}, \mathbf{p}_{\mathrm{T}}^{\mathrm{miss}}) > 1.5$ region. This OS/SS ratio was found to be constant and equal to 1 for $E_{\mathrm{T}}^{\mathrm{miss}} > 200$ GeV, indicating that low-mass resonances do not contribute significantly to the OS sample in the SR-E-$1\ell 1T$ region. The uncertainty is computed as the value of the fitting function at $E_{\mathrm{T}}^{\mathrm{miss}} = 200$ GeV, where the deviation from unity is largest, summed linearly with the corresponding fit uncertainty. The $m_{\ell\mathrm{track}} > 2$ GeV region is instead mainly populated by $W+$jets events, in which the correlation between the lepton and the track charge may introduce differences between the SS and OS expectations. A 12% uncertainty, extracted from $W+$jets simulated events, is assigned.

The $m_{\ell\mathrm{track}} > 2$ GeV region is instead mainly populated by $W+$jets events, in which the correlation between the

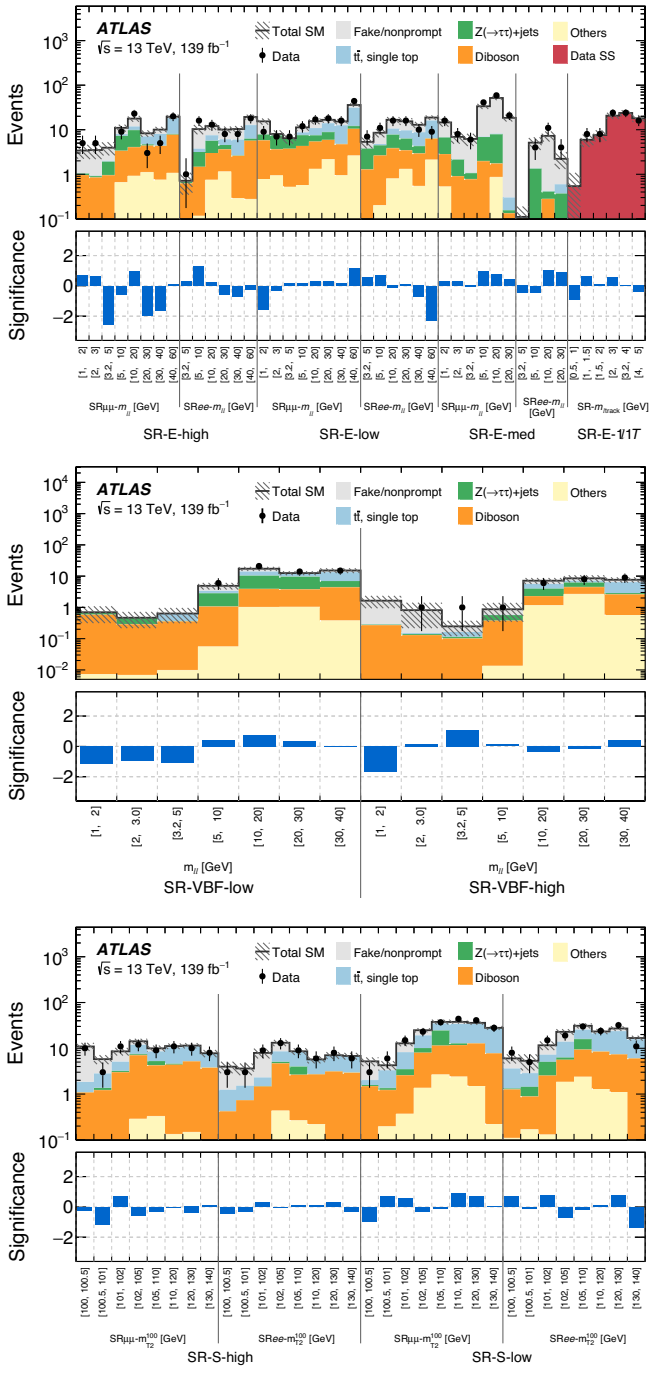

FIG. 10. Comparison of observed and expected event yields in the SRs after the CR + SR background-only fits. The SRs used in searches for electroweakinos recoiling against ISR are shown at the top, and the SRs used for the VBF electroweakino search are shown in the middle, all binned in $m_{\ell\ell}$. The SRs used in searches for sleptons recoiling against ISR are shown at the bottom, binned in m_{T2}^{100}. Uncertainties in the background estimates include both the statistical and systematic uncertainties. The bottom panel in all three plots shows the significance of the difference between the expected and observed yields, computed following the profile likelihood method of Ref. [118] in the case where the observed yield exceeds the prediction, and using the same expression with an overall minus sign if the yield is below the prediction.

lepton and the track charge may introduce differences between the SS and OS expectations. A 12% uncertainty, extracted from W + jets simulated events, is assigned.

Uncertainties in the expected yields for non-VBF SUSY samples arising from generator modeling are determined *in situ* by comparing the yields from $Z \to \mu\mu$ events in data with those from $Z(\to \mu\mu)$ + jets events generated using the same MG5_aMC@NLO configuration as the signal samples. The muon four-momenta are added to the $E_{\mathrm{T}}^{\mathrm{miss}}$ to emulate the p_{T} of the SUSY system in signal events, and uncertainties are derived from observed differences in $E_{\mathrm{T}}^{\mathrm{miss}}$ between data and simulation. The largest modeling uncertainties are approximately 20% for samples with the most compressed mass spectrum and in high-$E_{\mathrm{T}}^{\mathrm{miss}}$ channels, while low-$E_{\mathrm{T}}^{\mathrm{miss}}$ channels and noncompressed signal points have uncertainties ranging from 1% to 10%. Uncertainties in the signal acceptance due to PDF uncertainties are evaluated following the PDF4LHC15 recommendations [121] and amount to at most 15% for large $\tilde{\chi}_2^0$ or $\tilde{\ell}$ masses. Uncertainties in the shape of the $m_{\ell\ell}$ or m_{T2}^{100} signal distributions due to the sources above are found to be small, and are neglected.

Uncertainties due to generator modeling in the acceptance of the VBF signal samples are evaluated by varying by a factor of 2 the MG5_aMC@NLO parameters corresponding to the renormalization, factorization and CKKW-L matching scales, as well as the PYTHIA8 shower tune parameters and α_{s}. The largest uncertainties arise from renormalization and factorization scale variations (13%–22%), with smaller contributions from matching and α_{s} variations (0.5%–5%).

Additional uncertainties are assigned to the predictions from signal simulation in the $1\ell 1T$ SR. An uncertainty in the modeling of the rate for reconstructed tracks that do not match a generated charged particle is accounted for. It is estimated by comparing the nonlinear component of the per-event track multiplicity as a function of pileup, in data and simulation. Furthermore, the calibration procedure applied to MC events to match the track impact parameter resolution in different data-taking periods is also a source of systematic uncertainty. Finally, uncertainties are assigned to the track–lepton matching efficiency and the track-isolation efficiency, as derived from the studies of events with a J/ψ meson or Z boson decaying into a lepton and a track, described in Sec. IV.

VIII. RESULTS

Data in the control regions, validation regions, and signal regions are compared with SM predictions using a profile likelihood method [122] implemented in the HISTFITTER package [123]. Most systematic uncertainties are treated as nuisance parameters with Gaussian constraints in the likelihood, apart from those of a statistical nature, for which Poisson constraints are used. Experimental systematic

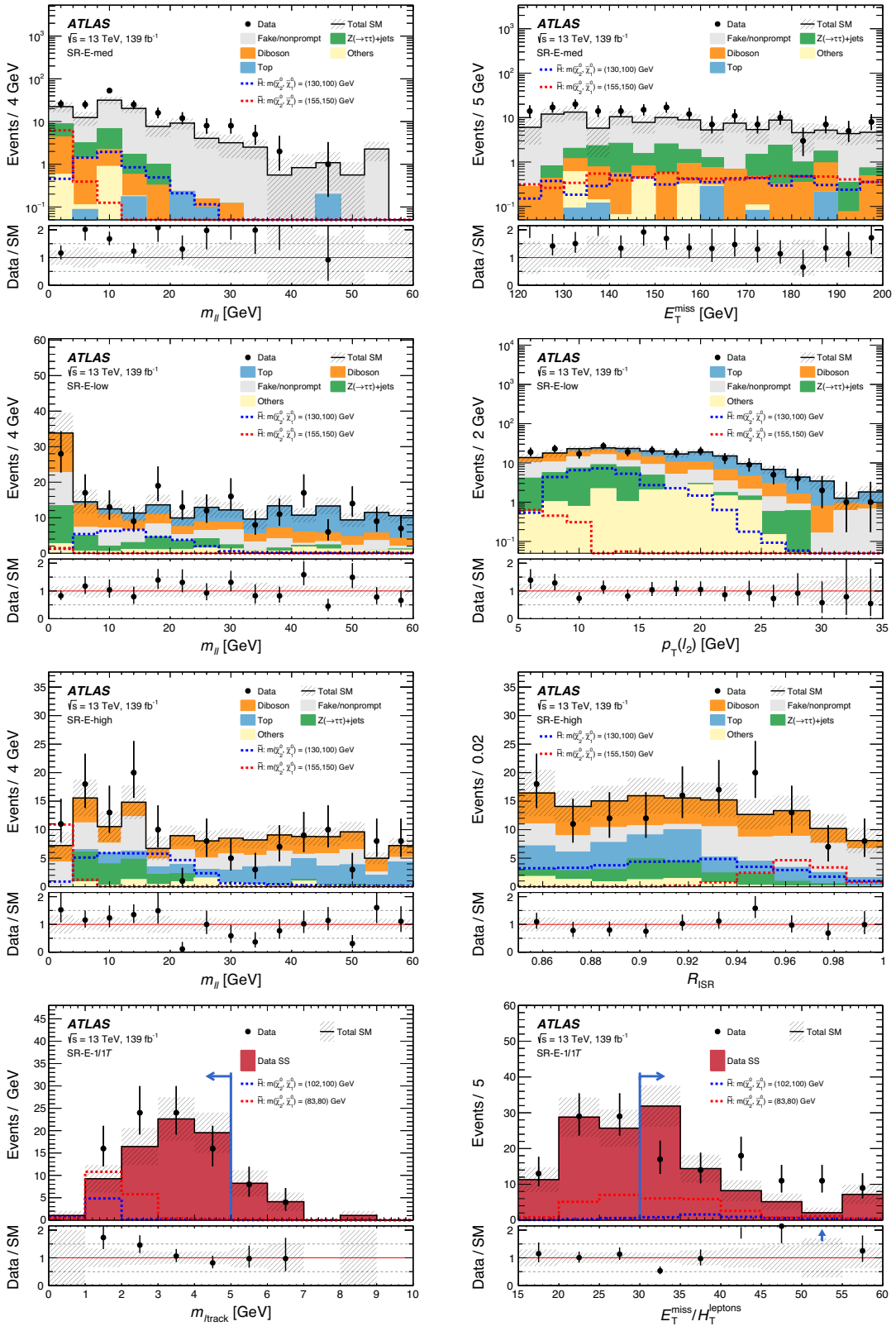

FIG. 11. Examples of kinematic distributions after the background-only fit of the CRs showing the data as well as the expected background in the signal regions sensitive to electroweakinos. The full event selection of the corresponding regions is applied, except for distributions showing blue arrows, where the requirement on the variable being plotted is removed and indicated by the arrows in the distributions instead. The first (last) bin includes underflow (overflow). The uncertainty bands plotted include all statistical and systematic uncertainties.

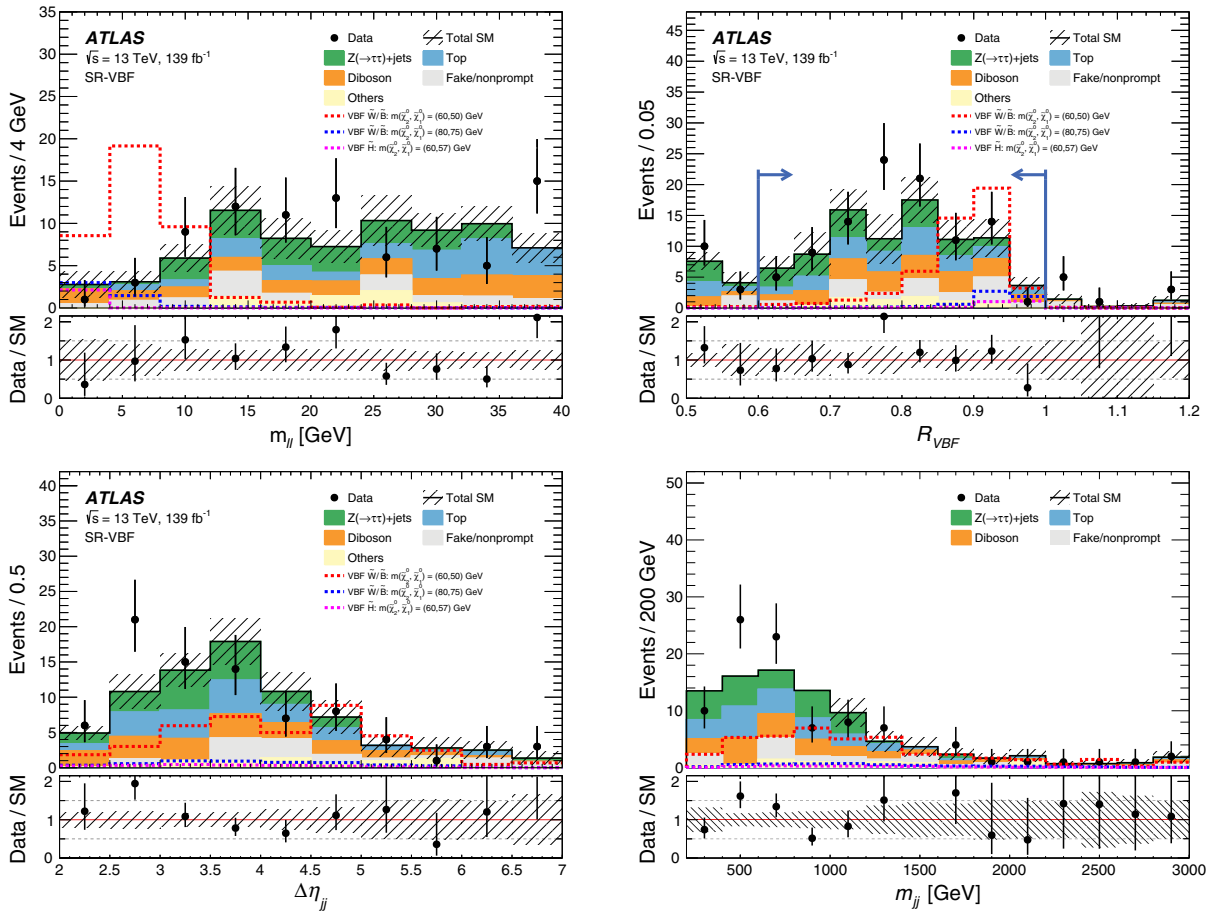

FIG. 12. Examples of kinematic distributions after the background-only fit of the CRs showing the data as well as the expected background in the signal regions sensitive to electroweakinos produced through VBF. The full event selection of the corresponding regions is applied, except for distributions showing blue arrows, where the requirement on the variable being plotted is removed and indicated by the arrows instead in the distributions. The first (last) bin includes underflow (overflow). The uncertainty bands plotted include all statistical and systematic uncertainties.

uncertainties are correlated between signal and backgrounds for all regions.

A. Control and validation regions

A background-only fit of the CRs is constructed using only the control regions to constrain the fit parameters. The data in the control regions CRtop, CRtau, and CRVV are fit simultaneously in each search to constrain overall normalization factors for the $t\bar{t}/Wt$, $Z^{(*)}/\gamma^{*}(\rightarrow \tau\tau)+\text{jets}$, and VV background predictions. The resulting normalization parameters are presented in Table IX.

The background prediction as obtained from the background-only fit of the CRs is then compared with data in the validation regions to verify the accuracy of the background modeling. Figure 6 shows a comparison of the data yields with background predictions in the VRDF regions, binned in $m_{\ell\ell}$ and m_{T2}^{100} using the same intervals as defined for the corresponding SRs. Good agreement is observed in all event selection categories, with deviations below 2σ. Examples of kinematic distributions in control and validation regions are presented in Figs. 7, 8, and 9, where good agreement between data and MC simulation is seen in both the shape and normalization of the discriminating variables.

B. Inclusive signal regions

The inclusive signal regions defined in Sec. V are used to test for excesses of events above the SM predictions. Each fit only considers one single-bin inclusive signal region, and includes a signal model with an unconstrained normalization parameter to estimate the contributions of any phenomena beyond those predicted by the Standard Model. The signal region is fit simultaneously with the control regions, which are assumed to contain no signal, resulting in background estimates constrained by the background-only fit of the CRs.

To quantify the probability under the background-only hypothesis to produce event yields greater than or

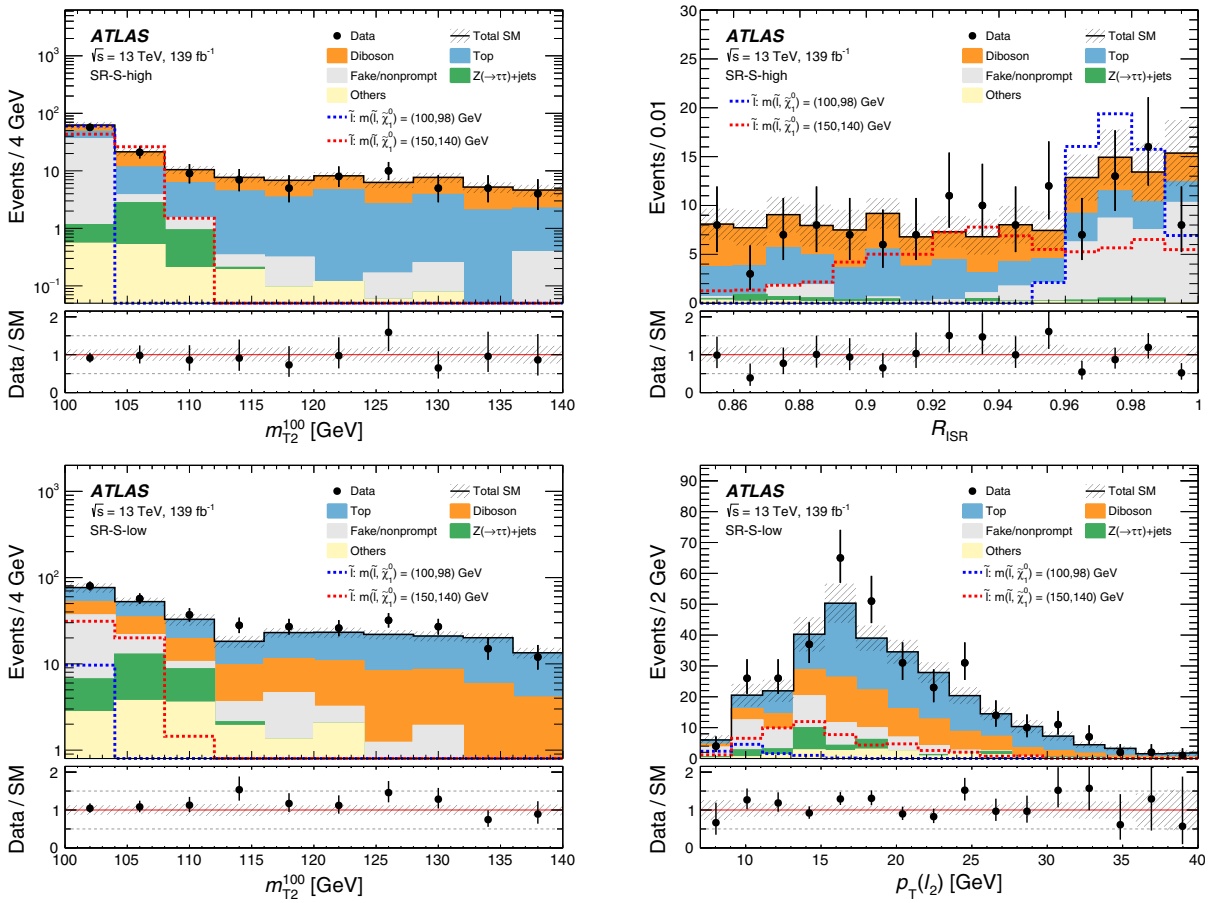

FIG. 13. Examples of kinematic distributions after the background-only fit of the CRs showing the data as well as the expected background in the signal regions sensitive to sleptons. The full event selection of the corresponding regions is applied, except for distributions showing blue arrows, where the requirement on the variable being plotted is removed and indicated by the arrows instead in the distributions. The first (last) bin includes underflow (overflow). The uncertainty bands plotted include all statistical and systematic uncertainties.

equal to the observed data, the discovery p-values are calculated for each inclusive signal region. The results for the electroweakino, VBF, and slepton regions are shown in Table X. Several electroweakino regions have low p-values, with the lowest observed in the $m_{\ell\ell} < 20$ GeV bin corresponding to a local significance of 2.7σ. The CL_s prescription [124] is used to perform a hypothesis test that sets upper limits at the 95% confidence level (C.L.) on the observed (expected) number of signal events $S^{95}_{\mathrm{obs(exp)}}$ in each inclusive signal region. Dividing S^{95}_{obs} by the integrated luminosity defines the upper limits on the visible cross sections $\langle \epsilon\sigma \rangle^{95}_{\mathrm{obs}}$.

C. Exclusive signal regions and model-dependent interpretations

The exclusive signal regions are used to constrain specific SUSY models. An exclusion fit extends a background-only fit of the CRs to include signal regions relevant for the model under study. All regions are fit simultaneously with a parameter of interest corresponding to the signal strength, a factor that coherently scales the signal yield across all regions. In order to assess the stability of the exclusion fit, a "CR + SR background-only fit" of the CRs and the exclusive signal regions is performed in which the signal strength is fixed to zero. Comparisons of the data yields with the background prediction in the $m_{\ell\ell}$ and m_{T2}^{100} bins of the SRs, after the CR + SR background-only fit, are shown in Tables XI–XIV and Fig. 10, with all deviations less than 2σ. Examples of kinematic distributions in the SRs after a background-only fit of the CRs are presented in Figs. 11, 12, and 13, where good agreement between data and the background predictions is seen in both the shape and the normalization of the discriminating variables.

The CL_s prescription is used to perform hypothesis tests of specific SUSY models. The SRs defined using $m_{\ell\ell}$ are used for electroweakino models, while regions defined using m_{T2}^{100} are used for slepton models. Exclusions at

TABLE XI. Observed event yields and fit results using a CR + SR background-only fit for the exclusive electroweakino signal regions. Background processes containing fewer than two prompt leptons are categorized as "Fake/nonprompt." The category "Others" contains rare backgrounds from triboson, Higgs-boson, and the remaining top-quark production processes listed in Table I. Uncertainties in the fitted background estimates combine statistical and systematic uncertainties.

	SR bin [GeV]	[1, 2]	[2, 3]	[3.2, 5]	[5, 10]	[10, 20]	[20, 30]	[30, 40]	[40, 60]
SR-E-high ee	Observed			1	16	13	8	8	18
	Fitted SM events			0.7 ± 0.4	10.3 ± 2.5	12.1 ± 2.2	10.1 ± 1.7	10.4 ± 1.7	19.3 ± 2.5
	Fake/nonprompt			$0.03^{+0.19}_{-0.03}$	6.6 ± 2.7	4.6 ± 2.0	4.0 ± 1.5	4.4 ± 1.6	6.7 ± 2.3
	$t\bar{t}$, single top			$0.01^{+0.06}_{-0.01}$	0.59 ± 0.27	1.9 ± 0.5	1.6 ± 0.4	3.3 ± 0.6	6.4 ± 0.9
	Diboson			0.62 ± 0.23	1.4 ± 0.5	2.3 ± 0.7	2.5 ± 0.7	2.3 ± 0.6	5.4 ± 1.3
	$Z(\rightarrow \tau\tau) + \text{jets}$			$0.06^{+0.29}_{-0.06}$	1.7 ± 0.7	2.6 ± 1.2	0.93 ± 0.24	0.04 ± 0.04	0.62 ± 0.23
	Others			$0.000^{+0.004}_{-0.000}$	0.12 ± 0.05	0.74 ± 0.18	1.14 ± 0.19	0.29 ± 0.07	0.27 ± 0.14
SR-E-high $\mu\mu$	Observed	5	5	0	9	23	3	5	20
	Fitted SM events	3.4 ± 1.2	3.5 ± 1.3	3.9 ± 1.3	11.0 ± 2.0	17.8 ± 2.7	8.3 ± 1.4	10.1 ± 1.5	19.6 ± 2.3
	Fake/nonprompt	2.4 ± 1.2	2.6 ± 1.4	1.9 ± 1.0	3.1 ± 1.7	6.0 ± 2.8	1.3 ± 0.8	2.0 ± 0.9	1.4 ± 1.3
	$t\bar{t}$, single top	$0.01^{+0.06}_{-0.01}$	$0.01^{+0.06}_{-0.01}$	0.09 ± 0.07	0.67 ± 0.25	2.0 ± 0.5	2.4 ± 0.5	3.7 ± 0.9	10.2 ± 1.7
	Diboson	0.92 ± 0.32	0.84 ± 0.32	0.9 ± 0.4	2.7 ± 0.7	3.1 ± 0.8	3.3 ± 0.8	3.6 ± 0.8	6.6 ± 1.5
	$Z(\rightarrow \tau\tau) + \text{jets}$	$0.07^{+0.34}_{-0.07}$	$0.06^{+0.34}_{-0.06}$	1.0 ± 0.4	3.9 ± 0.9	5.7 ± 1.6	0.31 ± 0.25	$0.00^{+0.04}_{-0.00}$	0.31 ± 0.16
	Others	$0.032^{+0.035}_{-0.032}$	...	0.025 ± 0.018	0.66 ± 0.33	0.91 ± 0.14	1.10 ± 0.18	0.75 ± 0.16	1.06 ± 0.09
SR-E-med ee	Observed			0	4	11	4		
	Fitted SM events			0.11 ± 0.08	5.1 ± 1.6	7.3 ± 1.9	2.2 ± 0.9		
	Fake/nonprompt			$0.000^{+0.016}_{-0.000}$	3.8 ± 1.3	6.9 ± 2.0	1.6 ± 1.1		
	$t\bar{t}$, single top			$0.00^{+0.05}_{-0.00}$	$0.00^{+0.04}_{-0.00}$	$0.01^{+0.06}_{-0.01}$	$0.23^{+0.25}_{-0.23}$		
	Diboson			0.10 ± 0.05	0.10 ± 0.09	0.28 ± 0.26	$0.02^{+0.13}_{-0.02}$		
	$Z(\rightarrow \tau\tau) + \text{jets}$			$0.000^{+0.028}_{-0.000}$	1.2 ± 1.2	$0.1^{+0.5}_{-0.1}$	$0.3^{+0.6}_{-0.3}$		
	Others			$0.000^{+0.012}_{-0.000}$	...	...	...		
SR-E-med $\mu\mu$	Observed	16	8	6	41	59	21		
	Fitted SM events	14.6 ± 2.9	6.9 ± 2.1	6.2 ± 1.9	34 ± 4	52 ± 6	18.5 ± 3.2		
	Fake/nonprompt	7.9 ± 3.2	4.8 ± 2.1	5.1 ± 2.0	27 ± 5	44 ± 6	18.2 ± 3.2		
	$t\bar{t}$, single top	$0.01^{+0.06}_{-0.01}$	$0.01^{+0.06}_{-0.01}$	$0.00^{+0.05}_{-0.00}$	$0.12^{+0.13}_{-0.12}$	0.24 ± 0.08	$0.14^{+0.19}_{-0.14}$		
	Diboson	2.3 ± 0.8	0.9 ± 0.4	0.73 ± 0.24	1.9 ± 0.7	0.87 ± 0.26	0.13 ± 0.07		
	$Z(\rightarrow \tau\tau) + \text{jets}$	3.8 ± 1.8	1.2 ± 0.5	$0.3^{+0.6}_{-0.3}$	4.9 ± 1.6	6.1 ± 2.1	$0.02^{+0.29}_{-0.02}$		
	Others	0.5 ± 0.4	$0.000^{+0.026}_{-0.000}$	0.036 ± 0.015	0.019 ± 0.017	0.9 ± 0.6	...		
SR-E-low ee	Observed			7	11	16	16	10	9
	Fitted SM events			5.3 ± 1.5	8.6 ± 1.8	16.7 ± 2.5	15.5 ± 2.6	12.9 ± 2.1	18.8 ± 2.2
	Fake/nonprompt			1.6 ± 1.1	3.8 ± 1.8	6.2 ± 2.2	5.8 ± 2.3	4.2 ± 1.8	2.8 ± 1.4
	$t\bar{t}$, single top			0.015 ± 0.006	0.32 ± 0.30	2.8 ± 0.6	3.4 ± 1.1	4.5 ± 0.9	9.7 ± 1.5
	Diboson			1.3 ± 0.6	2.4 ± 0.8	3.0 ± 0.7	2.1 ± 0.7	2.4 ± 0.7	4.2 ± 1.0
	$Z(\rightarrow \tau\tau) + \text{jets}$			2.5 ± 1.1	1.8 ± 0.7	3.9 ± 1.3	2.8 ± 1.0	1.4 ± 0.7	$0.07^{+0.20}_{-0.07}$
	Others			$0.01^{+0.05}_{-0.01}$	0.20 ± 0.05	0.79 ± 0.23	1.3 ± 0.8	0.54 ± 0.09	2.10 ± 0.34
SR-E-low $\mu\mu$	Observed	9	7	7	12	17	18	16	44
	Fitted SM events	15.4 ± 2.4	8.0 ± 1.7	6.5 ± 1.6	11.3 ± 1.9	15.6 ± 2.3	16.7 ± 2.3	15.3 ± 2.0	35.9 ± 3.3
	Fake/nonprompt	7.7 ± 1.9	$0.3^{+0.6}_{-0.3}$	$0.01^{+0.22}_{-0.01}$	2.6 ± 1.3	4.7 ± 1.9	2.8 ± 1.6	2.8 ± 1.6	4.9 ± 2.3
	$t\bar{t}$, single top	$0.00^{+0.04}_{-0.00}$	0.26 ± 0.07	$0.01^{+0.06}_{-0.01}$	1.2 ± 0.5	3.4 ± 0.7	5.1 ± 1.5	7.8 ± 1.3	18.9 ± 2.7
	Diboson	4.9 ± 1.3	2.7 ± 0.7	3.2 ± 0.9	3.8 ± 0.9	4.1 ± 1.0	3.7 ± 0.9	3.8 ± 0.8	7.8 ± 1.6
	$Z(\rightarrow \tau\tau) + \text{jets}$	2.0 ± 0.7	3.8 ± 1.1	2.7 ± 1.2	3.2 ± 1.1	2.0 ± 1.2	2.9 ± 0.8	$0.01^{+0.27}_{-0.01}$	1.6 ± 0.6
	Others	0.8 ± 0.5	0.9 ± 0.8	0.52 ± 0.24	0.57 ± 0.16	1.32 ± 0.18	2.1 ± 0.4	0.94 ± 0.11	2.60 ± 0.20

TABLE XII. Observed event yields and fit results using a CR + SR background-only fit for the exclusive electroweakino $1\ell 1T$ regions. All backgrounds are determined from the same-sign method. Uncertainties in the fitted background estimates combine statistical and systematic uncertainties.

SR bin [GeV]	[0.5, 1.0]	[1.0, 1.5]	[1.5, 2.0]	[2.0, 3.0]	[3.2, 4.0]	[4.0, 5.0]
Observed	0	8	8	24	24	16
Fitted SM events	0.5 ± 0.5	6.0 ± 1.9	7.6 ± 2.1	20.7 ± 3.4	24 ± 4	18.1 ± 3.1

TABLE XIII. Observed event yields and fit results using a CR + SR background-only fit for the exclusive VBF signal regions. Background processes containing fewer than two prompt leptons are categorized as "Fake/nonprompt." The category "Others" contains rare backgrounds from triboson, Higgs-boson, and the remaining top-quark production processes listed in Table I. Uncertainties in the fitted background estimates combine statistical and systematic uncertainties.

	SR bin [GeV]	[1, 2]	[2, 3]	[3.2, 5]	[5, 10]	[10, 20]	[20, 30]	[30, 40]
SR-VBF-low	Observed	0	0	0	6	21	14	15
	Fitted SM events	0.7 ± 0.4	0.47 ± 0.25	0.64 ± 0.32	4.9 ± 1.2	17.3 ± 2.6	12.5 ± 1.8	15.2 ± 2.7
	$Z(\to \tau\tau) + \text{jets}$	$0.11^{+0.22}_{-0.11}$	0.17 ± 0.12	$0.009^{+0.018}_{-0.009}$	1.8 ± 0.7	6.4 ± 1.4	5.7 ± 1.3	2.6 ± 1.0
	Fake/nonprompt	$0.01^{+0.05}_{-0.01}$	$0.01^{+0.05}_{-0.01}$	$0.01^{+0.05}_{-0.01}$	1.5 ± 1.0	3.4 ± 2.0	$0.01^{+0.06}_{-0.01}$	$1.8^{+2.5}_{-1.8}$
	Diboson	0.57 ± 0.29	0.28 ± 0.17	0.35 ± 0.20	1.0 ± 0.4	2.8 ± 1.1	2.7 ± 1.004	4.0 ± 1.4
	$t\bar{t}$, single top	$0.01^{+0.04}_{-0.01}$	$0.01^{+0.05}_{-0.01}$	0.26 ± 0.18	0.55 ± 0.27	3.6 ± 1.3	3.1 ± 0.7	6.4 ± 1.1
	Others	0.007 ± 0.007	0.007 ± 0.004	$0.01^{+0.05}_{-0.01}$	0.056 ± 0.026	1.0 ± 0.4	1.03 ± 0.32	0.37 ± 0.13
SR-VBF-high	Observed	0	1	1	1	6	8	9
	Fitted SM events	1.6 ± 0.7	0.8 ± 0.6	0.25 ± 0.13	0.9 ± 0.5	7.1 ± 1.5	8.5 ± 2.2	7.7 ± 1.5
	$Z(\to \tau\tau) + \text{jets}$	$0.009^{+0.018}_{-0.009}$	$0.010^{+0.021}_{-0.010}$	$0.012^{+0.026}_{-0.012}$	$0.19^{+0.29}_{-0.19}$	1.7 ± 0.8	1.8 ± 1.3	0.27 ± 0.09
	Fake/nonprompt	1.4 ± 0.7	0.7 ± 0.6	$0.08^{+0.11}_{-0.08}$	$0.3^{+0.5}_{-0.3}$	1.5 ± 1.0	$1.4^{+1.5}_{-1.4}$	1.2 ± 1.2
	Diboson	0.27 ± 0.17	0.13 ± 0.11	0.10 ± 0.05	0.37 ± 0.19	1.1 ± 0.5	1.8 ± 0.7	2.0 ± 0.8
	$t\bar{t}$, single top	$0.01^{+0.05}_{-0.01}$	$0.01^{+0.06}_{-0.01}$	$0.05^{+0.09}_{-0.05}$	$0.01^{+0.06}_{-0.01}$	1.7 ± 0.6	0.9 ± 0.6	3.5 ± 0.8
	Others	⋯	⋯	⋯	$0.01^{+0.02}_{-0.01}$	1.2 ± 0.4	2.6 ± 1.5	0.57 ± 0.21

TABLE XIV. Observed event yields and fit results using a CR + SR background-only fit for the exclusive slepton signal regions. Background processes containing fewer than two prompt leptons are categorized as "Fake/nonprompt." The category "Others" contains rare backgrounds from triboson, Higgs-boson, and the remaining top-quark production processes listed in Table I. Uncertainties in the fitted background estimates combine statistical and systematic uncertainties.

	SR bin [GeV]	[100, 100.5]	[100.5, 101]	[101, 102]	[102, 105]	[105, 110]	[110, 120]	[120, 130]	[130, 140]
SR-S-high ee	Observed	3	3	9	13	9	6	8	6
	Fitted SM events	4.0 ± 1.1	3.6 ± 1.0	7.9 ± 1.9	13.2 ± 2.1	8.6 ± 1.4	5.7 ± 1.0	7.0 ± 1.2	6.8 ± 1.1
	Fake/nonprompt	2.7 ± 1.1	2.1 ± 1.0	5.6 ± 1.9	4.7 ± 1.9	$0.2^{+0.5}_{-0.2}$	$0.01^{+0.17}_{-0.01}$	$0.01^{+0.17}_{-0.01}$	$0.00^{+0.15}_{-0.00}$
	$t\bar{t}$, single top	0.8 ± 0.4	0.8 ± 0.5	0.8 ± 0.4	3.5 ± 0.7	4.5 ± 1.2	3.0 ± 0.7	3.9 ± 0.9	3.9 ± 0.9
	Diboson	0.42 ± 0.16	0.68 ± 0.23	1.4 ± 0.4	4.2 ± 1.1	2.4 ± 0.7	2.5 ± 0.7	3.0 ± 0.8	2.8 ± 0.7
	$Z(\to \tau\tau) + \text{jets}$	$0.00^{+0.08}_{-0.00}$	$0.00^{+0.18}_{-0.00}$	0.027 ± 0.012	0.38 ± 0.16	1.32 ± 0.31	$0.00^{+0.12}_{-0.00}$	$0.02^{+0.22}_{-0.02}$	$0.00^{+0.19}_{-0.00}$
	Others	0.0 ± 0.0	$0.06^{+0.11}_{-0.06}$	0.09 ± 0.05	0.43 ± 0.32	0.26 ± 0.14	$0.2^{+0.5}_{-0.2}$	$0.06^{+0.08}_{-0.06}$	0.05 ± 0.05
SR-S-high $\mu\mu$	Observed	10	3	11	12	9	11	10	8
	Fitted SM events	11.0 ± 2.2	5.8 ± 1.3	8.6 ± 1.6	14.2 ± 1.9	10.0 ± 1.5	11.2 ± 1.6	11.5 ± 1.5	7.8 ± 1.4
	Fake/nonprompt	9.1 ± 2.2	3.0 ± 1.1	3.5 ± 1.4	2.4 ± 1.2	1.5 ± 1.0	$0.7^{+0.8}_{-0.7}$	$0.4^{+0.5}_{-0.4}$	$0.19^{+0.33}_{-0.19}$
	$t\bar{t}$, single top	0.8 ± 0.5	1.5 ± 0.5	1.9 ± 0.5	4.4 ± 0.8	3.3 ± 0.7	5.9 ± 1.1	5.9 ± 0.9	3.9 ± 1.3
	Diboson	1.1 ± 0.4	1.2 ± 0.4	2.9 ± 1.3	6.7 ± 1.7	3.9 ± 1.1	4.2 ± 1.0	5.0 ± 1.3	3.7 ± 0.9
	$Z(\to \tau\tau) + \text{jets}$	$0.00^{+0.19}_{-0.00}$	0.15 ± 0.04	0.22 ± 0.19	0.40 ± 0.34	1.03 ± 0.34	0.19 ± 0.12	$0.00^{+0.19}_{-0.00}$	$0.00^{+0.21}_{-0.00}$
	Others	$0.000^{+0.019}_{-0.000}$	0.029 ± 0.017	0.09 ± 0.05	0.29 ± 0.14	0.32 ± 0.22	0.13 ± 0.11	0.15 ± 0.12	0.06 ± 0.05

(Table continued)

TABLE XIV. *(Continued)*

	SR bin [GeV]	[100, 100.5]	[100.5, 101]	[101, 102]	[102, 105]	[105, 110]	[110, 120]	[120, 130]	[130, 140]
SR-S-low ee	Observed	8	5	15	19	30	24	32	11
	Fitted SM events	6.0 ± 1.4	5.3 ± 2.1	11.6 ± 2.5	22.9 ± 3.3	31 ± 4	23.3 ± 3.0	27.1 ± 3.1	16.8 ± 2.1
	Fake/nonprompt	2.4 ± 1.2	2.5 ± 1.2	4.4 ± 2.0	9.0 ± 2.8	5.7 ± 2.7	$1.6^{+1.7}_{-1.6}$	3.4 ± 2.3	1.0 ± 0.9
	$t\bar{t}$, single top	2.3 ± 0.9	1.4 ± 0.5	2.2 ± 0.7	7.6 ± 1.7	9.6 ± 1.7	13.3 ± 3.3	16.4 ± 3.0	9.8 ± 1.5
	Diboson	1.1 ± 0.6	0.71 ± 0.30	2.4 ± 0.8	3.8 ± 1.3	6.9 ± 2.1	7.1 ± 2.1	6.2 ± 2.0	5.9 ± 1.6
	$Z(\to \tau\tau) + \text{jets}$	$0.1^{+0.4}_{-0.1}$	$0.6^{+2.0}_{-0.6}$	2.5 ± 2.4	$0.7^{+1.5}_{-0.7}$	6.5 ± 2.2	$0.01^{+0.26}_{-0.01}$	$0.03^{+0.30}_{-0.03}$	$0.000^{+0.032}_{-0.000}$
	Others	0.11 ± 0.06	0.17 ± 0.15	0.13 ± 0.09	1.8 ± 0.9	2.4 ± 2.4	1.3 ± 1.2	1.1 ± 1.0	0.042 ± 0.034
SR-S-low $\mu\mu$	Observed	3	6	15	23	37	44	41	28
	Fitted SM events	5.2 ± 1.1	4.3 ± 1.0	12.8 ± 1.8	24.8 ± 2.6	38 ± 5	37.8 ± 3.3	36.0 ± 3.4	28.0 ± 2.7
	Fake/nonprompt	3.2 ± 1.0	0.9 ± 0.7	4.6 ± 1.5	5.6 ± 1.8	2.8 ± 1.7	3.8 ± 2.0	1.5 ± 1.2	$0.00^{+0.10}_{-0.00}$
	$t\bar{t}$, single top	0.45 ± 0.18	2.0 ± 0.5	4.7 ± 1.0	9.1 ± 1.6	10.6 ± 1.9	21.2 ± 2.9	21.8 ± 2.6	20.2 ± 2.7
	Diboson	1.4 ± 0.5	1.02 ± 0.34	2.2 ± 0.8	6.7 ± 1.9	8.8 ± 2.6	9.4 ± 2.6	11.2 ± 3.2	7.5 ± 2.2
	$Z(\to \tau\tau) + \text{jets}$	$0.09^{+0.16}_{-0.09}$	$0.1^{+0.5}_{-0.1}$	0.9 ± 0.4	2.1 ± 1.0	13 ± 5	1.0 ± 0.6	$0.02^{+0.29}_{-0.02}$	$0.00^{+0.26}_{-0.00}$
	Others	0.032 ± 0.026	0.19 ± 0.11	0.37 ± 0.19	1.4 ± 0.8	2.6 ± 1.5	2.4 ± 1.2	1.5 ± 0.8	0.22 ± 0.13

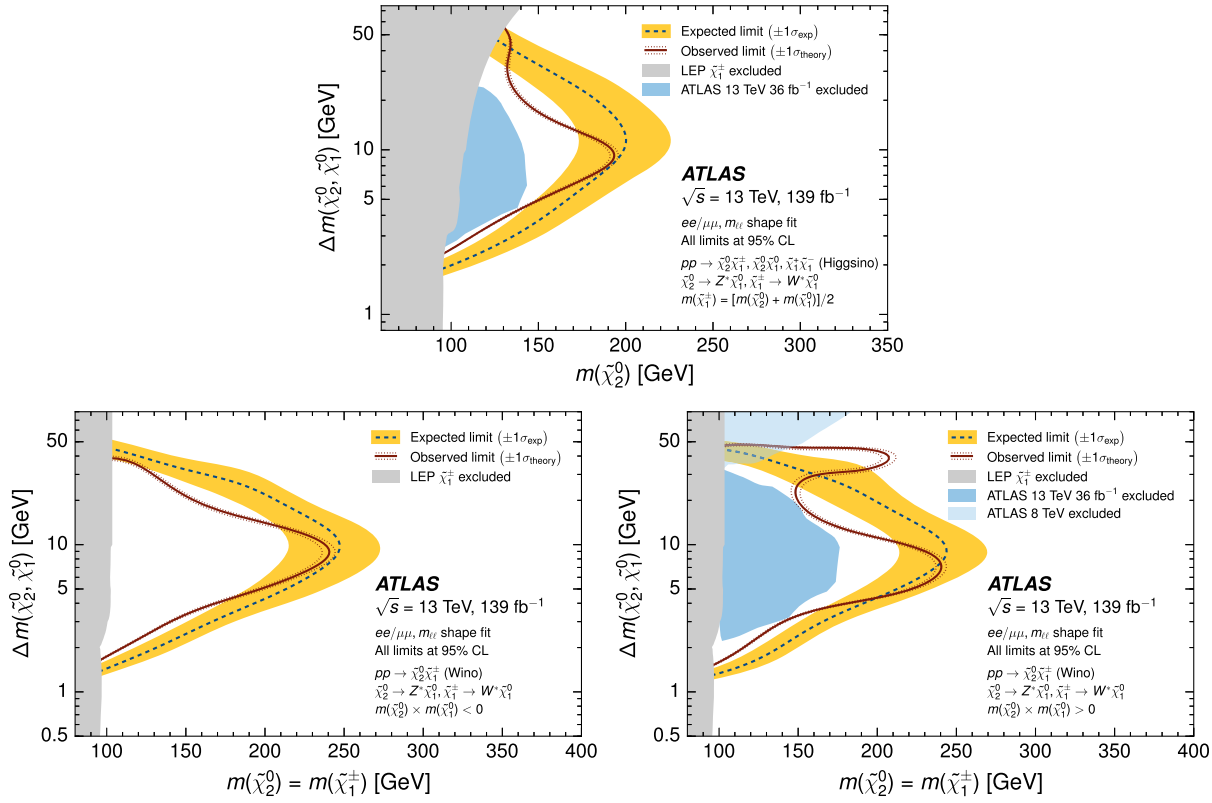

FIG. 14. Expected 95% C.L. exclusion sensitivity (blue dashed line), with $\pm1\sigma_{\text{exp}}$ (yellow band) from experimental systematic uncertainties and statistical uncertainties on the data yields, and observed limits (red solid line) with $\pm1\sigma_{\text{theory}}$ (dotted red line) from signal cross-section uncertainties for simplified models of direct Higgsino (top) and wino (bottom) production. A fit of signals to the $m_{\ell\ell}$ spectrum is used to derive the limit, which is projected into the $\Delta m(\tilde{\chi}_2^0, \tilde{\chi}_1^0)$ vs $m(\tilde{\chi}_2^0)$ plane. For Higgsino production, the chargino $\tilde{\chi}_1^\pm$ mass is assumed to be halfway between the $\tilde{\chi}_2^0$ and $\tilde{\chi}_1^0$ masses, while $m(\tilde{\chi}_2^0) = m(\tilde{\chi}_1^\pm)$ is assumed for the wino/bino model. Following the discussion in Sec. III, the $m_{\ell\ell}$ shape in the wino/bino model depends on the relative sign of the $\tilde{\chi}_1^0$ and $\tilde{\chi}_2^0$ mass parameters. The bottom-left plot assumes $m(\tilde{\chi}_1^0) \times m(\tilde{\chi}_2^0) < 0$, while $m(\tilde{\chi}_1^0) \times m(\tilde{\chi}_2^0) > 0$ is assumed on the bottom right. The gray regions denote the lower chargino mass limit from LEP [30]. The blue regions indicate the limits from ATLAS searches at 8 TeV [125,126] and at 13 TeV with 36 fb^{-1} [45].

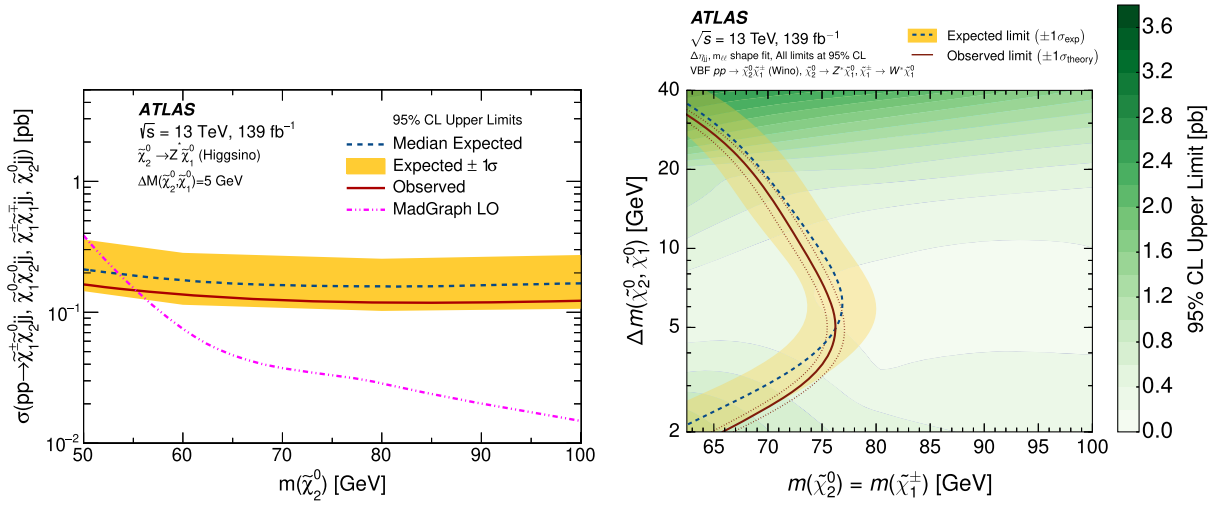

FIG. 15. Expected 95% C.L. exclusion sensitivity (blue dashed line) and observed limits (red solid line) for simplified models of Higgsino (left) and wino (right) production through VBF. A fit of signals to the $m_{\ell\ell}$ spectrum in the VBF signal regions is used to derive the limit. On the left, the limit for Higgsinos is shown as a function of $m(\tilde{\chi}_2^0)$ for a mass splitting of $\Delta m(\tilde{\chi}_2^0, \tilde{\chi}_1^0) = 5$ GeV (the chargino $\tilde{\chi}_1^\pm$ mass is assumed to be halfway between the $\tilde{\chi}_2^0$ and $\tilde{\chi}_1^0$ masses). The yellow band indicates $\pm 1\sigma_{\text{exp}}$ from experimental systematic uncertainties and statistical uncertainties on the data yields. On the right, the limit for winos is projected into the $\Delta m(\tilde{\chi}_2^0, \tilde{\chi}_1^0)$ vs $m(\tilde{\chi}_2^0)$ plane [$m(\tilde{\chi}_2^0) = m(\tilde{\chi}_1^\pm)$ is assumed for the wino/bino model]. The red dotted line indicates the $\pm 1\sigma_{\text{theory}}$ from signal cross-section uncertainties, and the colored map illustrates the 95% C.L. upper limits on the cross section. The cross section corresponds to the leading-order prediction from MG5_aMC@NLO for the process $pp \to \tilde{\chi}_2^0 \tilde{\chi}_1^\pm jj$ including the parton-level requirements described in Sec. III. The contour lines represent steps of 0.2 pb.

95% confidence level are presented in a two-dimensional plane with the horizontal axis given by the mass of the $\tilde{\chi}_2^0$ and the vertical axis defined by the difference in mass between the $\tilde{\chi}_2^0$ or slepton and the $\tilde{\chi}_1^0$.

Exclusion contours for both wino and Higgsino production are shown in Fig. 14. Most of the exclusion power originates from the high-$E_{\text{T}}^{\text{miss}}$ channel, with added sensitivity provided by the $1\ell 1T$ search at small mass splittings and by the low-$E_{\text{T}}^{\text{miss}}$ channels at higher mass splittings. The behavior of the observed exclusion contours at large $\Delta m(\tilde{\chi}_2^0, \tilde{\chi}_1^0)$ is due to the SM background expectation underestimating the data for events

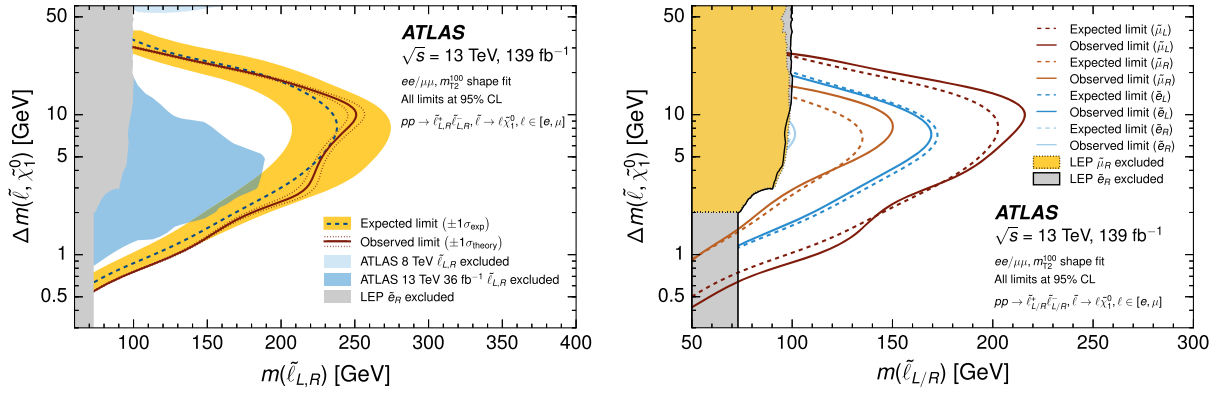

FIG. 16. Expected 95% C.L. sensitivity (dashed lines) and observed limits (solid lines) for simplified models of direct slepton production. A fit of slepton signals to the m_{T2}^{100} spectrum is used to derive the limits, which are projected into the $\Delta m(\tilde{\ell}, \tilde{\chi}_1^0)$ vs $m(\tilde{\ell})$ plane. Slepton $\tilde{\ell}$ refers to the scalar partners of left- and right-handed electrons and muons. The gray region is the $\tilde{e}_R$ limit from LEP [30]. On the left, the sleptons are assumed to be fourfold mass degenerate with $m(\tilde{e}_L) = m(\tilde{e}_R) = m(\tilde{\mu}_L) = m(\tilde{\mu}_R)$; the expected sensitivity (blue dashed line) is shown with $\pm 1\sigma_{\text{exp}}$ (yellow band) from experimental systematic uncertainties and statistical uncertainties on the data yields; the observed limit (red solid line) is shown with $\pm 1\sigma_{\text{theory}}$ (dotted red line) from signal cross-section uncertainties, and the blue regions are the fourfold mass-degenerate slepton limits from ATLAS Run 1 [125] and Run 2 [45]. On the right, no degeneracy is assumed for the masses of the sleptons, and the limits are presented separately for $\tilde{e}_L$, $\tilde{e}_R$, $\tilde{\mu}_L$, and $\tilde{\mu}_R$.

with $10 < m_{\mu\mu} < 20$ GeV in SR-E-high, while it overestimates for events with $20 < m_{\mu\mu} < 40$ GeV in the same signal region. This is also visible in Fig. 10, which shows the results of a CR + SR background-only fit assuming that no signal is present. The lack of allowed contributions from signal processes in the SR-constrained fit reduces the significance of bin-by-bin deviations, while the presence of a signal normalization parameter in the exclusion fit allows for larger deviations from the background constraints. When assuming wino production with $m(\tilde{\chi}_2^0) \times m(\tilde{\chi}_1^0) > 0$, electroweakino masses of up to 240 GeV for mass splittings of 7 GeV are excluded. For electroweakino masses at the edge of LEP exclusions, mass splittings from 1.5 GeV to 46 GeV are excluded. Assuming Higgsino production, $\tilde{\chi}_2^0$ masses below 193 GeV are excluded for mass splittings of 9.3 GeV. At the LEP bounds on $m(\tilde{\chi}_2^0)$, mass splittings from 2.4 GeV to 55 GeV are excluded. All observed limits are within 2σ of the median expected limit.

Models containing electroweakinos produced through VBF processes are constrained using the VBF signal regions. These constraints are shown in Fig. 15. The limits on VBF Higgsino production cross sections have a weak dependence on the mass splittings and are shown assuming $\Delta m = 5$ GeV. Higgsinos with masses below 55 GeV are excluded for mass splittings of 5 GeV. Assuming VBF production of winos, electroweakino masses up to 76 GeV for mass splittings of 4.5 GeV are excluded. For wino masses near half of the Higgs boson mass, mass splittings between 2 GeV and 32 GeV are excluded.

Exclusion contours for light-flavor sleptons are shown in Fig. 16. Assuming mass-degenerate selectrons and smuons, slepton masses below 251 GeV are excluded for mass splittings of 10 GeV. For sleptons with masses just above the LEP limits, mass splittings from 550 MeV to 30 GeV are excluded. Figure 16 also shows results where only the right-/left-handed selectron or smuon is produced. When producing these results, only ee or $\mu\mu$ events in the SRs are considered. Right-handed sleptons have smaller cross sections than their left-handed counterparts, due to their different couplings to the weak gauge fields [127]. Right-handed smuons are excluded up to 150 GeV for mass splittings of 8.2 GeV, while left-handed smuons are excluded up to 216 GeV for mass splittings of 10 GeV. Left-handed selectrons are excluded up to 169 GeV for mass splittings of 7.1 GeV. Right-handed selectrons are excluded up to 101 GeV for mass splittings of 7.5 GeV.

IX. CONCLUSION

Results of searches for the electroweak production of supersymmetric particles in models with compressed mass spectra are presented, using $\sqrt{s} = 13$ TeV proton-proton collision data corresponding to 139 fb^{-1} collected by the ATLAS experiment at the CERN Large Hadron Collider. Events with missing transverse momentum, two same-flavor, opposite-charge, low-transverse-momentum leptons, and hadronic activity from initial-state radiation or characteristic of vector-boson fusion production are selected. The data are found to be consistent with predictions from the Standard Model. Assuming wino production, constraints at a 95% confidence level are placed on the minimum mass of the $\tilde{\chi}_2^0$ at 240 GeV for a mass splitting of 7 GeV and extend down to a mass splitting of 1.5 GeV at the LEP chargino mass limit of 92.4 GeV. For Higgsino production, the corresponding lower limits are at 193 GeV at a mass splitting of 9.3 GeV and extend down to a mass splitting of 2.4 GeV at the LEP chargino mass limit. Events consistent with the production of electroweak SUSY states through vector-boson fusion processes are used to constrain wino/bino and Higgsino models while assuming a vanishing $q\bar{q}$ fusion production cross section. Light-flavor sleptons are constrained to have masses above 251 GeV for a mass splitting of 10 GeV, with constraints extending down to mass splittings of 550 MeV at the LEP slepton limits (73 GeV).

ACKNOWLEDGMENTS

We thank CERN for the very successful operation of the LHC, as well as the support staff from our institutions, without whom ATLAS could not be operated efficiently. We acknowledge the support of ANPCyT, Argentina; YerPhI, Armenia; ARC, Australia; BMWFW and FWF, Austria; ANAS, Azerbaijan; SSTC, Belarus; CNPq and FAPESP, Brazil; NSERC, NRC, and CFI, Canada; CERN; CONICYT, Chile; CAS, MOST, and NSFC, China; COLCIENCIAS, Colombia; MSMT CR, MPO CR, and VSC CR, Czech Republic; DNRF and DNSRC, Denmark; IN2P3-CNRS and CEA-DRF/IRFU, France; SRNSFG, Georgia; BMBF, HGF, and MPG, Germany; GSRT, Greece; RGC and Hong Kong SAR, China; ISF and Benoziyo Center, Israel; INFN, Italy; MEXT and JSPS, Japan; CNRST, Morocco; NWO, Netherlands; RCN, Norway; MNiSW and NCN, Poland; FCT, Portugal; MNE/IFA, Romania; MES of Russia and NRC KI, Russian Federation; JINR; MESTD, Serbia; MSSR, Slovakia; ARRS and MIZŠ, Slovenia; DST/NRF, South Africa; MINECO, Spain; SRC and Wallenberg Foundation, Sweden; SERI, SNSF, and Cantons of Bern and Geneva, Switzerland; MOST, Taiwan; TAEK, Turkey; STFC, United Kingdom; DOE and NSF, United States of America. In addition, individual groups and members have received support from BCKDF, CANARIE, Compute Canada, and CRC, Canada; ERC, ERDF, Horizon 2020, Marie Skłodowska-Curie Actions and COST, European Union; Investissements d'Avenir Labex, Investissements d'Avenir Idex, and ANR, France; DFG and AvH Foundation, Germany; Herakleitos, Thales, and Aristeia programs cofinanced by EU-ESF and the Greek NSRF,

Greece; BSF-NSF and GIF, Israel; CERCA Programme Generalitat de Catalunya and PROMETEO Programme Generalitat Valenciana, Spain; The Royal Society and Leverhulme Trust, United Kingdom. The crucial computing support from all WLCG partners is acknowledged gratefully, in particular from CERN, the ATLAS Tier-1 facilities at TRIUMF (Canada), NDGF (Denmark, Norway, Sweden), CC-IN2P3 (France), KIT/GridKA (Germany), INFN-CNAF (Italy), NL-T1 (Netherlands), PIC (Spain), ASGC (Taiwan), RAL (UK) and BNL (USA), the Tier-2 facilities worldwide and large non-WLCG resource providers. Major contributors of computing resources are listed in Ref. [128].

[1] Y. A. Golfand and E. P. Likhtman, Extension of the algebra of Poincaré group generators and violation of p invariance, Pis'ma Zh. Eksp. Teor. Fiz. **13**, 452 (1971) [JETP Lett. **13**, 323 (1971)].
[2] D. V. Volkov and V. P. Akulov, Is the neutrino a Goldstone particle?, Phys. Lett. B **46**, 109 (1973).
[3] J. Wess and B. Zumino, Supergauge transformations in four dimensions, Nucl. Phys. **B70**, 39 (1974).
[4] J. Wess and B. Zumino, Supergauge invariant extension of quantum electrodynamics, Nucl. Phys. **B78**, 1 (1974).
[5] S. Ferrara and B. Zumino, Supergauge invariant Yang-Mills theories, Nucl. Phys. **B79**, 413 (1974).
[6] A. Salam and J. A. Strathdee, Supersymmetry and non-Abelian gauges, Phys. Lett. B **51**, 353 (1974).
[7] G. R. Farrar and P. Fayet, Phenomenology of the production, decay, and detection of new hadronic states associated with supersymmetry, Phys. Lett. B **76**, 575 (1978).
[8] H. Goldberg, Constraint on the Photino Mass from Cosmology, Phys. Rev. Lett. **50**, 1419 (1983); Erratum, Phys. Rev. Lett. **103**, 099905 (2009).
[9] J. R. Ellis, J. S. Hagelin, D. V. Nanopoulos, K. A. Olive, and M. Srednicki, Supersymmetric relics from the big bang, Nucl. Phys. **B238**, 453 (1984).
[10] J. Alwall, M.-P. Le, M. Lisanti, and J. G. Wacker, Searching for directly decaying gluinos at the Tevatron, Phys. Lett. B **666**, 34 (2008).
[11] J. Alwall, P. Schuster, and N. Toro, Simplified models for a first characterization of new physics at the LHC, Phys. Rev. D **79**, 075020 (2009).
[12] D. Alves *et al.*, Simplified models for LHC new physics searches, J. Phys. G **39**, 105005 (2012).
[13] ATLAS Collaboration, The ATLAS experiment at the CERN large Hadron collider, J. Inst. **3**, S08003 (2008).
[14] P. Fayet, Supersymmetry and weak, electromagnetic and strong interactions, Phys. Lett. B **64**, 159 (1976).
[15] P. Fayet, Spontaneously broken supersymmetric theories of weak, electromagnetic and strong interactions, Phys. Lett. B **69**, 489 (1977).
[16] R. Barbieri and G. F. Giudice, Upper bounds on supersymmetric particle masses, Nucl. Phys. **B306**, 63 (1988).
[17] B. de Carlos and J. A. Casas, One loop analysis of the electroweak breaking in supersymmetric models and the fine tuning problem, Phys. Lett. B **309**, 320 (1993).
[18] R. Barbieri and D. Pappadopulo, *S*-particles at their naturalness limits, J. High Energy Phys. 10 (2009) 061.
[19] H. Baer, V. Barger, and P. Huang, Hidden SUSY at the LHC: The light Higgsino-world scenario and the role of a lepton collider, J. High Energy Phys. 11 (2011) 031.
[20] M. Papucci, J. T. Ruderman, and A. Weiler, Natural SUSY endures, J. High Energy Phys. 09 (2012) 035.
[21] H. Baer, V. Barger, P. Huang, A. Mustafayev, and X. Tata, Radiative Natural SUSY with a 125 GeV Higgs Boson, Phys. Rev. Lett. **109**, 161802 (2012).
[22] K. Griest and D. Seckel, Three exceptions in the calculation of relic abundances, Phys. Rev. D **43**, 3191 (1991).
[23] J. Edsjo and P. Gondolo, Neutralino relic density including coannihilations, Phys. Rev. D **56**, 1879 (1997).
[24] S. Profumo, T. Stefaniak, and L. Stephenson Haskins, Not-so-well-tempered neutralino, Phys. Rev. D **96**, 055018 (2017).
[25] A. Nelson, P. Tanedo, and D. Whiteson, Limiting SUSY compressed spectra scenarios, Phys. Rev. D **93**, 115029 (2016).
[26] G. W. Bennett *et al.*, Final report of the E821 muon anomalous magnetic moment measurement at BNL, Phys. Rev. D **73**, 072003 (2006).
[27] A. S. Belyaev, S. F. King, and P. B. Schaefers, Muon $g-2$ and dark matter suggest nonuniversal gaugino masses: $\mathbf{SU}(\mathbf{5}) \times \mathbf{A_4}$ case study at the LHC, Phys. Rev. D **97**, 115002 (2018).
[28] C. G. Lester and D. J. Summers, Measuring masses of semi-invisibly decaying particles pair produced at hadron colliders, Phys. Lett. B **463**, 99 (1999).
[29] A. Barr, C. Lester, and P. Stephens, A variable for measuring masses at hadron colliders when missing energy is expected; m_{T2}: The truth behind the glamour, J. Phys. G **29**, 2343 (2003).
[30] ALEPH, DELPHI, L3, OPAL experiments, combined LEP Chargino results, up to 208 GeV for low DM, Report No. LEPSUSYWG/02-04.1, 2002, http://lepsusy.web.cern.ch/lepsusy/www/inoslowdmsummer02/charginolowdm_pub.html.
[31] ALEPH, DELPHI, L3, OPAL experiments, combined LEP Selectron/Smuon/Stau results, 183–208 GeV, Report No. LEPSUSYWG/04-01.1, 2004, http://lepsusy.web.cern.ch/lepsusy/www/sleptons_summer04/slep_final.html.
[32] ALEPH Collaboration, Search for scalar leptons in e^+e^- collisions at center-of-mass energies up to 209 GeV, Phys. Lett. B **526**, 206 (2002).
[33] ALEPH Collaboration, Search for charginos nearly mass degenerate with the lightest neutralino in e^+e^- collisions at center-of-mass energies up to 209 GeV, Phys. Lett. B **533**, 223 (2002).

[34] ALEPH Collaboration, Absolute lower limits on the masses of selectrons and sneutrinos in the MSSM, Phys. Lett. B **544**, 73 (2002).

[35] ALEPH Collaboration, Absolute mass lower limit for the lightest neutralino of the MSSM from e^+e^- data at $\sqrt{s}$ up to 209 GeV, Phys. Lett. B **583**, 247 (2004).

[36] DELPHI Collaboration, Searches for supersymmetric particles in e^+e^- collisions up to 208 GeV and interpretation of the results within the MSSM, Eur. Phys. J. C **31**, 421 (2003).

[37] L3 Collaboration, Search for charginos with a small mass difference with the lightest supersymmetric particle at $\sqrt{s} = 189$ GeV, Phys. Lett. B **482**, 31 (2000).

[38] L3 Collaboration, Search for scalar leptons and scalar quarks at LEP, Phys. Lett. B **580**, 37 (2004).

[39] OPAL Collaboration, Search for anomalous production of dilepton events with missing transverse momentum in e^+e^- collisions at $\sqrt{s} = 183$ GeV to 209 GeV, Eur. Phys. J. C **32**, 453 (2004).

[40] OPAL Collaboration, Search for nearly mass degenerate charginos and neutralinos at LEP, Eur. Phys. J. C **29**, 479 (2003).

[41] D. Egana-Ugrinovic, M. Low, and J. T. Ruderman, Charged fermions below 100 GeV, J. High Energy Phys. 05 (2018) 012.

[42] CMS Collaboration, Search for new physics in events with two soft oppositely charged leptons and missing transverse momentum in proton-proton collisions at $\sqrt{s} = 13$ TeV, Phys. Lett. B **782**, 440 (2018).

[43] CMS Collaboration, Combined search for electroweak production of charginos and neutralinos in proton-proton collisions at $\sqrt{s} = 13$ TeV, J. High Energy Phys. 03 (2018) 160.

[44] CMSCollaboration, Search for supersymmetry with a compressed mass spectrum in the vector boson fusion topology with 1-lepton and 0-lepton final states in proton-proton collisions at $\sqrt{s} = 13$ TeV, J. High Energy Phys. 08 (2019) 150.

[45] ATLAS Collaboration, Search for electroweak production of supersymmetric states in scenarios with compressed mass spectra at $\sqrt{s} = 13$ TeV with the ATLAS detector, Phys. Rev. D **97**, 052010 (2018).

[46] P. Jackson and C. Rogan, Recursive jigsaw reconstruction: HEP event analysis in the presence of kinematic and combinatoric ambiguities, Phys. Rev. D **96**, 112007 (2017).

[47] B. Abbott *et al.*, Production and integration of the ATLAS insertable B-layer, J. Inst. **13**, T05008 (2018).

[48] ATLAS Collaboration, ATLAS insertable B-layer technical design report, CERN Report No. ATLAS-TDR-19, 2010, https://cds.cern.ch/record/1291633; Addendum, CERN Report No. ATLAS-TDR-19-ADD-1, 2012, https://cds.cern.ch/record/1451888.

[49] ATLAS Collaboration, Performance of the ATLAS trigger system in 2015, Eur. Phys. J. C **77**, 317 (2017).

[50] ATLAS Collaboration, Luminosity determination in pp collisions at $\sqrt{s} = 13$ TeV using the ATLAS detector at the LHC, CERN Report No. ATLAS-CONF-2019-021, 2019, https://cds.cern.ch/record/2677054.

[51] G. Avoni *et al.*, The new LUCID-2 detector for luminosity measurement and monitoring in ATLAS, J. Inst. **13**, P07017 (2018).

[52] S. D. Thomas and J. D. Wells, Phenomenology of Massive Vectorlike Doublet Leptons, Phys. Rev. Lett. **81**, 34 (1998).

[53] J. Alwall *et al.*, The automated computation of tree-level and next-to-leading order differential cross sections, and their matching to parton shower simulations, J. High Energy Phys. 07 (2014) 079.

[54] R. D. Ball *et al.*, Parton distributions with LHC data, Nucl. Phys. **B867**, 244 (2013).

[55] P. Artoisenet, R. Frederix, O. Mattelaer, and R. Rietkerk, Automatic spin-entangled decays of heavy resonances in Monte Carlo simulations, J. High Energy Phys. 03 (2013) 015.

[56] T. Sjöstrand *et al.*, An introduction to PYTHIA 8.2, Comput. Phys. Commun. **191**, 159 (2015).

[57] ATLAS Collaboration, ATLAS Pythia 8 tunes to 7 TeV data, CERN Report No. ATL-PHYS-PUB-2014-021, 2014, https://cds.cern.ch/record/1966419.

[58] L. Lönnblad and S. Prestel, Matching tree-level matrix elements with interleaved showers, J. High Energy Phys. 03 (2012) 019.

[59] M. M. Muhlleitner, A. Djouadi, and M. Spira, Decays of supersymmetric particles: The Program SUSY-HIT, Acta Phys. Pol. B **38**, 635 (2007).

[60] U. De Sanctis, T. Lari, S. Montesano, and C. Troncon, Perspectives for the detection and measurement of supersymmetry in the focus point region of mSUGRA models with the ATLAS detector at LHC, Eur. Phys. J. C **52**, 743 (2007).

[61] B. C. Allanach *et al.*, SUSY Les Houches accord 2, Comput. Phys. Commun. **180**, 8 (2009).

[62] B. Fuks, M. Klasen, S. Schmiemann, and M. Sunder, Realistic simplified gaugino-Higgsino models in the MSSM, Eur. Phys. J. C **78**, 209 (2018).

[63] W. Beenakker, M. Klasen, M. Krämer, T. Plehn, M. Spira, and P. M. Zerwas, Production of Charginos, Neutralinos, and Sleptons at Hadron Colliders, Phys. Rev. Lett. **83**, 3780 (1999).

[64] J. Debove, B. Fuks, and M. Klasen, Threshold resummation for gaugino pair production at hadron colliders, Nucl. Phys. **B842**, 51 (2011).

[65] B. Fuks, M. Klasen, D. R. Lamprea, and M. Rothering, Gaugino production in proton-proton collisions at a center-of-mass energy of 8 TeV, J. High Energy Phys. 10 (2012) 081.

[66] B. Fuks, M. Klasen, D. R. Lamprea, and M. Rothering, Precision predictions for electroweak superpartner production at hadron colliders with Resummino, Eur. Phys. J. C **73**, 2480 (2013).

[67] J. Fiaschi and M. Klasen, Neutralino-chargino pair production at NLO + NLL with resummation-improved parton density functions for LHC Run II, Phys. Rev. D **98**, 055014 (2018).

[68] G. Bozzi, B. Fuks, and M. Klasen, Threshold resummation for slepton-pair production at Hadron colliders, Nucl. Phys. **B777**, 157 (2007).

[69] B. Fuks, M. Klasen, D. R. Lamprea, and M. Rothering, Revisiting slepton pair production at the Large Hadron Collider, J. High Energy Phys. 01 (2014) 168.
[70] J. Fiaschi and M. Klasen, Slepton pair production at the LHC in NLO + NLL with resummation-improved parton densities, J. High Energy Phys. 03 (2018) 094.
[71] C. Borschensky, M. Krämer, A. Kulesza, M. Mangano, S. Padhi, T. Plehn, and X. Portell, Squark and gluino production cross sections in pp collisions at $\sqrt{s} = 13$, 14, 33 and 100 TeV, Eur. Phys. J. C **74**, 3174 (2014).
[72] T. Gleisberg, S. Höche, F. Krauss, M. Schönherr, S. Schumann, F. Siegert, and J. Winter, Event generation with SHERPA 1.1, J. High Energy Phys. 02 (2009) 007.
[73] S. Alioli, P. Nason, C. Oleari, and E. Re, A general framework for implementing NLO calculations in shower Monte Carlo programs: The POWHEG BOX, J. High Energy Phys. 06 (2010) 043.
[74] S. Frixione, P. Nason, and G. Ridolfi, A positive-weight next-to-leading-order Monte Carlo for heavy flavour hadroproduction, J. High Energy Phys. 09 (2007) 126.
[75] P. Nason, A new method for combining NLO QCD with shower Monte Carlo algorithms, J. High Energy Phys. 11 (2004) 040.
[76] S. Frixione, P. Nason, and C. Oleari, Matching NLO QCD computations with parton shower simulations: The POWHEG method, J. High Energy Phys. 11 (2007) 070.
[77] R. Frederix, E. Re, and P. Torrielli, Single-top t-channel hadroproduction in the four-flavour scheme with POWHEG and aMC@NLO, J. High Energy Phys. 09 (2012) 130.
[78] E. Re, Single-top Wt-channel production matched with parton showers using the POWHEG method, Eur. Phys. J. C **71**, 1547 (2011).
[79] ATLAS Collaboration, Multi-Boson simulation for 13 TeV ATLAS analyses, CERN Report No. ATL-PHYS-PUB-2017-005, 2017, https://cds.cern.ch/record/2261933.
[80] ATLAS Collaboration, ATLAS simulation of boson plus jets processes in Run 2, CERN Report No. ATL-PHYS-PUB-2017-006, 2017, https://cds.cern.ch/record/2261937.
[81] ATLASCollaboration, Studies on top-quark Monte Carlo modelling with Sherpa and MG5_aMC@NLO, CERN Report No. ATL-PHYS-PUB-2017-007, 2017, https://cds.cern.ch/record/2261938.
[82] ATLAS Collaboration, A study of different colour reconnection settings for PYTHIA8 generator using underlying event observables, CERN Report No. ATL-PHYS-PUB-2017-008, 2017, https://cds.cern.ch/record/2262253.
[83] ATLAS Collaboration, Modelling of the $t\bar{t}H$ and $t\bar{t}V(V = W, Z)$ processes for $\sqrt{s} = 13$ TeV ATLAS analyses, CERN Report No. ATL-PHYS-PUB-2016-005, 2016, https://cds.cern.ch/record/2120826.
[84] R. D. Ball *et al.*, Parton distributions for the LHC Run II, J. High Energy Phys. 04 (2015) 040.
[85] C. Anastasiou, L. J. Dixon, K. Melnikov, and F. Petriello, High precision QCD at hadron colliders: Electroweak gauge boson rapidity distributions at NNLO, Phys. Rev. D **69**, 094008 (2004).
[86] J. Pumplin, D. R. Stump, J. Huston, H.-L. Lai, P. Nadolsky, and W.-K. Tung, New generation of parton distributions with uncertainties from global QCD analysis, J. High Energy Phys. 07 (2002) 012.
[87] D. de Florian *et al.*, Handbook of LHC Higgs cross sections: 4. Deciphering the Nature of the Higgs sector, CERN Report No. CERN-2017-002-M, 2016.
[88] M. Cacciari, M. Czakon, M. Mangano, A. Mitov, and P. Nason, Top-pair production at hadron colliders with next-to-next-to-leading logarithmic soft-gluon resummation, Phys. Lett. B **710**, 612 (2012).
[89] M. Czakon and A. Mitov, NNLO corrections to top-pair production at hadron colliders: The all-fermionic scattering channels, J. High Energy Phys. 12 (2012) 054.
[90] M. Czakon and A. Mitov, NNLO corrections to top pair production at hadron colliders: The quark-gluon reaction, J. High Energy Phys. 01 (2013) 080.
[91] M. Czakon, P. Fiedler, and A. Mitov, Total Top-Quark Pair-Production Cross Section at Hadron Colliders Through $O(\alpha_S^4)$, Phys. Rev. Lett. **110**, 252004 (2013).
[92] M. Czakon and A. Mitov, Top++: A program for the calculation of the top-pair cross-section at hadron colliders, Comput. Phys. Commun. **185**, 2930 (2014).
[93] N. Kidonakis, NNLL resummation for s-channel single top quark production, Phys. Rev. D **81**, 054028 (2010).
[94] N. Kidonakis, Next-to-next-to-leading-order collinear and soft gluon corrections for t-channel single top quark production, Phys. Rev. D **83**, 091503 (2011).
[95] N. Kidonakis, Two-loop soft anomalous dimensions for single top quark associated production with a W^- or H^-, Phys. Rev. D **82**, 054018 (2010).
[96] ATLAS Collaboration, The Pythia 8 A3 tune description of ATLAS minimum bias and inelastic measurements incorporating the Donnachie–Landshoff diffractive model, CERN Report No. ATL-PHYS-PUB-2016-017, 2016, https://cds.cern.ch/record/2206965.
[97] A. D. Martin, W. Stirling, R. S. Thorne, and G. Watt, Parton distributions for the LHC, Eur. Phys. J. C **63**, 189 (2009).
[98] D. J. Lange, The EvtGen particle decay simulation package, Nucl. Instrum. Methods Phys. Res., Sect. A **462**, 152 (2001).
[99] ATLAS Collaboration, The ATLAS simulation infrastructure, Eur. Phys. J. C **70**, 823 (2010).
[100] S. Agostinelli *et al.*, GEANT4—A simulation toolkit, Nucl. Instrum. Methods Phys. Res., Sect. A **506**, 250 (2003).
[101] ATLAS Collaboration, Characterisation and mitigation of beam-induced backgrounds observed in the ATLAS detector during the 2011 proton-proton run, J. Inst. **8**, P07004 (2013).
[102] ATLAS Collaboration, Muon reconstruction performance of the ATLAS detector in proton-proton collision data at $\sqrt{s} = 13$ TeV, Eur. Phys. J. C **76**, 292 (2016).
[103] ATLAS Collaboration, Electron and photon performance measurements with the ATLAS detector using the 2015–2017 LHC proton-proton collision data, J. Inst. **14**, P12006 (2019).
[104] ATLAS Collaboration, Identification of very-low transverse momentum muons in the ATLAS experiment, CERN Report No. ATL-PHYS-PUB-2020-002, https://cds.cern.ch/record/2710574.
[105] ATLAS Collaboration, Topological cell clustering in the ATLAS calorimeters and its performance in LHC Run 1, Eur. Phys. J. C **77**, 490 (2017).

[106] M. Cacciari, G. P. Salam, and G. Soyez, The anti-k_t jet clustering algorithm, J. High Energy Phys. 04 (2008) 063.
[107] M. Cacciari, G. P. Salam, and G. Soyez, FastJet user manual, Eur. Phys. J. C **72**, 1896 (2012).
[108] ATLAS Collaboration, Jet energy scale measurements and their systematic uncertainties in proton-proton collisions at $\sqrt{s} = 13$ TeV with the ATLAS detector, Phys. Rev. D **96**, 072002 (2017).
[109] ATLAS Collaboration, Performance of pile-up mitigation techniques for jets in pp collisions at $\sqrt{s} = 8$ TeV using the ATLAS detector, Eur. Phys. J. C **76**, 581 (2016).
[110] ATLAS Collaboration, Forward Jet Vertex Tagging: A new technique for the identification and rejection of forward pileup jets, CERN Report No. ATL-PHYS-PUB-2015-034, 2015, https://cds.cern.ch/record/2042098.
[111] ATLAS Collaboration, ATLAS b-jet identification performance and efficiency measurement with $t\bar{t}$ events in pp collisions at $\sqrt{s} = 13$ TeV, Eur. Phys. J. C **79**, 970 (2019).
[112] ATLAS Collaboration, Early inner detector tracking performance in the 2015 data at $\sqrt{s} = 13$ TeV, CERN Report No. ATL-PHYS-PUB-2015-051, 2015, https://cds.cern.ch/record/2110140.
[113] ATLAS Collaboration, $E_{\mathrm{T}}^{\mathrm{miss}}$ performance in the ATLAS detector using 2015–2016 LHC pp collisions, CERN Report No. ATLAS-CONF-2018-023, 2018, https://cds.cern.ch/record/2625233.
[114] ATLAS Collaboration, Performance of missing transverse momentum reconstruction with the ATLAS detector using proton-proton collisions at $\sqrt{s} = 13$ TeV, Eur. Phys. J. C **78**, 903 (2018).
[115] Z. Han, G. D. Kribs, A. Martin, and A. Menon, Hunting quasidegenerate Higgsinos, Phys. Rev. D **89**, 075007 (2014).
[116] H. Baer, A. Mustafayev, and X. Tata, Monojet plus soft dilepton signal from light Higgsino pair production at LHC14, Phys. Rev. D **90**, 115007 (2014).
[117] A. Barr and J. Scoville, A boost for the EW SUSY hunt: Monojet-like search for compressed sleptons at LHC14 with 100 fb^{-1}, J. High Energy Phys. 04 (2015) 147.
[118] R. D. Cousins, J. T. Linnemann, and J. Tucker, Evaluation of three methods for calculating statistical significance when incorporating a systematic uncertainty into a test of the background-only hypothesis for a Poisson process, Nucl. Instrum. Methods Phys. Res., Sect. A **595**, 480 (2008).
[119] ATLAS Collaboration, Measurement of the WW cross section in $\sqrt{s} = 7$ TeV pp collisions with the ATLAS detector and limits on anomalous gauge couplings, Phys. Lett. B **712**, 289 (2012).
[120] ATLAS Collaboration, Prospects for Higgs boson searches using the $H \to WW^{(*)} \to \ell\nu\ell\nu$ decay mode with the ATLAS detector at 10 TeV, CERN Report No. ATL-PHYS-PUB-2010-005, 2010, https://cds.cern.ch/record/1270568.
[121] J. Butterworth *et al.*, PDF4LHC recommendations for LHC Run II, J. Phys. G **43**, 023001 (2016).
[122] G. Cowan, K. Cranmer, E. Gross, and O. Vitells, Asymptotic formulae for likelihood-based tests of new physics, Eur. Phys. J. C **71**, 1554 (2011).
[123] M. Baak, G. J. Besjes, D. Côté, A. Koutsman, J. Lorenz, and D. Short, HistFitter software framework for statistical data analysis, Eur. Phys. J. C **75**, 153 (2015).
[124] A. L. Read, Presentation of search results: The CL_S technique, J. Phys. G **28**, 2693 (2002).
[125] ATLAS Collaboration, Search for direct production of charginos, neutralinos and sleptons in final states with two leptons and missing transverse momentum in pp collisions at $\sqrt{s} = 8$ TeV with the ATLAS detector, J. High Energy Phys. 05 (2014) 071.
[126] ATLAS Collaboration, Search for direct production of charginos and neutralinos in events with three leptons and missing transverse momentum in $\sqrt{s} = 8$ TeV pp collisions with the ATLAS detector, J. High Energy Phys. 04 (2014) 169.
[127] S. P. Martin, A supersymmetry primer, Adv. Ser. Dir. High Energy Phys. **18**, 1 (1998).
[128] ATLAS Collaboration, ATLAS computing acknowledgements, CERN Report No. ATL-GEN-PUB-2016-002, https://cds.cern.ch/record/2202407.

G. Aad,[102] B. Abbott,[129] D. C. Abbott,[103] A. Abed Abud,[36] K. Abeling,[53] D. K. Abhayasinghe,[94] S. H. Abidi,[167] O. S. AbouZeid,[40] N. L. Abraham,[156] H. Abramowicz,[161] H. Abreu,[160] Y. Abulaiti,[6] B. S. Acharya,[67a,67b,b] B. Achkar,[53] S. Adachi,[163] L. Adam,[100] C. Adam Bourdarios,[5] L. Adamczyk,[84a] L. Adamek,[167] J. Adelman,[121] M. Adersberger,[114] A. Adiguzel,[12c] S. Adorni,[54] T. Adye,[144] A. A. Affolder,[146] Y. Afik,[160] C. Agapopoulou,[65] M. N. Agaras,[38] A. Aggarwal,[119] C. Agheorghiesei,[27c] J. A. Aguilar-Saavedra,[140f,140a,c] F. Ahmadov,[80] W. S. Ahmed,[104] X. Ai,[18] G. Aielli,[74a,74b] S. Akatsuka,[86] T. P. A. Åkesson,[97] E. Akilli,[54] A. V. Akimov,[111] K. Al Khoury,[65] G. L. Alberghi,[23b,23a] J. Albert,[176] M. J. Alconada Verzini,[161] S. Alderweireldt,[36] M. Aleksa,[36] I. N. Aleksandrov,[80] C. Alexa,[27b] T. Alexopoulos,[10] A. Alfonsi,[120] F. Alfonsi,[23b,23a] M. Alhroob,[129] B. Ali,[142] M. Aliev,[166] G. Alimonti,[69a] C. Allaire,[65] B. M. M. Allbrooke,[156] B. W. Allen,[132] P. P. Allport,[21] A. Aloisio,[70a,70b] F. Alonso,[89] C. Alpigiani,[148] A. A. Alshehri,[57] M. Alvarez Estevez,[99] M. G. Alviggi,[70a,70b] Y. Amaral Coutinho,[81b] A. Ambler,[104] L. Ambroz,[135] C. Amelung,[26] D. Amidei,[106] S. P. Amor Dos Santos,[140a] S. Amoroso,[46] C. S. Amrouche,[54] F. An,[79] C. Anastopoulos,[149] N. Andari,[145] T. Andeen,[11] C. F. Anders,[61b] J. K. Anders,[20] A. Andreazza,[69a,69b] V. Andrei,[61a] C. R. Anelli,[176] S. Angelidakis,[38] A. Angerami,[39] A. V. Anisenkov,[122b,122a] A. Annovi,[72a] C. Antel,[54] M. T. Anthony,[149] E. Antipov,[130] M. Antonelli,[51] D. J. A. Antrim,[171] F. Anulli,[73a] M. Aoki,[82] J. A. Aparisi Pozo,[174] L. Aperio Bella,[15a] J. P. Araque,[140a] V. Araujo Ferraz,[81b] R. Araujo Pereira,[81b]

C. Arcangeletti,[51] A. T. H. Arce,[49] F. A. Arduh,[89] J-F. Arguin,[110] S. Argyropoulos,[52] J.-H. Arling,[46] A. J. Armbruster,[36] A. Armstrong,[171] O. Arnaez,[167] H. Arnold,[120] Z. P. Arrubarrena Tame,[114] G. Artoni,[135] S. Artz,[100] S. Asai,[163] T. Asawatavonvanich,[165] N. Asbah,[59] E. M. Asimakopoulou,[172] L. Asquith,[156] J. Assahsah,[35d] K. Assamagan,[29] R. Astalos,[28a] R. J. Atkin,[33a] M. Atkinson,[173] N. B. Atlay,[19] H. Atmani,[65] K. Augsten,[142] A. T. Aukerman,[139] G. Avolio,[36] M. K. Ayoub,[15a] G. Azuelos,[110,d] H. Bachacou,[145] K. Bachas,[68a,68b] M. Backes,[135] F. Backman,[45a,45b] P. Bagnaia,[73a,73b] M. Bahmani,[85] H. Bahrasemani,[152] A. J. Bailey,[174] V. R. Bailey,[173] J. T. Baines,[144] C. Bakalis,[10] O. K. Baker,[183] P. J. Bakker,[120] D. Bakshi Gupta,[8] S. Balaji,[157] E. M. Baldin,[122b,122a] P. Balek,[180] F. Balli,[145] W. K. Balunas,[135] J. Balz,[100] E. Banas,[85] A. Bandyopadhyay,[24] Sw. Banerjee,[181,e] A. A. E. Bannoura,[182] L. Barak,[161] W. M. Barbe,[38] E. L. Barberio,[105] D. Barberis,[55b,55a] M. Barbero,[102] G. Barbour,[95] T. Barillari,[115] M-S. Barisits,[36] J. Barkeloo,[132] T. Barklow,[153] R. Barnea,[160] B. M. Barnett,[144] R. M. Barnett,[18] Z. Barnovska-Blenessy,[60a] A. Baroncelli,[60a] G. Barone,[29] A. J. Barr,[135] L. Barranco Navarro,[45a,45b] F. Barreiro,[99] J. Barreiro Guimarães da Costa,[15a] S. Barsov,[138] R. Bartoldus,[153] G. Bartolini,[102] A. E. Barton,[90] P. Bartos,[28a] A. Basalaev,[46] A. Basan,[100] A. Bassalat,[65,f] M. J. Basso,[167] R. L. Bates,[57] S. Batlamous,[35e] J. R. Batley,[32] B. Batool,[151] M. Battaglia,[146] M. Bauce,[73a,73b] F. Bauer,[145] K. T. Bauer,[171] H. S. Bawa,[31] J. B. Beacham,[49] T. Beau,[136] P. H. Beauchemin,[170] F. Becherer,[52] P. Bechtle,[24] H. C. Beck,[53] H. P. Beck,[20,g] K. Becker,[178] C. Becot,[46] A. Beddall,[12d] A. J. Beddall,[12a] V. A. Bednyakov,[80] M. Bedognetti,[120] C. P. Bee,[155] T. A. Beermann,[182] M. Begalli,[81b] M. Begel,[29] A. Behera,[155] J. K. Behr,[46] F. Beisiegel,[24] A. S. Bell,[95] G. Bella,[161] L. Bellagamba,[23b] A. Bellerive,[34] P. Bellos,[9] K. Beloborodov,[122b,122a] K. Belotskiy,[112] N. L. Belyaev,[112] D. Benchekroun,[35a] N. Benekos,[10] Y. Benhammou,[161] D. P. Benjamin,[6] M. Benoit,[54] J. R. Bensinger,[26] S. Bentvelsen,[120] L. Beresford,[135] M. Beretta,[51] D. Berge,[19] E. Bergeaas Kuutmann,[172] N. Berger,[5] B. Bergmann,[142] L. J. Bergsten,[26] J. Beringer,[18] S. Berlendis,[7] G. Bernardi,[136] C. Bernius,[153] F. U. Bernlochner,[24] T. Berry,[94] P. Berta,[100] C. Bertella,[15a] I. A. Bertram,[90] O. Bessidskaia Bylund,[182] N. Besson,[145] A. Bethani,[101] S. Bethke,[115] A. Betti,[42] A. J. Bevan,[93] J. Beyer,[115] D. S. Bhattacharya,[177] P. Bhattarai,[26] R. Bi,[139] R. M. Bianchi,[139] O. Biebel,[114] D. Biedermann,[19] R. Bielski,[36] K. Bierwagen,[100] N. V. Biesuz,[72a,72b] M. Biglietti,[75a] T. R. V. Billoud,[110] M. Bindi,[53] A. Bingul,[12d] C. Bini,[73a,73b] S. Biondi,[23b,23a] M. Birman,[180] T. Bisanz,[53] J. P. Biswal,[3] D. Biswas,[181,e] A. Bitadze,[101] C. Bittrich,[48] K. Bjørke,[134] T. Blazek,[28a] I. Bloch,[46] C. Blocker,[26] A. Blue,[57] U. Blumenschein,[93] G. J. Bobbink,[120] V. S. Bobrovnikov,[122b,122a] S. S. Bocchetta,[97] A. Bocci,[49] D. Boerner,[46] D. Bogavac,[14] A. G. Bogdanchikov,[122b,122a] C. Bohm,[45a] V. Boisvert,[94] P. Bokan,[53] T. Bold,[84a] A. E. Bolz,[61b] M. Bomben,[136] M. Bona,[93] J. S. Bonilla,[132] M. Boonekamp,[145] C. D. Booth,[94] H. M. Borecka-Bielska,[91] L. S. Borgna,[95] A. Borisov,[123] G. Borissov,[90] J. Bortfeldt,[36] D. Bortoletto,[135] D. Boscherini,[23b] M. Bosman,[14] J. D. Bossio Sola,[104] K. Bouaouda,[35a] J. Boudreau,[139] E. V. Bouhova-Thacker,[90] D. Boumediene,[38] S. K. Boutle,[57] A. Boveia,[127] J. Boyd,[36] D. Boye,[33b,h] I. R. Boyko,[80] A. J. Bozson,[94] J. Bracinik,[21] N. Brahimi,[102] G. Brandt,[182] O. Brandt,[32] F. Braren,[46] B. Brau,[103] J. E. Brau,[132] W. D. Breaden Madden,[57] K. Brendlinger,[46] L. Brenner,[46] R. Brenner,[172] S. Bressler,[180] B. Brickwedde,[100] D. L. Briglin,[21] D. Britton,[57] D. Britzger,[115] I. Brock,[24] R. Brock,[107] G. Brooijmans,[39] W. K. Brooks,[147c] E. Brost,[29] J. H Broughton,[21] P. A. Bruckman de Renstrom,[85] D. Bruncko,[28b] A. Bruni,[23b] G. Bruni,[23b] L. S. Bruni,[120] S. Bruno,[74a,74b] M. Bruschi,[23b] N. Bruscino,[73a,73b] P. Bryant,[37] L. Bryngemark,[97] T. Buanes,[17] Q. Buat,[36] P. Buchholz,[151] A. G. Buckley,[57] I. A. Budagov,[80] M. K. Bugge,[134] F. Bührer,[52] O. Bulekov,[112] T. J. Burch,[121] S. Burdin,[91] C. D. Burgard,[120] A. M. Burger,[130] B. Burghgrave,[8] J. T. P. Burr,[46] C. D. Burton,[11] J. C. Burzynski,[103] V. Büscher,[100] E. Buschmann,[53] P. J. Bussey,[57] J. M. Butler,[25] C. M. Buttar,[57] J. M. Butterworth,[95] P. Butti,[36] W. Buttinger,[36] C. J. Buxo Vazquez,[107] A. Buzatu,[158] A. R. Buzykaev,[122b,122a] G. Cabras,[23b,23a] S. Cabrera Urbán,[174] D. Caforio,[56] H. Cai,[173] V. M. M. Cairo,[153] O. Cakir,[4a] N. Calace,[36] P. Calafiura,[18] A. Calandri,[102] G. Calderini,[136] P. Calfayan,[66] G. Callea,[57] L. P. Caloba,[81b] A. Caltabiano,[74a,74b] S. Calvente Lopez,[99] D. Calvet,[38] S. Calvet,[38] T. P. Calvet,[155] M. Calvetti,[72a,72b] R. Camacho Toro,[136] S. Camarda,[36] D. Camarero Munoz,[99] P. Camarri,[74a,74b] D. Cameron,[134] C. Camincher,[36] S. Campana,[36] M. Campanelli,[95] A. Camplani,[40] A. Campoverde,[151] V. Canale,[70a,70b] A. Canesse,[104] M. Cano Bret,[60c] J. Cantero,[130] T. Cao,[161] Y. Cao,[173] M. D. M. Capeans Garrido,[36] M. Capua,[41b,41a] R. Cardarelli,[74a] F. Cardillo,[149] G. Carducci,[41b,41a] I. Carli,[143] T. Carli,[36] G. Carlino,[70a] B. T. Carlson,[139] L. Carminati,[69a,69b] R. M. D. Carney,[153] S. Caron,[119] E. Carquin,[147c] S. Carrá,[46] J. W. S. Carter,[167] M. P. Casado,[14,i] A. F. Casha,[167] R. Castelijn,[120] F. L. Castillo,[174] L. Castillo Garcia,[14] V. Castillo Gimenez,[174] N. F. Castro,[140a,140e] A. Catinaccio,[36] J. R. Catmore,[134] A. Cattai,[36] V. Cavaliere,[29] E. Cavallaro,[14] M. Cavalli-Sforza,[14] V. Cavasinni,[72a,72b] E. Celebi,[12b] L. Cerda Alberich,[174] K. Cerny,[131] A. S. Cerqueira,[81a] A. Cerri,[156] L. Cerrito,[74a,74b] F. Cerutti,[18] A. Cervelli,[23b,23a] S. A. Cetin,[12b] Z. Chadi,[35a] D. Chakraborty,[121] J. Chan,[181] W. S. Chan,[120] W. Y. Chan,[91] J. D. Chapman,[32] B. Chargeishvili,[159b] D. G. Charlton,[21] T. P. Charman,[93] C. C. Chau,[34] S. Che,[127] S. Chekanov,[6] S. V. Chekulaev,[168a]

G. A. Chelkov,[80,j] B. Chen,[79] C. Chen,[60a] C. H. Chen,[79] H. Chen,[29] J. Chen,[60a] J. Chen,[39] J. Chen,[26] S. Chen,[137] S. J. Chen,[15c] X. Chen,[15b] Y-H. Chen,[46] H. C. Cheng,[63a] H. J. Cheng,[15a] A. Cheplakov,[80] E. Cheremushkina,[123] R. Cherkaoui El Moursli,[35e] E. Cheu,[7] K. Cheung,[64] T. J. A. Chevalérias,[145] L. Chevalier,[145] V. Chiarella,[51] G. Chiarelli,[72a] G. Chiodini,[68a] A. S. Chisholm,[21] A. Chitan,[27b] I. Chiu,[163] Y. H. Chiu,[176] M. V. Chizhov,[80] K. Choi,[11] A. R. Chomont,[73a,73b] S. Chouridou,[162] Y. S. Chow,[120] M. C. Chu,[63a] X. Chu,[15a,15d] J. Chudoba,[141] J. J. Chwastowski,[85] L. Chytka,[131] D. Cieri,[115] K. M. Ciesla,[85] D. Cinca,[47] V. Cindro,[92] I. A. Cioară,[27b] A. Ciocio,[18] F. Cirotto,[70a,70b] Z. H. Citron,[180,k] M. Citterio,[69a] D. A. Ciubotaru,[27b] B. M. Ciungu,[167] A. Clark,[54] M. R. Clark,[39] P. J. Clark,[50] C. Clement,[45a,45b] Y. Coadou,[102] M. Cobal,[67a,67c] A. Coccaro,[55b] J. Cochran,[79] H. Cohen,[161] A. E. C. Coimbra,[36] B. Cole,[39] A. P. Colijn,[120] J. Collot,[58] P. Conde Muiño,[140a,140h] S. H. Connell,[33b] I. A. Connelly,[57] S. Constantinescu,[27b] F. Conventi,[70a,l] A. M. Cooper-Sarkar,[135] F. Cormier,[175] K. J. R. Cormier,[167] L. D. Corpe,[95] M. Corradi,[73a,73b] E. E. Corrigan,[97] F. Corriveau,[104,m] A. Cortes-Gonzalez,[36] M. J. Costa,[174] F. Costanza,[5] D. Costanzo,[149] G. Cowan,[94] J. W. Cowley,[32] J. Crane,[101] K. Cranmer,[125] S. J. Crawley,[57] R. A. Creager,[137] S. Crépé-Renaudin,[58] F. Crescioli,[136] M. Cristinziani,[24] V. Croft,[170] G. Crosetti,[41b,41a] A. Cueto,[5] T. Cuhadar Donszelmann,[149] A. R. Cukierman,[153] W. R. Cunningham,[57] S. Czekierda,[85] P. Czodrowski,[36] M. J. Da Cunha Sargedas De Sousa,[60b] J. V. Da Fonseca Pinto,[81b] C. Da Via,[101] W. Dabrowski,[84a] F. Dachs,[36] T. Dado,[28a] S. Dahbi,[33d] T. Dai,[106] C. Dallapiccola,[103] M. Dam,[40] G. D'amen,[29] V. D'Amico,[75a,75b] J. Damp,[100] J. R. Dandoy,[137] M. F. Daneri,[30] N. S. Dann,[101] M. Danninger,[152] V. Dao,[36] G. Darbo,[55b] O. Dartsi,[5] A. Dattagupta,[132] T. Daubney,[46] S. D'Auria,[69a,69b] C. David,[168b] T. Davidek,[143] D. R. Davis,[49] I. Dawson,[149] K. De,[8] R. De Asmundis,[70a] M. De Beurs,[120] S. De Castro,[23b,23a] S. De Cecco,[73a,73b] N. De Groot,[119] P. de Jong,[120] H. De la Torre,[107] A. De Maria,[15c] D. De Pedis,[73a] A. De Salvo,[73a] U. De Sanctis,[74a,74b] M. De Santis,[74a,74b] A. De Santo,[156] K. De Vasconcelos Corga,[102] J. B. De Vivie De Regie,[65] C. Debenedetti,[146] D. V. Dedovich,[80] A. M. Deiana,[42] J. Del Peso,[99] Y. Delabat Diaz,[46] D. Delgove,[65] F. Deliot,[145,n] C. M. Delitzsch,[7] M. Della Pietra,[70a,70b] D. Della Volpe,[54] A. Dell'Acqua,[36] L. Dell'Asta,[74a,74b] M. Delmastro,[5] C. Delporte,[65] P. A. Delsart,[58] D. A. DeMarco,[167] S. Demers,[183] M. Demichev,[80] G. Demontigny,[110] S. P. Denisov,[123] L. D'Eramo,[136] D. Derendarz,[85] J. E. Derkaoui,[35d] F. Derue,[136] P. Dervan,[91] K. Desch,[24] C. Deterre,[46] K. Dette,[167] C. Deutsch,[24] M. R. Devesa,[30] P. O. Deviveiros,[36] F. A. Di Bello,[73a,73b] A. Di Ciaccio,[74a,74b] L. Di Ciaccio,[5] W. K. Di Clemente,[137] C. Di Donato,[70a,70b] A. Di Girolamo,[36] G. Di Gregorio,[72a,72b] B. Di Micco,[75a,75b] R. Di Nardo,[75a,75b] K. F. Di Petrillo,[59] R. Di Sipio,[167] C. Diaconu,[102] F. A. Dias,[40] T. Dias Do Vale,[140a] M. A. Diaz,[147a] J. Dickinson,[18] E. B. Diehl,[106] J. Dietrich,[19] S. Díez Cornell,[46] A. Dimitrievska,[18] W. Ding,[15b] J. Dingfelder,[24] F. Dittus,[36] F. Djama,[102] T. Djobava,[159b] J. I. Djuvsland,[17] M. A. B. Do Vale,[81c] M. Dobre,[27b] D. Dodsworth,[26] C. Doglioni,[97] J. Dolejsi,[143] Z. Dolezal,[143] M. Donadelli,[81d] B. Dong,[60c] J. Donini,[38] A. D'onofrio,[15c] M. D'Onofrio,[91] J. Dopke,[144] A. Doria,[70a] M. T. Dova,[89] A. T. Doyle,[57] E. Drechsler,[152] E. Dreyer,[152] T. Dreyer,[53] A. S. Drobac,[170] D. Du,[60b] Y. Duan,[60b] F. Dubinin,[111] M. Dubovsky,[28a] A. Dubreuil,[54] E. Duchovni,[180] G. Duckeck,[114] A. Ducourthial,[136] O. A. Ducu,[110] D. Duda,[115] A. Dudarev,[36] A. C. Dudder,[100] E. M. Duffield,[18] L. Duflot,[65] M. Dührssen,[36] C. Dülsen,[182] M. Dumancic,[180] A. E. Dumitriu,[27b] A. K. Duncan,[57] M. Dunford,[61a] A. Duperrin,[102] H. Duran Yildiz,[4a] M. Düren,[56] A. Durglishvili,[159b] D. Duschinger,[48] B. Dutta,[46] D. Duvnjak,[1] G. I. Dyckes,[137] M. Dyndal,[36] S. Dysch,[101] B. S. Dziedzic,[85] K. M. Ecker,[115] M. G. Eggleston,[49] T. Eifert,[8] G. Eigen,[17] K. Einsweiler,[18] T. Ekelof,[172] H. El Jarrari,[35e] R. El Kosseifi,[102] V. Ellajosyula,[172] M. Ellert,[172] F. Ellinghaus,[182] A. A. Elliot,[93] N. Ellis,[36] J. Elmsheuser,[29] M. Elsing,[36] D. Emeliyanov,[144] A. Emerman,[39] Y. Enari,[163] M. B. Epland,[49] J. Erdmann,[47] A. Ereditato,[20] P. A. Erland,[85] M. Errenst,[36] M. Escalier,[65] C. Escobar,[174] O. Estrada Pastor,[174] E. Etzion,[161] H. Evans,[66] A. Ezhilov,[138] F. Fabbri,[57] L. Fabbri,[23b,23a] V. Fabiani,[119] G. Facini,[178] R. M. Faisca Rodrigues Pereira,[140a] R. M. Fakhrutdinov,[123] S. Falciano,[73a] P. J. Falke,[5] S. Falke,[5] J. Faltova,[143] Y. Fang,[15a] Y. Fang,[15a] G. Fanourakis,[44] M. Fanti,[69a,69b] M. Faraj,[67a,67c,o] A. Farbin,[8] A. Farilla,[75a] E. M. Farina,[71a,71b] T. Farooque,[107] S. M. Farrington,[50] P. Farthouat,[36] F. Fassi,[35e] P. Fassnacht,[36] D. Fassouliotis,[9] M. Faucci Giannelli,[50] W. J. Fawcett,[32] L. Fayard,[65] O. L. Fedin,[138,p] W. Fedorko,[175] A. Fehr,[20] M. Feickert,[173] L. Feligioni,[102] A. Fell,[149] C. Feng,[60b] M. Feng,[49] M. J. Fenton,[171] A. B. Fenyuk,[123] S. W. Ferguson,[43] J. Ferrando,[46] A. Ferrante,[173] A. Ferrari,[172] P. Ferrari,[120] R. Ferrari,[71a] D. E. Ferreira de Lima,[61b] A. Ferrer,[174] D. Ferrere,[54] C. Ferretti,[106] F. Fiedler,[100] A. Filipčič,[92] F. Filthaut,[119] K. D. Finelli,[25] M. C. N. Fiolhais,[140a,140c,q] L. Fiorini,[174] F. Fischer,[114] W. C. Fisher,[107] I. Fleck,[151] P. Fleischmann,[106] T. Flick,[182] B. M. Flierl,[114] L. Flores,[137] L. R. Flores Castillo,[63a] F. M. Follega,[76a,76b] N. Fomin,[17] J. H. Foo,[167] G. T. Forcolin,[76a,76b] A. Formica,[145] F. A. Förster,[14] A. C. Forti,[101] A. G. Foster,[21] M. G. Foti,[135] D. Fournier,[65] H. Fox,[90] P. Francavilla,[72a,72b] S. Francescato,[73a,73b] M. Franchini,[23b,23a] S. Franchino,[61a] D. Francis,[36] L. Franconi,[20] M. Franklin,[59] A. N. Fray,[93] P. M. Freeman,[21] B. Freund,[110] W. S. Freund,[81b] E. M. Freundlich,[47] D. C. Frizzell,[129] D. Froidevaux,[36] J. A. Frost,[135]

C. Fukunaga,[164] E. Fullana Torregrosa,[174] T. Fusayasu,[116] J. Fuster,[174] A. Gabrielli,[23b,23a] A. Gabrielli,[18] S. Gadatsch,[54] P. Gadow,[115] G. Gagliardi,[55b,55a] L. G. Gagnon,[110] B. Galhardo,[140a] G. E. Gallardo,[135] E. J. Gallas,[135] B. J. Gallop,[144] G. Galster,[40] R. Gamboa Goni,[93] K. K. Gan,[127] S. Ganguly,[180] J. Gao,[60a] Y. Gao,[50] Y. S. Gao,[31,r] C. García,[174] J. E. García Navarro,[174] J. A. García Pascual,[15a] C. Garcia-Argos,[52] M. Garcia-Sciveres,[18] R. W. Gardner,[37] N. Garelli,[153] S. Gargiulo,[52] C. A. Garner,[167] V. Garonne,[134] S. J. Gasiorowski,[148] P. Gaspar,[81b] A. Gaudiello,[55b,55a] G. Gaudio,[71a] I. L. Gavrilenko,[111] A. Gavrilyuk,[124] C. Gay,[175] G. Gaycken,[46] E. N. Gazis,[10] A. A. Geanta,[27b] C. M. Gee,[146] C. N. P. Gee,[144] J. Geisen,[97] M. Geisen,[100] C. Gemme,[55b] M. H. Genest,[58] C. Geng,[106] S. Gentile,[73a,73b] S. George,[94] T. Geralis,[44] L. O. Gerlach,[53] P. Gessinger-Befurt,[100] G. Gessner,[47] S. Ghasemi,[151] M. Ghasemi Bostanabad,[176] M. Ghneimat,[151] A. Ghosh,[65] A. Ghosh,[78] B. Giacobbe,[23b] S. Giagu,[73a,73b] N. Giangiacomi,[23b,23a] P. Giannetti,[72a] A. Giannini,[70a,70b] G. Giannini,[14] S. M. Gibson,[94] M. Gignac,[146] D. Gillberg,[34] G. Gilles,[182] D. M. Gingrich,[3,d] M. P. Giordani,[67a,67c] P. F. Giraud,[145] G. Giugliarelli,[67a,67c] D. Giugni,[69a] F. Giuli,[74a,74b] S. Gkaitatzis,[162] I. Gkialas,[9,s] E. L. Gkougkousis,[14] P. Gkountoumis,[10] L. K. Gladilin,[113] C. Glasman,[99] J. Glatzer,[14] P. C. F. Glaysher,[46] A. Glazov,[46] G. R. Gledhill,[132] M. Goblirsch-Kolb,[26] D. Godin,[110] S. Goldfarb,[105] T. Golling,[54] D. Golubkov,[123] A. Gomes,[140a,140b] R. Goncalves Gama,[53] R. Gonçalo,[140a] G. Gonella,[132] L. Gonella,[21] A. Gongadze,[80] F. Gonnella,[21] J. L. Gonski,[39] S. González de la Hoz,[174] S. Gonzalez Fernandez,[14] S. Gonzalez-Sevilla,[54] G. R. Gonzalvo Rodriguez,[174] L. Goossens,[36] N. A. Gorasia,[21] P. A. Gorbounov,[124] H. A. Gordon,[29] B. Gorini,[36] E. Gorini,[68a,68b] A. Gorišek,[92] A. T. Goshaw,[49] M. I. Gostkin,[80] C. A. Gottardo,[119] M. Gouighri,[35b] A. G. Goussiou,[148] N. Govender,[33b] C. Goy,[5] E. Gozani,[160] I. Grabowska-Bold,[84a] E. C. Graham,[91] J. Gramling,[171] E. Gramstad,[134] S. Grancagnolo,[19] M. Grandi,[156] V. Gratchev,[138] P. M. Gravila,[27f] F. G. Gravili,[68a,68b] C. Gray,[57] H. M. Gray,[18] C. Grefe,[24] K. Gregersen,[97] I. M. Gregor,[46] P. Grenier,[153] K. Grevtsov,[46] C. Grieco,[14] N. A. Grieser,[129] A. A. Grillo,[146] K. Grimm,[31,t] S. Grinstein,[14,u] J.-F. Grivaz,[65] S. Groh,[100] E. Gross,[180] J. Grosse-Knetter,[53] Z. J. Grout,[95] C. Grud,[106] A. Grummer,[118] L. Guan,[106] W. Guan,[181] C. Gubbels,[175] J. Guenther,[36] A. Guerguichon,[65] J. G. R. Guerrero Rojas,[174] F. Guescini,[115] D. Guest,[171] R. Gugel,[52] T. Guillemin,[5] S. Guindon,[36] U. Gul,[57] J. Guo,[60c] W. Guo,[106] Y. Guo,[60a] Z. Guo,[102] R. Gupta,[46] S. Gurbuz,[12c] G. Gustavino,[129] M. Guth,[52] P. Gutierrez,[129] C. Gutschow,[95] C. Guyot,[145] C. Gwenlan,[135] C. B. Gwilliam,[91] A. Haas,[125] C. Haber,[18] H. K. Hadavand,[8] A. Hadef,[60a] M. Haleem,[177] J. Haley,[130] G. Halladjian,[107] G. D. Hallewell,[102] K. Hamacher,[182] P. Hamal,[131] K. Hamano,[176] H. Hamdaoui,[35e] M. Hamer,[24] G. N. Hamity,[50] K. Han,[60a,v] L. Han,[60a] S. Han,[15a] Y. F. Han,[167] K. Hanagaki,[82,w] M. Hance,[146] D. M. Handl,[114] B. Haney,[137] R. Hankache,[136] E. Hansen,[97] J. B. Hansen,[40] J. D. Hansen,[40] M. C. Hansen,[24] P. H. Hansen,[40] E. C. Hanson,[101] K. Hara,[169] T. Harenberg,[182] S. Harkusha,[108] P. F. Harrison,[178] N. M. Hartmann,[114] Y. Hasegawa,[150] A. Hasib,[50] S. Hassani,[145] S. Haug,[20] R. Hauser,[107] L. B. Havener,[39] M. Havranek,[142] C. M. Hawkes,[21] R. J. Hawkings,[36] D. Hayden,[107] C. Hayes,[106] R. L. Hayes,[175] C. P. Hays,[135] J. M. Hays,[93] H. S. Hayward,[91] S. J. Haywood,[144] F. He,[60a] M. P. Heath,[50] V. Hedberg,[97] S. Heer,[24] K. K. Heidegger,[52] W. D. Heidorn,[79] J. Heilman,[34] S. Heim,[46] T. Heim,[18] B. Heinemann,[46,x] J. J. Heinrich,[132] L. Heinrich,[36] J. Hejbal,[141] L. Helary,[61b] A. Held,[125] S. Hellesund,[134] C. M. Helling,[146] S. Hellman,[45a,45b] C. Helsens,[36] R. C. W. Henderson,[90] Y. Heng,[181] L. Henkelmann,[61a] S. Henkelmann,[175] A. M. Henriques Correia,[36] H. Herde,[26] V. Herget,[177] Y. Hernández Jiménez,[33d] H. Herr,[100] M. G. Herrmann,[114] T. Herrmann,[48] G. Herten,[52] R. Hertenberger,[114] L. Hervas,[36] T. C. Herwig,[137] G. G. Hesketh,[95] N. P. Hessey,[168a] A. Higashida,[163] S. Higashino,[82] E. Higón-Rodriguez,[174] K. Hildebrand,[37] J. C. Hill,[32] K. K. Hill,[29] K. H. Hiller,[46] S. J. Hillier,[21] M. Hils,[48] I. Hinchliffe,[18] F. Hinterkeuser,[24] M. Hirose,[133] S. Hirose,[52] D. Hirschbuehl,[182] B. Hiti,[92] O. Hladik,[141] D. R. Hlaluku,[33d] J. Hobbs,[155] N. Hod,[180] M. C. Hodgkinson,[149] A. Hoecker,[36] D. Hohn,[52] D. Hohov,[65] T. Holm,[24] T. R. Holmes,[37] M. Holzbock,[114] L. B. A. H. Hommels,[32] S. Honda,[169] T. M. Hong,[139] J. C. Honig,[52] A. Hönle,[115] B. H. Hooberman,[173] W. H. Hopkins,[6] Y. Horii,[117] P. Horn,[48] L. A. Horyn,[37] S. Hou,[158] A. Hoummada,[35a] J. Howarth,[101] J. Hoya,[89] M. Hrabovsky,[131] J. Hrdinka,[77] I. Hristova,[19] J. Hrivnac,[65] A. Hrynevich,[109] T. Hryn'ova,[5] P. J. Hsu,[64] S.-C. Hsu,[148] Q. Hu,[29] S. Hu,[60c] Y. F. Hu,[15a,15d] D. P. Huang,[95] Y. Huang,[60a] Y. Huang,[15a] Z. Hubacek,[142] F. Hubaut,[102] M. Huebner,[24] F. Huegging,[24] T. B. Huffman,[135] M. Huhtinen,[36] R. F. H. Hunter,[34] P. Huo,[155] N. Huseynov,[80,y] J. Huston,[107] J. Huth,[59] R. Hyneman,[106] S. Hyrych,[28a] G. Iacobucci,[54] G. Iakovidis,[29] I. Ibragimov,[151] L. Iconomidou-Fayard,[65] P. Iengo,[36] R. Ignazzi,[40] O. Igonkina,[120,a,z] R. Iguchi,[163] T. Iizawa,[54] Y. Ikegami,[82] M. Ikeno,[82] D. Iliadis,[162] N. Ilic,[119,167,m] F. Iltzsche,[48] G. Introzzi,[71a,71b] M. Iodice,[75a] K. Iordanidou,[168a] V. Ippolito,[73a,73b] M. F. Isacson,[172] M. Ishino,[163] W. Islam,[130] C. Issever,[19,46] S. Istin,[160] F. Ito,[169] J. M. Iturbe Ponce,[63a] R. Iuppa,[76a,76b] A. Ivina,[180] H. Iwasaki,[82] J. M. Izen,[43] V. Izzo,[70a] P. Jacka,[141] P. Jackson,[1] R. M. Jacobs,[24] B. P. Jaeger,[152] V. Jain,[2] G. Jäkel,[182] K. B. Jakobi,[100] K. Jakobs,[52] T. Jakoubek,[141] J. Jamieson,[57] K. W. Janas,[84a] R. Jansky,[54] M. Janus,[53] P. A. Janus,[84a] G. Jarlskog,[97] N. Javadov,[80,y] T. Javůrek,[36]

M. Javurkova,[103] F. Jeanneau,[145] L. Jeanty,[132] J. Jejelava,[159a] A. Jelinskas,[178] P. Jenni,[52,aa] N. Jeong,[46] S. Jézéquel,[5] H. Ji,[181] J. Jia,[155] H. Jiang,[79] Y. Jiang,[60a] Z. Jiang,[153,bb] S. Jiggins,[52] F. A. Jimenez Morales,[38] J. Jimenez Pena,[115] S. Jin,[15c] A. Jinaru,[27b] O. Jinnouchi,[165] H. Jivan,[33d] P. Johansson,[149] K. A. Johns,[7] C. A. Johnson,[66] R. W. L. Jones,[90] S. D. Jones,[156] S. Jones,[7] T. J. Jones,[91] J. Jongmanns,[61a] P. M. Jorge,[140a] J. Jovicevic,[36] X. Ju,[18] J. J. Junggeburth,[115] A. Juste Rozas,[14,u] A. Kaczmarska,[85] M. Kado,[73a,73b] H. Kagan,[127] M. Kagan,[153] A. Kahn,[39] C. Kahra,[100] T. Kaji,[179] E. Kajomovitz,[160] C. W. Kalderon,[29] A. Kaluza,[100] A. Kamenshchikov,[123] M. Kaneda,[163] N. J. Kang,[146] S. Kang,[79] L. Kanjir,[92] Y. Kano,[117] J. Kanzaki,[82] L. S. Kaplan,[181] D. Kar,[33d] K. Karava,[135] M. J. Kareem,[168b] S. N. Karpov,[80] Z. M. Karpova,[80] V. Kartvelishvili,[90] A. N. Karyukhin,[123] A. Kastanas,[45a,45b] C. Kato,[60d,60c] J. Katzy,[46] K. Kawade,[150] K. Kawagoe,[88] T. Kawaguchi,[117] T. Kawamoto,[145] G. Kawamura,[53] E. F. Kay,[176] V. F. Kazanin,[122b,122a] R. Keeler,[176] R. Kehoe,[42] J. S. Keller,[34] E. Kellermann,[97] D. Kelsey,[156] J. J. Kempster,[21] J. Kendrick,[21] K. E. Kennedy,[39] O. Kepka,[141] S. Kersten,[182] B. P. Kerševan,[92] S. Ketabchi Haghighat,[167] M. Khader,[173] F. Khalil-Zada,[13] M. Khandoga,[145] A. Khanov,[130] A. G. Kharlamov,[122b,122a] T. Kharlamova,[122b,122a] E. E. Khoda,[175] A. Khodinov,[166] T. J. Khoo,[54] E. Khramov,[80] J. Khubua,[159b] S. Kido,[83] M. Kiehn,[54] C. R. Kilby,[94] E. Kim,[165] Y. K. Kim,[37] N. Kimura,[95] O. M. Kind,[19] B. T. King,[91,a] D. Kirchmeier,[48] J. Kirk,[144] A. E. Kiryunin,[115] T. Kishimoto,[163] D. P. Kisliuk,[167] V. Kitali,[46] O. Kivernyk,[5] T. Klapdor-Kleingrothaus,[52] M. Klassen,[61a] C. Klein,[32] M. H. Klein,[106] M. Klein,[91] U. Klein,[91] K. Kleinknecht,[100] P. Klimek,[121] A. Klimentov,[29] T. Klingl,[24] T. Klioutchnikova,[36] F. F. Klitzner,[114] P. Kluit,[120] S. Kluth,[115] E. Kneringer,[77] E. B. F. G. Knoops,[102] A. Knue,[52] D. Kobayashi,[88] T. Kobayashi,[163] M. Kobel,[48] M. Kocian,[153] T. Kodama,[163] P. Kodys,[143] P. T. Koenig,[24] T. Koffas,[34] N. M. Köhler,[36] M. Kolb,[145] I. Koletsou,[5] T. Komarek,[131] T. Kondo,[82] K. Köneke,[52] A. X. Y. Kong,[1] A. C. König,[119] T. Kono,[126] V. Konstantinides,[95] N. Konstantinidis,[95] B. Konya,[97] R. Kopeliansky,[66] S. Koperny,[84a] K. Korcyl,[85] K. Kordas,[162] G. Koren,[161] A. Korn,[95] I. Korolkov,[14] E. V. Korolkova,[149] N. Korotkova,[113] O. Kortner,[115] S. Kortner,[115] T. Kosek,[143] V. V. Kostyukhin,[149,166] A. Kotsokechagia,[65] A. Kotwal,[49] A. Koulouris,[10] A. Kourkoumeli-Charalampidi,[71a,71b] C. Kourkoumelis,[9] E. Kourlitis,[149] V. Kouskoura,[29] A. B. Kowalewska,[85] R. Kowalewski,[176] W. Kozanecki,[101] A. S. Kozhin,[123] V. A. Kramarenko,[113] G. Kramberger,[92] D. Krasnopevtsev,[60a] M. W. Krasny,[136] A. Krasznahorkay,[36] D. Krauss,[115] J. A. Kremer,[84a] J. Kretzschmar,[91] P. Krieger,[167] F. Krieter,[114] A. Krishnan,[61b] K. Krizka,[18] K. Kroeninger,[47] H. Kroha,[115] J. Kroll,[141] J. Kroll,[137] K. S. Krowpman,[107] U. Kruchonak,[80] H. Krüger,[24] N. Krumnack,[79] M. C. Kruse,[49] J. A. Krzysiak,[85] T. Kubota,[105] O. Kuchinskaia,[166] S. Kuday,[4b] J. T. Kuechler,[46] S. Kuehn,[36] A. Kugel,[61a] T. Kuhl,[46] V. Kukhtin,[80] R. Kukla,[102] Y. Kulchitsky,[108,cc] S. Kuleshov,[147c] Y. P. Kulinich,[173] M. Kuna,[58] T. Kunigo,[86] A. Kupco,[141] T. Kupfer,[47] O. Kuprash,[52] H. Kurashige,[83] L. L. Kurchaninov,[168a] Y. A. Kurochkin,[108] A. Kurova,[112] M. G. Kurth,[15a,15d] E. S. Kuwertz,[36] M. Kuze,[165] A. K. Kvam,[148] J. Kvita,[131] T. Kwan,[104] L. La Rotonda,[41b,41a] F. La Ruffa,[41b,41a] C. Lacasta,[174] F. Lacava,[73a,73b] D. P. J. Lack,[101] H. Lacker,[19] D. Lacour,[136] E. Ladygin,[80] R. Lafaye,[5] B. Laforge,[136] T. Lagouri,[147b] S. Lai,[53] I. K. Lakomiec,[84a] S. Lammers,[66] W. Lampl,[7] C. Lampoudis,[162] E. Lançon,[29] U. Landgraf,[52] M. P. J. Landon,[93] M. C. Lanfermann,[54] V. S. Lang,[46] J. C. Lange,[53] R. J. Langenberg,[103] A. J. Lankford,[171] F. Lanni,[29] K. Lantzsch,[24] A. Lanza,[71a] A. Lapertosa,[55b,55a] S. Laplace,[136] J. F. Laporte,[145] T. Lari,[69a] F. Lasagni Manghi,[23b,23a] M. Lassnig,[36] T. S. Lau,[63a] A. Laudrain,[65] A. Laurier,[34] M. Lavorgna,[70a,70b] S. D. Lawlor,[94] M. Lazzaroni,[69a,69b] B. Le,[105] E. Le Guirriec,[102] A. Lebedev,[79] M. LeBlanc,[7] T. LeCompte,[6] F. Ledroit-Guillon,[58] A. C. A. Lee,[95] C. A. Lee,[29] G. R. Lee,[17] L. Lee,[59] S. C. Lee,[158] S. Lee,[79] B. Lefebvre,[168a] H. P. Lefebvre,[94] M. Lefebvre,[176] C. Leggett,[18] K. Lehmann,[152] N. Lehmann,[182] G. Lehmann Miotto,[36] W. A. Leight,[46] A. Leisos,[162,dd] M. A. L. Leite,[81d] C. E. Leitgeb,[114] R. Leitner,[143] D. Lellouch,[180,a] K. J. C. Leney,[42] T. Lenz,[24] R. Leone,[7] S. Leone,[72a] C. Leonidopoulos,[50] A. Leopold,[136] C. Leroy,[110] R. Les,[167] C. G. Lester,[32] M. Levchenko,[138] J. Levêque,[5] D. Levin,[106] L. J. Levinson,[180] D. J. Lewis,[21] B. Li,[15b] B. Li,[106] C-Q. Li,[60a] F. Li,[60c] H. Li,[60a] H. Li,[60b] J. Li,[60c] K. Li,[148] L. Li,[60c] M. Li,[15a,15d] Q. Li,[15a,15d] Q. Y. Li,[60a] S. Li,[60d,60c] X. Li,[46] Y. Li,[46] Z. Li,[60b] Z. Li,[104] Z. Liang,[15a] B. Liberti,[74a] A. Liblong,[167] K. Lie,[63c] S. Lim,[29] C. Y. Lin,[32] K. Lin,[107] T. H. Lin,[100] R. A. Linck,[66] J. H. Lindon,[21] A. L. Lionti,[54] E. Lipeles,[137] A. Lipniacka,[17] T. M. Liss,[173,ee] A. Lister,[175] J. D. Little,[8] B. Liu,[79] B. L. Liu,[6] H. B. Liu,[29] H. Liu,[106] J. B. Liu,[60a] J. K. K. Liu,[37] K. Liu,[60d] M. Liu,[60a] P. Liu,[15a] Y. Liu,[15a,15d] Y. L. Liu,[106] Y. W. Liu,[60a] M. Livan,[71a,71b] A. Lleres,[58] J. Llorente Merino,[152] S. L. Lloyd,[93] C. Y. Lo,[63b] E. M. Lobodzinska,[46] P. Loch,[7] S. Loffredo,[74a,74b] T. Lohse,[19] K. Lohwasser,[149] M. Lokajicek,[141] J. D. Long,[173] R. E. Long,[90] L. Longo,[36] K. A. Looper,[127] J. A. Lopez,[147c] I. Lopez Paz,[101] A. Lopez Solis,[149] J. Lorenz,[114] N. Lorenzo Martinez,[5] A. M. Lory,[114] M. Losada,[22] P. J. Lösel,[114] A. Lösle,[52] X. Lou,[46] X. Lou,[15a] A. Lounis,[65] J. Love,[6] P. A. Love,[90] J. J. Lozano Bahilo,[174] M. Lu,[60a] Y. J. Lu,[64] H. J. Lubatti,[148] C. Luci,[73a,73b] A. Lucotte,[58] C. Luedtke,[52] F. Luehring,[66] I. Luise,[136] L. Luminari,[73a]

B. Lund-Jensen,[154] M. S. Lutz,[103] D. Lynn,[29] H. Lyons,[91] R. Lysak,[141] E. Lytken,[97] F. Lyu,[15a] V. Lyubushkin,[80] T. Lyubushkina,[80] H. Ma,[29] L. L. Ma,[60b] Y. Ma,[60b] G. Maccarrone,[51] A. Macchiolo,[115] C. M. Macdonald,[149] J. Machado Miguens,[137] D. Madaffari,[174] R. Madar,[38] W. F. Mader,[48] M. Madugoda Ralalage Don,[130] N. Madysa,[48] J. Maeda,[83] T. Maeno,[29] M. Maerker,[48] V. Magerl,[52] N. Magini,[79] D. J. Mahon,[39] C. Maidantchik,[81b] T. Maier,[114] A. Maio,[140a,140b,140d] K. Maj,[84a] O. Majersky,[28a] S. Majewski,[132] Y. Makida,[82] N. Makovec,[65] B. Malaescu,[136] Pa. Malecki,[85] V. P. Maleev,[138] F. Malek,[58] U. Mallik,[78] D. Malon,[6] C. Malone,[32] S. Maltezos,[10] S. Malyukov,[80] J. Mamuzic,[174] G. Mancini,[51] I. Mandić,[92] L. Manhaes de Andrade Filho,[81a] I. M. Maniatis,[162] J. Manjarres Ramos,[48] K. H. Mankinen,[97] A. Mann,[114] A. Manousos,[77] B. Mansoulie,[145] I. Manthos,[162] S. Manzoni,[120] A. Marantis,[162] G. Marceca,[30] L. Marchese,[135] G. Marchiori,[136] M. Marcisovsky,[141] L. Marcoccia,[74a,74b] C. Marcon,[97] C. A. Marin Tobon,[36] M. Marjanovic,[129] Z. Marshall,[18] M. U. F. Martensson,[172] S. Marti-Garcia,[174] C. B. Martin,[127] T. A. Martin,[178] V. J. Martin,[50] B. Martin dit Latour,[17] L. Martinelli,[75a,75b] M. Martinez,[14,u] V. I. Martinez Outschoorn,[103] S. Martin-Haugh,[144] V. S. Martoiu,[27b] A. C. Martyniuk,[95] A. Marzin,[36] S. R. Maschek,[115] L. Masetti,[100] T. Mashimo,[163] R. Mashinistov,[111] J. Masik,[101] A. L. Maslennikov,[122b,122a] L. Massa,[74a,74b] P. Massarotti,[70a,70b] P. Mastrandrea,[72a,72b] A. Mastroberardino,[41b,41a] T. Masubuchi,[163] D. Matakias,[29] A. Matic,[114] N. Matsuzawa,[163] P. Mättig,[24] J. Maurer,[27b] B. Maček,[92] D. A. Maximov,[122b,122a] R. Mazini,[158] I. Maznas,[162] S. M. Mazza,[146] S. P. Mc Kee,[106] T. G. McCarthy,[115] W. P. McCormack,[18] E. F. McDonald,[105] J. A. Mcfayden,[36] G. Mchedlidze,[159b] M. A. McKay,[42] K. D. McLean,[176] S. J. McMahon,[144] P. C. McNamara,[105] C. J. McNicol,[178] R. A. McPherson,[176,m] J. E. Mdhluli,[33d] Z. A. Meadows,[103] S. Meehan,[36] T. Megy,[52] S. Mehlhase,[114] A. Mehta,[91] T. Meideck,[58] B. Meirose,[43] D. Melini,[160] B. R. Mellado Garcia,[33d] J. D. Mellenthin,[53] M. Melo,[28a] F. Meloni,[46] A. Melzer,[24] S. B. Menary,[101] E. D. Mendes Gouveia,[140a,140e] L. Meng,[36] X. T. Meng,[106] S. Menke,[115] E. Meoni,[41b,41a] S. Mergelmeyer,[19] S. A. M. Merkt,[139] C. Merlassino,[135] P. Mermod,[54] L. Merola,[70a,70b] C. Meroni,[69a] G. Merz,[106] O. Meshkov,[113,111] J. K. R. Meshreki,[151] A. Messina,[73a,73b] J. Metcalfe,[6] A. S. Mete,[6] C. Meyer,[66] J-P. Meyer,[145] H. Meyer Zu Theenhausen,[61a] F. Miano,[156] M. Michetti,[19] R. P. Middleton,[144] L. Mijović,[50] G. Mikenberg,[180] M. Mikestikova,[141] M. Mikuž,[92] H. Mildner,[149] M. Milesi,[105] A. Milic,[167] D. A. Millar,[93] D. W. Miller,[37] A. Milov,[180] D. A. Milstead,[45a,45b] R. A. Mina,[153] A. A. Minaenko,[123] M. Miñano Moya,[174] I. A. Minashvili,[159b] A. I. Mincer,[125] B. Mindur,[84a] M. Mineev,[80] Y. Minegishi,[163] L. M. Mir,[14] A. Mirto,[68a,68b] K. P. Mistry,[137] T. Mitani,[179] J. Mitrevski,[114] V. A. Mitsou,[174] M. Mittal,[60c] O. Miu,[167] A. Miucci,[20] P. S. Miyagawa,[149] A. Mizukami,[82] J. U. Mjörnmark,[97] T. Mkrtchyan,[61a] M. Mlynarikova,[143] T. Moa,[45a,45b] K. Mochizuki,[110] P. Mogg,[52] S. Mohapatra,[39] R. Moles-Valls,[24] M. C. Mondragon,[107] K. Mönig,[46] J. Monk,[40] E. Monnier,[102] A. Montalbano,[152] J. Montejo Berlingen,[36] M. Montella,[95] F. Monticelli,[89] S. Monzani,[69a] N. Morange,[65] D. Moreno,[22] M. Moreno Llácer,[174] C. Moreno Martinez,[14] P. Morettini,[55b] M. Morgenstern,[160] S. Morgenstern,[48] D. Mori,[152] M. Morii,[59] M. Morinaga,[179] V. Morisbak,[134] A. K. Morley,[36] G. Mornacchi,[36] A. P. Morris,[95] L. Morvaj,[155] P. Moschovakos,[36] B. Moser,[120] M. Mosidze,[159b] T. Moskalets,[145] H. J. Moss,[149] J. Moss,[31,ff] E. J. W. Moyse,[103] S. Muanza,[102] J. Mueller,[139] R. S. P. Mueller,[114] D. Muenstermann,[90] G. A. Mullier,[97] D. P. Mungo,[69a,69b] J. L. Munoz Martinez,[14] F. J. Munoz Sanchez,[101] P. Murin,[28b] W. J. Murray,[178,144] A. Murrone,[69a,69b] M. Muškinja,[18] C. Mwewa,[33a] A. G. Myagkov,[123,gg] A. A. Myers,[139] J. Myers,[132] M. Myska,[142] B. P. Nachman,[18] O. Nackenhorst,[47] A. Nag Nag,[48] K. Nagai,[135] K. Nagano,[82] Y. Nagasaka,[62] J. L. Nagle,[29] E. Nagy,[102] A. M. Nairz,[36] Y. Nakahama,[117] K. Nakamura,[82] T. Nakamura,[163] I. Nakano,[128] H. Nanjo,[133] F. Napolitano,[61a] R. F. Naranjo Garcia,[46] R. Narayan,[42] I. Naryshkin,[138] T. Naumann,[46] G. Navarro,[22] P. Y. Nechaeva,[111] F. Nechansky,[46] T. J. Neep,[21] A. Negri,[71a,71b] M. Negrini,[23b] C. Nellist,[119] M. E. Nelson,[45a,45b] S. Nemecek,[141] M. Nessi,[36,hh] M. S. Neubauer,[173] F. Neuhaus,[100] M. Neumann,[182] R. Newhouse,[175] P. R. Newman,[21] C. W. Ng,[139] Y. S. Ng,[19] Y. W. Y. Ng,[171] B. Ngair,[35e] H. D. N. Nguyen,[102] T. Nguyen Manh,[110] E. Nibigira,[38] R. B. Nickerson,[135] R. Nicolaidou,[145] D. S. Nielsen,[40] J. Nielsen,[146] N. Nikiforou,[11] V. Nikolaenko,[123,gg] I. Nikolic-Audit,[136] K. Nikolopoulos,[21] P. Nilsson,[29] H. R. Nindhito,[54] Y. Ninomiya,[82] A. Nisati,[73a] N. Nishu,[60c] R. Nisius,[115] I. Nitsche,[47] T. Nitta,[179] T. Nobe,[163] Y. Noguchi,[86] I. Nomidis,[136] M. A. Nomura,[29] M. Nordberg,[36] T. Novak,[92] O. Novgorodova,[48] R. Novotny,[142] L. Nozka,[131] K. Ntekas,[171] E. Nurse,[95] F. G. Oakham,[34,d] H. Oberlack,[115] J. Ocariz,[136] A. Ochi,[83] I. Ochoa,[39] J. P. Ochoa-Ricoux,[147a] K. O'Connor,[26] S. Oda,[88] S. Odaka,[82] S. Oerdek,[53] A. Ogrodnik,[84a] A. Oh,[101] S. H. Oh,[49] C. C. Ohm,[154] H. Oide,[165] M. L. Ojeda,[167] H. Okawa,[169] Y. Okazaki,[86] M. W. O'Keefe,[91] Y. Okumura,[163] T. Okuyama,[82] A. Olariu,[27b] L. F. Oleiro Seabra,[140a] S. A. Olivares Pino,[147a] D. Oliveira Damazio,[29] J. L. Oliver,[1] M. J. R. Olsson,[171] A. Olszewski,[85] J. Olszowska,[85] D. C. O'Neil,[152] A. P. O'neill,[135] A. Onofre,[140a,140e] P. U. E. Onyisi,[11] H. Oppen,[134] M. J. Oreglia,[37] G. E. Orellana,[89] D. Orestano,[75a,75b] N. Orlando,[14] R. S. Orr,[167] V. O'Shea,[57] R. Ospanov,[60a]

G. Otero y Garzon,[30] H. Otono,[88] P. S. Ott,[61a] M. Ouchrif,[35d] J. Ouellette,[29] F. Ould-Saada,[134] A. Ouraou,[145] Q. Ouyang,[15a] M. Owen,[57] R. E. Owen,[21] V. E. Ozcan,[12c] N. Ozturk,[8] J. Pacalt,[131] H. A. Pacey,[32] K. Pachal,[49] A. Pacheco Pages,[14] C. Padilla Aranda,[14] S. Pagan Griso,[18] M. Paganini,[183] G. Palacino,[66] S. Palazzo,[50] S. Palestini,[36] M. Palka,[84b] D. Pallin,[38] P. Palni,[84a] I. Panagoulias,[10] C. E. Pandini,[36] J. G. Panduro Vazquez,[94] P. Pani,[46] G. Panizzo,[67a,67c] L. Paolozzi,[54] C. Papadatos,[110] K. Papageorgiou,[9,s] S. Parajuli,[42] A. Paramonov,[6] D. Paredes Hernandez,[63b] S. R. Paredes Saenz,[135] B. Parida,[166] T. H. Park,[167] A. J. Parker,[31] M. A. Parker,[32] F. Parodi,[55b,55a] E. W. Parrish,[121] J. A. Parsons,[39] U. Parzefall,[52] L. Pascual Dominguez,[136] V. R. Pascuzzi,[167] J. M. P. Pasner,[146] F. Pasquali,[120] E. Pasqualucci,[73a] S. Passaggio,[55b] F. Pastore,[94] P. Pasuwan,[45a,45b] S. Pataraia,[100] J. R. Pater,[101] A. Pathak,[181,e] J. Patton,[91] T. Pauly,[36] J. Pearkes,[153] B. Pearson,[115] M. Pedersen,[134] L. Pedraza Diaz,[119] R. Pedro,[140a] T. Peiffer,[53] S. V. Peleganchuk,[122b,122a] O. Penc,[141] H. Peng,[60a] B. S. Peralva,[81a] M. M. Perego,[65] A. P. Pereira Peixoto,[140a] D. V. Perepelitsa,[29] F. Peri,[19] L. Perini,[69a,69b] H. Pernegger,[36] S. Perrella,[140a] A. Perrevoort,[120] K. Peters,[46] R. F. Y. Peters,[101] B. A. Petersen,[36] T. C. Petersen,[40] E. Petit,[102] A. Petridis,[1] C. Petridou,[162] P. Petroff,[65] M. Petrov,[135] F. Petrucci,[75a,75b] M. Pettee,[183] N. E. Pettersson,[103] K. Petukhova,[143] A. Peyaud,[145] R. Pezoa,[147c] L. Pezzotti,[71a,71b] T. Pham,[105] F. H. Phillips,[107] P. W. Phillips,[144] M. W. Phipps,[173] G. Piacquadio,[155] E. Pianori,[18] A. Picazio,[103] R. H. Pickles,[101] R. Piegaia,[30] D. Pietreanu,[27b] J. E. Pilcher,[37] A. D. Pilkington,[101] M. Pinamonti,[67a,67c] J. L. Pinfold,[3] M. Pitt,[161] L. Pizzimento,[74a,74b] M.-A. Pleier,[29] V. Pleskot,[143] E. Plotnikova,[80] P. Podberezko,[122b,122a] R. Poettgen,[97] R. Poggi,[54] L. Poggioli,[136] I. Pogrebnyak,[107] D. Pohl,[24] I. Pokharel,[53] G. Polesello,[71a] A. Poley,[18] A. Policicchio,[73a,73b] R. Polifka,[143] A. Polini,[23b] C. S. Pollard,[46] V. Polychronakos,[29] D. Ponomarenko,[112] L. Pontecorvo,[36] S. Popa,[27a] G. A. Popeneciu,[27d] L. Portales,[5] D. M. Portillo Quintero,[58] S. Pospisil,[142] K. Potamianos,[46] I. N. Potrap,[80] C. J. Potter,[32] H. Potti,[11] T. Poulsen,[97] J. Poveda,[36] T. D. Powell,[149] G. Pownall,[46] M. E. Pozo Astigarraga,[36] P. Pralavorio,[102] S. Prell,[79] D. Price,[101] M. Primavera,[68a] S. Prince,[104] M. L. Proffitt,[148] N. Proklova,[112] K. Prokofiev,[63c] F. Prokoshin,[80] S. Protopopescu,[29] J. Proudfoot,[6] M. Przybycien,[84a] D. Pudzha,[138] A. Puri,[173] P. Puzo,[65] J. Qian,[106] Y. Qin,[101] A. Quadt,[53] M. Queitsch-Maitland,[36] A. Qureshi,[1] M. Racko,[28a] F. Ragusa,[69a,69b] G. Rahal,[98] J. A. Raine,[54] S. Rajagopalan,[29] A. Ramirez Morales,[93] K. Ran,[15a,15d] T. Rashid,[65] S. Raspopov,[5] D. M. Rauch,[46] F. Rauscher,[114] S. Rave,[100] B. Ravina,[149] I. Ravinovich,[180] J. H. Rawling,[101] M. Raymond,[36] A. L. Read,[134] N. P. Readioff,[58] M. Reale,[68a,68b] D. M. Rebuzzi,[71a,71b] A. Redelbach,[177] G. Redlinger,[29] K. Reeves,[43] L. Rehnisch,[19] J. Reichert,[137] D. Reikher,[161] A. Reiss,[100] A. Rej,[151] C. Rembser,[36] A. Renardi,[46] M. Renda,[27b] M. Rescigno,[73a] S. Resconi,[69a] E. D. Resseguie,[18] S. Rettie,[95] B. Reynolds,[127] E. Reynolds,[21] O. L. Rezanova,[122b,122a] P. Reznicek,[143] E. Ricci,[76a,76b] R. Richter,[115] S. Richter,[46] E. Richter-Was,[84b] O. Ricken,[24] M. Ridel,[136] P. Rieck,[115] O. Rifki,[46] M. Rijssenbeek,[155] A. Rimoldi,[71a,71b] M. Rimoldi,[46] L. Rinaldi,[23b] G. Ripellino,[154] I. Riu,[14] J. C. Rivera Vergara,[176] F. Rizatdinova,[130] E. Rizvi,[93] C. Rizzi,[36] R. T. Roberts,[101] S. H. Robertson,[104,m] M. Robin,[46] D. Robinson,[32] C. M. Robles Gajardo,[147c] M. Robles Manzano,[100] A. Robson,[57] A. Rocchi,[74a,74b] E. Rocco,[100] C. Roda,[72a,72b] S. Rodriguez Bosca,[174] A. Rodriguez Perez,[14] D. Rodriguez Rodriguez,[174] A. M. Rodríguez Vera,[168b] S. Roe,[36] O. Røhne,[134] R. Röhrig,[115] R. A. Rojas,[147c] B. Roland,[52] C. P. A. Roland,[66] J. Roloff,[29] A. Romaniouk,[112] M. Romano,[23b,23a] N. Rompotis,[91] M. Ronzani,[125] L. Roos,[136] S. Rosati,[73a] G. Rosin,[103] B. J. Rosser,[137] E. Rossi,[46] E. Rossi,[75a,75b] E. Rossi,[70a,70b] L. P. Rossi,[55b] L. Rossini,[69a,69b] R. Rosten,[14] M. Rotaru,[27b] J. Rothberg,[148] B. Rottler,[52] D. Rousseau,[65] G. Rovelli,[71a,71b] A. Roy,[11] D. Roy,[33d] A. Rozanov,[102] Y. Rozen,[160] X. Ruan,[33d] F. Rühr,[52] A. Ruiz-Martinez,[174] A. Rummler,[36] Z. Rurikova,[52] N. A. Rusakovich,[80] H. L. Russell,[104] L. Rustige,[38,47] J. P. Rutherfoord,[7] E. M. Rüttinger,[149] M. Rybar,[39] G. Rybkin,[65] E. B. Rye,[134] A. Ryzhov,[123] J. A. Sabater Iglesias,[46] P. Sabatini,[53] G. Sabato,[120] S. Sacerdoti,[65] H. F-W. Sadrozinski,[146] R. Sadykov,[80] F. Safai Tehrani,[73a] B. Safarzadeh Samani,[156] M. Safdari,[153] P. Saha,[121] S. Saha,[104] M. Sahinsoy,[61a] A. Sahu,[182] M. Saimpert,[46] M. Saito,[163] T. Saito,[163] H. Sakamoto,[163] D. Salamani,[54] G. Salamanna,[75a,75b] J. E. Salazar Loyola,[147c] A. Salnikov,[153] J. Salt,[174] D. Salvatore,[41b,41a] F. Salvatore,[156] A. Salvucci,[63a,63b,63c] A. Salzburger,[36] J. Samarati,[36] D. Sammel,[52] D. Sampsonidis,[162] D. Sampsonidou,[162] J. Sánchez,[174] A. Sanchez Pineda,[67a,36,67c] H. Sandaker,[134] C. O. Sander,[46] I. G. Sanderswood,[90] M. Sandhoff,[182] C. Sandoval,[22] D. P. C. Sankey,[144] M. Sannino,[55b,55a] Y. Sano,[117] A. Sansoni,[51] C. Santoni,[38] H. Santos,[140a,140b] S. N. Santpur,[18] A. Santra,[174] A. Sapronov,[80] J. G. Saraiva,[140a,140d] O. Sasaki,[82] K. Sato,[169] F. Sauerburger,[52] E. Sauvan,[5] P. Savard,[167,d] R. Sawada,[163] C. Sawyer,[144] L. Sawyer,[96,ii] C. Sbarra,[23b] A. Sbrizzi,[23a] T. Scanlon,[95] J. Schaarschmidt,[148] P. Schacht,[115] B. M. Schachtner,[114] D. Schaefer,[37] L. Schaefer,[137] J. Schaeffer,[100] S. Schaepe,[36] U. Schäfer,[100] A. C. Schaffer,[65] D. Schaile,[114] R. D. Schamberger,[155] N. Scharmberg,[101] V. A. Schegelsky,[138] D. Scheirich,[143] F. Schenck,[19] M. Schernau,[171] C. Schiavi,[55b,55a] L. K. Schildgen,[24] Z. M. Schillaci,[26] E. J. Schioppa,[36] M. Schioppa,[41b,41a] K. E. Schleicher,[52] S. Schlenker,[36] K. R. Schmidt-Sommerfeld,[115] K. Schmieden,[36]

C. Schmitt,[100] S. Schmitt,[46] S. Schmitz,[100] J. C. Schmoeckel,[46] L. Schoeffel,[145] A. Schoening,[61b] P. G. Scholer,[52] E. Schopf,[135] M. Schott,[100] J. F. P. Schouwenberg,[119] J. Schovancova,[36] S. Schramm,[54] F. Schroeder,[182] A. Schulte,[100] H-C. Schultz-Coulon,[61a] M. Schumacher,[52] B. A. Schumm,[146] Ph. Schune,[145] A. Schwartzman,[153] T. A. Schwarz,[106] Ph. Schwemling,[145] R. Schwienhorst,[107] A. Sciandra,[146] G. Sciolla,[26] M. Scodeggio,[46] M. Scornajenghi,[41b,41a] F. Scuri,[72a] F. Scutti,[105] L. M. Scyboz,[115] C. D. Sebastiani,[73a,73b] P. Seema,[19] S. C. Seidel,[118] A. Seiden,[146] B. D. Seidlitz,[29] T. Seiss,[37] J. M. Seixas,[81b] G. Sekhniaidze,[70a] S. J. Sekula,[42] N. Semprini-Cesari,[23b,23a] S. Sen,[49] C. Serfon,[77] L. Serin,[65] L. Serkin,[67a,67b] M. Sessa,[60a] H. Severini,[129] S. Sevova,[153] T. Šfiligoj,[92] F. Sforza,[55b,55a] A. Sfyrla,[54] E. Shabalina,[53] J. D. Shahinian,[146] N. W. Shaikh,[45a,45b] D. Shaked Renous,[180] L. Y. Shan,[15a] M. Shapiro,[18] A. Sharma,[135] A. S. Sharma,[1] P. B. Shatalov,[124] K. Shaw,[156] S. M. Shaw,[101] M. Shehade,[180] Y. Shen,[129] A. D. Sherman,[25] P. Sherwood,[95] L. Shi,[158] S. Shimizu,[82] C. O. Shimmin,[183] Y. Shimogama,[179] M. Shimojima,[116] I. P. J. Shipsey,[135] S. Shirabe,[165] M. Shiyakova,[80,jj] J. Shlomi,[180] A. Shmeleva,[111] M. J. Shochet,[37] J. Shojaii,[105] D. R. Shope,[129] S. Shrestha,[127] E. M. Shrif,[33d] E. Shulga,[180] P. Sicho,[141] A. M. Sickles,[173] P. E. Sidebo,[154] E. Sideras Haddad,[33d] O. Sidiropoulou,[36] A. Sidoti,[23b,23a] F. Siegert,[48] Dj. Sijacki,[16] M. Silva Jr.,[181] M. V. Silva Oliveira,[81a] S. B. Silverstein,[45a] S. Simion,[65] R. Simoniello,[100] S. Simsek,[12b] P. Sinervo,[167] V. Sinetckii,[113] S. Singh,[152] M. Sioli,[23b,23a] I. Siral,[132] S. Yu. Sivoklokov,[113] J. Sjölin,[45a,45b] E. Skorda,[97] P. Skubic,[129] M. Slawinska,[85] K. Sliwa,[170] R. Slovak,[143] V. Smakhtin,[180] B. H. Smart,[144] J. Smiesko,[28b] N. Smirnov,[112] S. Yu. Smirnov,[112] Y. Smirnov,[112] L. N. Smirnova,[113,kk] O. Smirnova,[97] J. W. Smith,[53] M. Smizanska,[90] K. Smolek,[142] A. Smykiewicz,[85] A. A. Snesarev,[111] H. L. Snoek,[120] I. M. Snyder,[132] S. Snyder,[29] R. Sobie,[176,m] A. Soffer,[161] A. Søgaard,[50] F. Sohns,[53] C. A. Solans Sanchez,[36] E. Yu. Soldatov,[112] U. Soldevila,[174] A. A. Solodkov,[123] A. Soloshenko,[80] O. V. Solovyanov,[123] V. Solovyev,[138] P. Sommer,[149] H. Son,[170] W. Song,[144] W. Y. Song,[168b] A. Sopczak,[142] A. L. Sopio,[95] F. Sopkova,[28b] C. L. Sotiropoulou,[72a,72b] S. Sottocornola,[71a,71b] R. Soualah,[67a,67c,ll] A. M. Soukharev,[122b,122a] D. South,[46] S. Spagnolo,[68a,68b] M. Spalla,[115] M. Spangenberg,[178] F. Spanò,[94] D. Sperlich,[52] T. M. Spieker,[61a] G. Spigo,[36] M. Spina,[156] D. P. Spiteri,[57] M. Spousta,[143] A. Stabile,[69a,69b] B. L. Stamas,[121] R. Stamen,[61a] M. Stamenkovic,[120] E. Stanecka,[85] B. Stanislaus,[135] M. M. Stanitzki,[46] M. Stankaityte,[135] B. Stapf,[120] E. A. Starchenko,[123] G. H. Stark,[146] J. Stark,[58] P. Staroba,[141] P. Starovoitov,[61a] S. Stärz,[104] R. Staszewski,[85] G. Stavropoulos,[44] M. Stegler,[46] P. Steinberg,[29] A. L. Steinhebel,[132] B. Stelzer,[152] H. J. Stelzer,[139] O. Stelzer-Chilton,[168a] H. Stenzel,[56] T. J. Stevenson,[156] G. A. Stewart,[36] M. C. Stockton,[36] G. Stoicea,[27b] M. Stolarski,[140a] S. Stonjek,[115] A. Straessner,[48] J. Strandberg,[154] S. Strandberg,[45a,45b] M. Strauss,[129] P. Strizenec,[28b] R. Ströhmer,[177] D. M. Strom,[132] R. Stroynowski,[42] A. Strubig,[50] S. A. Stucci,[29] B. Stugu,[17] J. Stupak,[129] N. A. Styles,[46] D. Su,[153] W. Su,[60c] S. Suchek,[61a] V. V. Sulin,[111] M. J. Sullivan,[91] D. M. S. Sultan,[54] S. Sultansoy,[4c] T. Sumida,[86] S. Sun,[106] X. Sun,[101] K. Suruliz,[156] C. J. E. Suster,[157] M. R. Sutton,[156] S. Suzuki,[82] M. Svatos,[141] M. Swiatlowski,[37] S. P. Swift,[2] T. Swirski,[177] A. Sydorenko,[100] I. Sykora,[28a] M. Sykora,[143] T. Sykora,[143] D. Ta,[100] K. Tackmann,[46,mm] J. Taenzer,[161] A. Taffard,[171] R. Tafirout,[168a] R. Takashima,[87] K. Takeda,[83] T. Takeshita,[150] E. P. Takeva,[50] Y. Takubo,[82] M. Talby,[102] A. A. Talyshev,[122b,122a] N. M. Tamir,[161] J. Tanaka,[163] M. Tanaka,[165] R. Tanaka,[65] S. Tapia Araya,[173] S. Tapprogge,[100] A. Tarek Abouelfadl Mohamed,[136] S. Tarem,[160] K. Tariq,[60b] G. Tarna,[27b,nn] G. F. Tartarelli,[69a] P. Tas,[143] M. Tasevsky,[141] T. Tashiro,[86] E. Tassi,[41b,41a] A. Tavares Delgado,[140a] Y. Tayalati,[35e] A. J. Taylor,[50] G. N. Taylor,[105] W. Taylor,[168b] A. S. Tee,[90] R. Teixeira De Lima,[153] P. Teixeira-Dias,[94] H. Ten Kate,[36] J. J. Teoh,[120] S. Terada,[82] K. Terashi,[163] J. Terron,[99] S. Terzo,[14] M. Testa,[51] R. J. Teuscher,[167,m] S. J. Thais,[183] T. Theveneaux-Pelzer,[46] F. Thiele,[40] D. W. Thomas,[94] J. O. Thomas,[42] J. P. Thomas,[21] P. D. Thompson,[21] L. A. Thomsen,[183] E. Thomson,[137] E. J. Thorpe,[93] R. E. Ticse Torres,[53] V. O. Tikhomirov,[111,oo] Yu. A. Tikhonov,[122b,122a] S. Timoshenko,[112] P. Tipton,[183] S. Tisserant,[102] K. Todome,[23b,23a] S. Todorova-Nova,[143] S. Todt,[48] J. Tojo,[88] S. Tokár,[28a] K. Tokushuku,[82] E. Tolley,[127] K. G. Tomiwa,[33d] M. Tomoto,[117] L. Tompkins,[153,bb] B. Tong,[59] P. Tornambe,[103] E. Torrence,[132] H. Torres,[48] E. Torró Pastor,[148] C. Tosciri,[135] J. Toth,[102,pp] D. R. Tovey,[149] A. Traeet,[17] C. J. Treado,[125] T. Trefzger,[177] F. Tresoldi,[156] A. Tricoli,[29] I. M. Trigger,[168a] S. Trincaz-Duvoid,[136] D. T. Trischuk,[175] W. Trischuk,[167] B. Trocmé,[58] A. Trofymov,[145] C. Troncon,[69a] F. Trovato,[156] L. Truong,[33b] M. Trzebinski,[85] A. Trzupek,[85] F. Tsai,[46] J. C-L. Tseng,[135] P. V. Tsiareshka,[108,cc] A. Tsirigotis,[162,dd] V. Tsiskaridze,[155] E. G. Tskhadadze,[159a] M. Tsopoulou,[162] I. I. Tsukerman,[124] V. Tsulaia,[18] S. Tsuno,[82] D. Tsybychev,[155] Y. Tu,[63b] A. Tudorache,[27b] V. Tudorache,[27b] T. T. Tulbure,[27a] A. N. Tuna,[59] S. Turchikhin,[80] D. Turgeman,[180] I. Turk Cakir,[4b,qq] R. J. Turner,[21] R. T. Turra,[69a] P. M. Tuts,[39] S. Tzamarias,[162] E. Tzovara,[100] G. Ucchielli,[47] K. Uchida,[163] F. Ukegawa,[169] G. Unal,[36] A. Undrus,[29] G. Unel,[171] F. C. Ungaro,[105] Y. Unno,[82] K. Uno,[163] J. Urban,[28b] P. Urquijo,[105] G. Usai,[8] Z. Uysal,[12d] V. Vacek,[142] B. Vachon,[104] K. O. H. Vadla,[134] A. Vaidya,[95] C. Valderanis,[114] E. Valdes Santurio,[45a,45b] M. Valente,[54] S. Valentinetti,[23b,23a] A. Valero,[174] L. Valéry,[46] R. A. Vallance,[21] A. Vallier,[36] J. A. Valls Ferrer,[174]

T. R. Van Daalen,[14] P. Van Gemmeren,[6] I. Van Vulpen,[120] M. Vanadia,[74a,74b] W. Vandelli,[36] M. Vandenbroucke,[145] E. R. Vandewall,[130] A. Vaniachine,[166] D. Vannicola,[73a,73b] R. Vari,[73a] E. W. Varnes,[7] C. Varni,[55b,55a] T. Varol,[158] D. Varouchas,[65] K. E. Varvell,[157] M. E. Vasile,[27b] G. A. Vasquez,[176] F. Vazeille,[38] D. Vazquez Furelos,[14] T. Vazquez Schroeder,[36] J. Veatch,[53] V. Vecchio,[75a,75b] M. J. Veen,[120] L. M. Veloce,[167] F. Veloso,[140a,140c] S. Veneziano,[73a] A. Ventura,[68a,68b] N. Venturi,[36] A. Verbytskyi,[115] V. Vercesi,[71a] M. Verducci,[72a,72b] C. M. Vergel Infante,[79] C. Vergis,[24] W. Verkerke,[120] A. T. Vermeulen,[120] J. C. Vermeulen,[120] M. C. Vetterli,[152,d] N. Viaux Maira,[147c] M. Vicente Barreto Pinto,[54] T. Vickey,[149] O. E. Vickey Boeriu,[149] G. H. A. Viehhauser,[135] L. Vigani,[61b] M. Villa,[23b,23a] M. Villaplana Perez,[3] E. Vilucchi,[51] M. G. Vincter,[34] G. S. Virdee,[21] A. Vishwakarma,[46] C. Vittori,[23b,23a] I. Vivarelli,[156] M. Vogel,[182] P. Vokac,[142] S. E. von Buddenbrock,[33d] E. Von Toerne,[24] V. Vorobel,[143] K. Vorobev,[112] M. Vos,[174] J. H. Vossebeld,[91] M. Vozak,[101] N. Vranjes,[16] M. Vranjes Milosavljevic,[16] V. Vrba,[142] M. Vreeswijk,[120] R. Vuillermet,[36] I. Vukotic,[37] P. Wagner,[24] W. Wagner,[182] J. Wagner-Kuhr,[114] S. Wahdan,[182] H. Wahlberg,[89] V. M. Walbrecht,[115] J. Walder,[90] R. Walker,[114] S. D. Walker,[94] W. Walkowiak,[151] V. Wallangen,[45a,45b] A. M. Wang,[59] A. Z. Wang,[181] C. Wang,[60c] F. Wang,[181] H. Wang,[18] H. Wang,[3] J. Wang,[63a] J. Wang,[61b] P. Wang,[42] Q. Wang,[129] R.-J. Wang,[100] R. Wang,[60a] R. Wang,[6] S. M. Wang,[158] W. T. Wang,[60a] W. Wang,[15c] W. X. Wang,[60a] Y. Wang,[60a] Z. Wang,[60c] C. Wanotayaroj,[46] A. Warburton,[104] C. P. Ward,[32] D. R. Wardrope,[95] N. Warrack,[57] A. Washbrook,[50] A. T. Watson,[21] M. F. Watson,[21] G. Watts,[148] B. M. Waugh,[95] A. F. Webb,[11] S. Webb,[100] C. Weber,[183] M. S. Weber,[20] S. A. Weber,[34] S. M. Weber,[61a] A. R. Weidberg,[135] J. Weingarten,[47] M. Weirich,[100] C. Weiser,[52] P. S. Wells,[36] T. Wenaus,[29] T. Wengler,[36] S. Wenig,[36] N. Wermes,[24] M. D. Werner,[79] M. Wessels,[61a] T. D. Weston,[20] K. Whalen,[132] N. L. Whallon,[148] A. M. Wharton,[90] A. S. White,[106] A. White,[8] M. J. White,[1] D. Whiteson,[171] B. W. Whitmore,[90] W. Wiedenmann,[181] C. Wiel,[48] M. Wielers,[144] N. Wieseotte,[100] C. Wiglesworth,[40] L. A. M. Wiik-Fuchs,[52] H. G. Wilkens,[36] L. J. Wilkins,[94] H. H. Williams,[137] S. Williams,[32] C. Willis,[107] S. Willocq,[103] I. Wingerter-Seez,[5] E. Winkels,[156] F. Winklmeier,[132] O. J. Winston,[156] B. T. Winter,[52] M. Wittgen,[153] M. Wobisch,[96] A. Wolf,[100] T. M. H. Wolf,[120] R. Wolff,[102] R. W. Wölker,[135] J. Wollrath,[52] M. W. Wolter,[85] H. Wolters,[140a,140c] V. W. S. Wong,[175] N. L. Woods,[146] S. D. Worm,[46] B. K. Wosiek,[85] K. W. Woźniak,[85] K. Wraight,[57] S. L. Wu,[181] X. Wu,[54] Y. Wu,[60a] T. R. Wyatt,[101] B. M. Wynne,[50] S. Xella,[40] Z. Xi,[106] L. Xia,[178] X. Xiao,[106] I. Xiotidis,[156] D. Xu,[15a] H. Xu,[60a] H. Xu,[60a] L. Xu,[29] T. Xu,[145] W. Xu,[106] Z. Xu,[60b] Z. Xu,[153] B. Yabsley,[157] S. Yacoob,[33a] K. Yajima,[133] D. P. Yallup,[95] N. Yamaguchi,[88] Y. Yamaguchi,[165] A. Yamamoto,[82] M. Yamatani,[163] T. Yamazaki,[163] Y. Yamazaki,[83] Z. Yan,[25] H. J. Yang,[60c,60d] H. T. Yang,[18] S. Yang,[60a] T. Yang,[63c] X. Yang,[60b,58] Y. Yang,[163] W-M. Yao,[18] Y. C. Yap,[46] Y. Yasu,[82] E. Yatsenko,[60c,60d] H. Ye,[15c] J. Ye,[42] S. Ye,[29] I. Yeletskikh,[80] M. R. Yexley,[90] E. Yigitbasi,[25] K. Yorita,[179] K. Yoshihara,[137] C. J. S. Young,[36] C. Young,[153] J. Yu,[79] R. Yuan,[60b,rr] X. Yue,[61a] M. Zaazoua,[35e] B. Zabinski,[85] G. Zacharis,[10] E. Zaffaroni,[54] J. Zahreddine,[136] A. M. Zaitsev,[123,gg] T. Zakareishvili,[159b] N. Zakharchuk,[34] S. Zambito,[59] D. Zanzi,[36] D. R. Zaripovas,[57] S. V. Zeißner,[47] C. Zeitnitz,[182] G. Zemaityte,[135] J. C. Zeng,[173] O. Zenin,[123] T. Ženiš,[28a] D. Zerwas,[65] M. Zgubič,[135] B. Zhang,[15c] D. F. Zhang,[15b] G. Zhang,[15b] H. Zhang,[15c] J. Zhang,[6] L. Zhang,[15c] L. Zhang,[60a] M. Zhang,[173] R. Zhang,[181] S. Zhang,[106] X. Zhang,[60b] Y. Zhang,[15a,15d] Z. Zhang,[63a] Z. Zhang,[65] P. Zhao,[49] Z. Zhao,[60a] A. Zhemchugov,[80] Z. Zheng,[106] D. Zhong,[173] B. Zhou,[106] C. Zhou,[181] M. S. Zhou,[15a,15d] M. Zhou,[155] N. Zhou,[60c] Y. Zhou,[7] C. G. Zhu,[60b] C. Zhu,[15a,15d] H. L. Zhu,[60a] H. Zhu,[15a] J. Zhu,[106] Y. Zhu,[60a] X. Zhuang,[15a] K. Zhukov,[111] V. Zhulanov,[122b,122a] D. Zieminska,[66] N. I. Zimine,[80] S. Zimmermann,[52] Z. Zinonos,[115] M. Ziolkowski,[151] L. Živković,[16] G. Zobernig,[181] A. Zoccoli,[23b,23a] K. Zoch,[53] T. G. Zorbas,[149] R. Zou,[37] and L. Zwalinski[36]

(ATLAS Collaboration)

[1]*Department of Physics, University of Adelaide, Adelaide, Australia*
[2]*Physics Department, SUNY Albany, Albany, New York, USA*
[3]*Department of Physics, University of Alberta, Edmonton, Alberta, Canada*
[4a]*Department of Physics, Ankara University, Ankara, Turkey*
[4b]*Istanbul Aydin University, Istanbul, Turkey*
[4c]*Division of Physics, TOBB University of Economics and Technology, Ankara, Turkey*
[5]*LAPP, Université Grenoble Alpes, Université Savoie Mont Blanc, CNRS/IN2P3, Annecy, France*
[6]*High Energy Physics Division, Argonne National Laboratory, Argonne, Illinois, USA*
[7]*Department of Physics, University of Arizona, Tucson, Arizona, USA*
[8]*Department of Physics, University of Texas at Arlington, Arlington, Texas, USA*
[9]*Physics Department, National and Kapodistrian University of Athens, Athens, Greece*

[10]Physics Department, National Technical University of Athens, Zografou, Greece
[11]Department of Physics, University of Texas at Austin, Austin, Texas, USA
[12a]Bahcesehir University, Faculty of Engineering and Natural Sciences, Istanbul, Turkey
[12b]Istanbul Bilgi University, Faculty of Engineering and Natural Sciences, Istanbul, Turkey
[12c]Department of Physics, Bogazici University, Istanbul, Turkey
[12d]Department of Physics Engineering, Gaziantep University, Gaziantep, Turkey
[13]Institute of Physics, Azerbaijan Academy of Sciences, Baku, Azerbaijan
[14]Institut de Física d'Altes Energies (IFAE), Barcelona Institute of Science and Technology, Barcelona, Spain
[15a]Institute of High Energy Physics, Chinese Academy of Sciences, Beijing, China
[15b]Physics Department, Tsinghua University, Beijing, China
[15c]Department of Physics, Nanjing University, Nanjing, China
[15d]University of Chinese Academy of Science (UCAS), Beijing, China
[16]Institute of Physics, University of Belgrade, Belgrade, Serbia
[17]Department for Physics and Technology, University of Bergen, Bergen, Norway
[18]Physics Division, Lawrence Berkeley National Laboratory and University of California, Berkeley, California, USA
[19]Institut für Physik, Humboldt Universität zu Berlin, Berlin, Germany
[20]Albert Einstein Center for Fundamental Physics and Laboratory for High Energy Physics, University of Bern, Bern, Switzerland
[21]School of Physics and Astronomy, University of Birmingham, Birmingham, United Kingdom
[22]Facultad de Ciencias y Centro de Investigaciónes, Universidad Antonio Nariño, Bogota, Colombia
[23a]INFN Bologna and Universita' di Bologna, Dipartimento di Fisica, Bologna, Italy
[23b]INFN Sezione di Bologna, Bologna, Italy
[24]Physikalisches Institut, Universität Bonn, Bonn, Germany
[25]Department of Physics, Boston University, Boston, Massachusetts, USA
[26]Department of Physics, Brandeis University, Waltham, Massachusetts, USA
[27a]Transilvania University of Brasov, Brasov, Romania
[27b]Horia Hulubei National Institute of Physics and Nuclear Engineering, Bucharest, Romania
[27c]Department of Physics, Alexandru Ioan Cuza University of Iasi, Iasi, Romania
[27d]National Institute for Research and Development of Isotopic and Molecular Technologies, Physics Department, Cluj-Napoca, Romania
[27e]University Politehnica Bucharest, Bucharest, Romania
[27f]West University in Timisoara, Timisoara, Romania
[28a]Faculty of Mathematics, Physics and Informatics, Comenius University, Bratislava, Slovak Republic
[28b]Department of Subnuclear Physics, Institute of Experimental Physics of the Slovak Academy of Sciences, Kosice, Slovak Republic
[29]Physics Department, Brookhaven National Laboratory, Upton, New York, USA
[30]Departamento de Física, Universidad de Buenos Aires, Buenos Aires, Argentina
[31]California State University, Los Angeles, California, USA
[32]Cavendish Laboratory, University of Cambridge, Cambridge, United Kingdom
[33a]Department of Physics, University of Cape Town, Cape Town, South Africa
[33b]Department of Mechanical Engineering Science, University of Johannesburg, Johannesburg, South Africa
[33c]University of South Africa, Department of Physics, Pretoria, South Africa
[33d]School of Physics, University of the Witwatersrand, Johannesburg, South Africa
[34]Department of Physics, Carleton University, Ottawa, Ontario, Canada
[35a]Faculté des Sciences Ain Chock, Réseau Universitaire de Physique des Hautes Energies—Université Hassan II, Casablanca, Morocco
[35b]Faculté des Sciences, Université Ibn-Tofail, Kénitra, Morocco
[35c]Faculté des Sciences Semlalia, Université Cadi Ayyad, LPHEA-Marrakech, Morocco
[35d]Faculté des Sciences, Université Mohamed Premier and LPTPM, Oujda, Morocco
[35e]Faculté des sciences, Université Mohammed V, Rabat, Morocco
[36]CERN, Geneva, Switzerland
[37]Enrico Fermi Institute, University of Chicago, Chicago, Illinois, USA
[38]LPC, Université Clermont Auvergne, CNRS/IN2P3, Clermont-Ferrand, France
[39]Nevis Laboratory, Columbia University, Irvington, New York, USA
[40]Niels Bohr Institute, University of Copenhagen, Copenhagen, Denmark
[41a]Dipartimento di Fisica, Università della Calabria, Rende, Italy
[41b]INFN Gruppo Collegato di Cosenza, Laboratori Nazionali di Frascati, Italy

[42]*Physics Department, Southern Methodist University, Dallas, Texas, USA*
[43]*Physics Department, University of Texas at Dallas, Richardson, Texas, USA*
[44]*National Centre for Scientific Research "Demokritos", Agia Paraskevi, Greece*
[45a]*Department of Physics, Stockholm University, Stockholm, Sweden*
[45b]*Oskar Klein Centre, Stockholm, Sweden*
[46]*Deutsches Elektronen-Synchrotron DESY, Hamburg and Zeuthen, Germany*
[47]*Lehrstuhl für Experimentelle Physik IV, Technische Universität Dortmund, Dortmund, Germany*
[48]*Institut für Kern- und Teilchenphysik, Technische Universität Dresden, Dresden, Germany*
[49]*Department of Physics, Duke University, Durham, North Carolina, USA*
[50]*SUPA—School of Physics and Astronomy, University of Edinburgh, Edinburgh, United Kingdom*
[51]*INFN e Laboratori Nazionali di Frascati, Frascati, Italy*
[52]*Physikalisches Institut, Albert-Ludwigs-Universität Freiburg, Freiburg, Germany*
[53]*II. Physikalisches Institut, Georg-August-Universität Göttingen, Göttingen, Germany*
[54]*Département de Physique Nucléaire et Corpusculaire, Université de Genève, Genève, Switzerland*
[55a]*Dipartimento di Fisica, Università di Genova, Genova, Italy*
[55b]*INFN Sezione di Genova, Genova, Italy*
[56]*II. Physikalisches Institut, Justus-Liebig-Universität Giessen, Giessen, Germany*
[57]*SUPA—School of Physics and Astronomy, University of Glasgow, Glasgow, United Kingdom*
[58]*LPSC, Université Grenoble Alpes, CNRS/IN2P3, Grenoble INP, Grenoble, France*
[59]*Laboratory for Particle Physics and Cosmology, Harvard University, Cambridge, Massachusetts, USA*
[60a]*Department of Modern Physics and State Key Laboratory of Particle Detection and Electronics, University of Science and Technology of China, Hefei, China*
[60b]*Institute of Frontier and Interdisciplinary Science and Key Laboratory of Particle Physics and Particle Irradiation (MOE), Shandong University, Qingdao, China*
[60c]*School of Physics and Astronomy, Shanghai Jiao Tong University, KLPPAC-MoE, SKLPPC, Shanghai, China*
[60d]*Tsung-Dao Lee Institute, Shanghai, China*
[61a]*Kirchhoff-Institut für Physik, Ruprecht-Karls-Universität Heidelberg, Heidelberg, Germany*
[61b]*Physikalisches Institut, Ruprecht-Karls-Universität Heidelberg, Heidelberg, Germany*
[62]*Faculty of Applied Information Science, Hiroshima Institute of Technology, Hiroshima, Japan*
[63a]*Department of Physics, Chinese University of Hong Kong, Shatin, N.T., Hong Kong, China*
[63b]*Department of Physics, University of Hong Kong, Hong Kong, China*
[63c]*Department of Physics and Institute for Advanced Study, Hong Kong University of Science and Technology, Clear Water Bay, Kowloon, Hong Kong, China*
[64]*Department of Physics, National Tsing Hua University, Hsinchu, Taiwan*
[65]*Université Paris-Saclay, CNRS/IN2P3, IJCLab, Orsay, France*
[66]*Department of Physics, Indiana University, Bloomington, Indiana, USA*
[67a]*INFN Gruppo Collegato di Udine, Sezione di Trieste, Udine, Italy*
[67b]*ICTP, Trieste, Italy*
[67c]*Dipartimento Politecnico di Ingegneria e Architettura, Università di Udine, Udine, Italy*
[68a]*INFN Sezione di Lecce, Lecce, Italy*
[68b]*Dipartimento di Matematica e Fisica, Università del Salento, Lecce, Italy*
[69a]*INFN Sezione di Milano, Italy*
[69b]*Dipartimento di Fisica, Università di Milano, Milano, Italy*
[70a]*INFN Sezione di Napoli, Napoli, Italy*
[70b]*Dipartimento di Fisica, Università di Napoli, Napoli, Italy*
[71a]*INFN Sezione di Pavia, Pavia, Italy*
[71b]*Dipartimento di Fisica, Università di Pavia, Pavia, Italy*
[72a]*INFN Sezione di Pisa, Pisa, Italy*
[72b]*Dipartimento di Fisica E. Fermi, Università di Pisa, Pisa, Italy*
[73a]*INFN Sezione di Roma, Roma, Italy*
[73b]*Dipartimento di Fisica, Sapienza Università di Roma, Roma, Italy*
[74a]*INFN Sezione di Roma Tor Vergata, Roma, Italy*
[74b]*Dipartimento di Fisica, Università di Roma Tor Vergata, Roma, Italy*
[75a]*INFN Sezione di Roma Tre, Roma, Italy*
[75b]*Dipartimento di Matematica e Fisica, Università Roma Tre, Roma, Italy*
[76a]*INFN-TIFPA, Trento, Italy*
[76b]*Università degli Studi di Trento, Trento, Italy*
[77]*Institut für Astro- und Teilchenphysik, Leopold-Franzens-Universität, Innsbruck, Austria*
[78]*University of Iowa, Iowa City, Iowa, USA*

[79]Department of Physics and Astronomy, Iowa State University, Ames, Iowa, USA
[80]Joint Institute for Nuclear Research, Dubna, Russia
[81a]Departamento de Engenharia Elétrica, Universidade Federal de Juiz de Fora (UFJF), Juiz de Fora, Brazil
[81b]Universidade Federal do Rio De Janeiro COPPE/EE/IF, Rio de Janeiro, Brazil
[81c]Universidade Federal de São João del Rei (UFSJ), São João del Rei, Brazil
[81d]Instituto de Física, Universidade de São Paulo, São Paulo, Brazil
[82]KEK, High Energy Accelerator Research Organization, Tsukuba, Japan
[83]Graduate School of Science, Kobe University, Kobe, Japan
[84a]AGH University of Science and Technology, Faculty of Physics and Applied Computer Science, Krakow, Poland
[84b]Marian Smoluchowski Institute of Physics, Jagiellonian University, Krakow, Poland
[85]Institute of Nuclear Physics Polish Academy of Sciences, Krakow, Poland
[86]Faculty of Science, Kyoto University, Kyoto, Japan
[87]Kyoto University of Education, Kyoto, Japan
[88]Research Center for Advanced Particle Physics and Department of Physics, Kyushu University, Fukuoka, Japan
[89]Instituto de Física La Plata, Universidad Nacional de La Plata and CONICET, La Plata, Argentina
[90]Physics Department, Lancaster University, Lancaster, United Kingdom
[91]Oliver Lodge Laboratory, University of Liverpool, Liverpool, United Kingdom
[92]Department of Experimental Particle Physics, Jožef Stefan Institute and Department of Physics, University of Ljubljana, Ljubljana, Slovenia
[93]School of Physics and Astronomy, Queen Mary University of London, London, United Kingdom
[94]Department of Physics, Royal Holloway University of London, Egham, United Kingdom
[95]Department of Physics and Astronomy, University College London, London, United Kingdom
[96]Louisiana Tech University, Ruston, Louisiana, USA
[97]Fysiska institutionen, Lunds universitet, Lund, Sweden
[98]Centre de Calcul de l'Institut National de Physique Nucléaire et de Physique des Particules (IN2P3), Villeurbanne, France
[99]Departamento de Física Teorica C-15 and CIAFF, Universidad Autónoma de Madrid, Madrid, Spain
[100]Institut für Physik, Universität Mainz, Mainz, Germany
[101]School of Physics and Astronomy, University of Manchester, Manchester, United Kingdom
[102]CPPM, Aix-Marseille Université, CNRS/IN2P3, Marseille, France
[103]Department of Physics, University of Massachusetts, Amherst, Massachusetts, USA
[104]Department of Physics, McGill University, Montreal, Quebec, Canada
[105]School of Physics, University of Melbourne, Victoria, Australia
[106]Department of Physics, University of Michigan, Ann Arbor, Michigan, USA
[107]Department of Physics and Astronomy, Michigan State University, East Lansing, Michigan, USA
[108]B.I. Stepanov Institute of Physics, National Academy of Sciences of Belarus, Minsk, Belarus
[109]Research Institute for Nuclear Problems of Byelorussian State University, Minsk, Belarus
[110]Group of Particle Physics, University of Montreal, Montreal, Quebec, Canada
[111]P.N. Lebedev Physical Institute of the Russian Academy of Sciences, Moscow, Russia
[112]National Research Nuclear University MEPhI, Moscow, Russia
[113]D.V. Skobeltsyn Institute of Nuclear Physics, M.V. Lomonosov Moscow State University, Moscow, Russia
[114]Fakultät für Physik, Ludwig-Maximilians-Universität München, München, Germany
[115]Max-Planck-Institut für Physik (Werner-Heisenberg-Institut), München, Germany
[116]Nagasaki Institute of Applied Science, Nagasaki, Japan
[117]Graduate School of Science and Kobayashi-Maskawa Institute, Nagoya University, Nagoya, Japan
[118]Department of Physics and Astronomy, University of New Mexico, Albuquerque, New Mexico, USA
[119]Institute for Mathematics, Astrophysics and Particle Physics, Radboud University Nijmegen/Nikhef, Nijmegen, Netherlands
[120]Nikhef National Institute for Subatomic Physics and University of Amsterdam, Amsterdam, Netherlands
[121]Department of Physics, Northern Illinois University, DeKalb, Illinois, USA
[122a]Budker Institute of Nuclear Physics and NSU, SB RAS, Novosibirsk, Russia
[122b]Novosibirsk State University, Novosibirsk, Russia
[123]Institute for High Energy Physics of the National Research Centre Kurchatov Institute, Protvino, Russia
[124]Institute for Theoretical and Experimental Physics named by A.I. Alikhanov of National Research Centre "Kurchatov Institute", Moscow, Russia
[125]Department of Physics, New York University, New York, New York, USA

[126]*Ochanomizu University, Otsuka, Bunkyo-ku, Tokyo, Japan*
[127]*Ohio State University, Columbus, Ohio, USA*
[128]*Faculty of Science, Okayama University, Okayama, Japan*
[129]*Homer L. Dodge Department of Physics and Astronomy, University of Oklahoma, Norman, Oklahoma, USA*
[130]*Department of Physics, Oklahoma State University, Stillwater, Oklahoma, USA*
[131]*Palacký University, RCPTM, Joint Laboratory of Optics, Olomouc, Czech Republic*
[132]*Center for High Energy Physics, University of Oregon, Eugene, Oregon, USA*
[133]*Graduate School of Science, Osaka University, Osaka, Japan*
[134]*Department of Physics, University of Oslo, Oslo, Norway*
[135]*Department of Physics, Oxford University, Oxford, United Kingdom*
[136]*LPNHE, Sorbonne Université, Université de Paris, CNRS/IN2P3, Paris, France*
[137]*Department of Physics, University of Pennsylvania, Philadelphia, Pennsylvania, USA*
[138]*Konstantinov Nuclear Physics Institute of National Research Centre "Kurchatov Institute", PNPI, St. Petersburg, Russia*
[139]*Department of Physics and Astronomy, University of Pittsburgh, Pittsburgh, Pennsylvania, USA*
[140a]*Laboratório de Instrumentação e Física Experimental de Partículas—LIP, Lisboa, Portugal*
[140b]*Departamento de Física, Faculdade de Ciências, Universidade de Lisboa, Lisboa, Portugal*
[140c]*Departamento de Física, Universidade de Coimbra, Coimbra, Portugal*
[140d]*Centro de Física Nuclear da Universidade de Lisboa, Lisboa, Portugal*
[140e]*Departamento de Física, Universidade do Minho, Braga, Portugal*
[140f]*Departamento de Física Teórica y del Cosmos, Universidad de Granada, Granada (Spain), Spain*
[140g]*Dep Física and CEFITEC of Faculdade de Ciências e Tecnologia, Universidade Nova de Lisboa, Caparica, Portugal*
[140h]*Instituto Superior Técnico, Universidade de Lisboa, Lisboa, Portugal*
[141]*Institute of Physics of the Czech Academy of Sciences, Prague, Czech Republic*
[142]*Czech Technical University in Prague, Prague, Czech Republic*
[143]*Charles University, Faculty of Mathematics and Physics, Prague, Czech Republic*
[144]*Particle Physics Department, Rutherford Appleton Laboratory, Didcot, United Kingdom*
[145]*IRFU, CEA, Université Paris-Saclay, Gif-sur-Yvette, France*
[146]*Santa Cruz Institute for Particle Physics, University of California Santa Cruz, Santa Cruz, California, USA*
[147a]*Departamento de Física, Pontificia Universidad Católica de Chile, Santiago, Chile*
[147b]*Universidad Andres Bello, Department of Physics, Santiago, Chile*
[147c]*Departamento de Física, Universidad Técnica Federico Santa María, Valparaíso, Chile*
[148]*Department of Physics, University of Washington, Seattle, Washington, USA*
[149]*Department of Physics and Astronomy, University of Sheffield, Sheffield, United Kingdom*
[150]*Department of Physics, Shinshu University, Nagano, Japan*
[151]*Department Physik, Universität Siegen, Siegen, Germany*
[152]*Department of Physics, Simon Fraser University, Burnaby, British Columbia, Canada*
[153]*SLAC National Accelerator Laboratory, Stanford, California, USA*
[154]*Physics Department, Royal Institute of Technology, Stockholm, Sweden*
[155]*Departments of Physics and Astronomy, Stony Brook University, Stony Brook, New York, USA*
[156]*Department of Physics and Astronomy, University of Sussex, Brighton, United Kingdom*
[157]*School of Physics, University of Sydney, Sydney, Australia*
[158]*Institute of Physics, Academia Sinica, Taipei, Taiwan*
[159a]*E. Andronikashvili Institute of Physics, Iv. Javakhishvili Tbilisi State University, Tbilisi, Georgia*
[159b]*High Energy Physics Institute, Tbilisi State University, Tbilisi, Georgia*
[160]*Department of Physics, Technion, Israel Institute of Technology, Haifa, Israel*
[161]*Raymond and Beverly Sackler School of Physics and Astronomy, Tel Aviv University, Tel Aviv, Israel*
[162]*Department of Physics, Aristotle University of Thessaloniki, Thessaloniki, Greece*
[163]*International Center for Elementary Particle Physics and Department of Physics, University of Tokyo, Tokyo, Japan*
[164]*Graduate School of Science and Technology, Tokyo Metropolitan University, Tokyo, Japan*
[165]*Department of Physics, Tokyo Institute of Technology, Tokyo, Japan*
[166]*Tomsk State University, Tomsk, Russia*
[167]*Department of Physics, University of Toronto, Toronto, Ontario, Canada*
[168a]*TRIUMF, Vancouver, British Columbia, Canada*
[168b]*Department of Physics and Astronomy, York University, Toronto, Ontario, Canada*

[169]*Division of Physics and Tomonaga Center for the History of the Universe, Faculty of Pure and Applied Sciences, University of Tsukuba, Tsukuba, Japan*
[170]*Department of Physics and Astronomy, Tufts University, Medford, Massachusetts, USA*
[171]*Department of Physics and Astronomy, University of California Irvine, Irvine, California, USA*
[172]*Department of Physics and Astronomy, University of Uppsala, Uppsala, Sweden*
[173]*Department of Physics, University of Illinois, Urbana, Illinois, USA*
[174]*Instituto de Física Corpuscular (IFIC), Centro Mixto Universidad de Valencia—CSIC, Valencia, Spain*
[175]*Department of Physics, University of British Columbia, Vancouver, British Columbia, Canada*
[176]*Department of Physics and Astronomy, University of Victoria, Victoria, British Columbia, Canada*
[177]*Fakultät für Physik und Astronomie, Julius-Maximilians-Universität Würzburg, Würzburg, Germany*
[178]*Department of Physics, University of Warwick, Coventry, United Kingdom*
[179]*Waseda University, Tokyo, Japan*
[180]*Department of Particle Physics, Weizmann Institute of Science, Rehovot, Israel*
[181]*Department of Physics, University of Wisconsin, Madison, Wisconsin, USA*
[182]*Fakultät für Mathematik und Naturwissenschaften, Fachgruppe Physik, Bergische Universität Wuppertal, Wuppertal, Germany*
[183]*Department of Physics, Yale University, New Haven, Connecticut, USA*

[a]Deceased.
[b]Also at Department of Physics, King's College London, London, United Kingdom.
[c]Also at Instituto de Fisica Teorica, IFT-UAM/CSIC, Madrid, Spain.
[d]Also at TRIUMF, Vancouver BC, Canada.
[e]Also at Department of Physics and Astronomy, University of Louisville, Louisville, Kentucky, USA.
[f]Also at Physics Department, An-Najah National University, Nablus, Palestine.
[g]Also at Department of Physics, University of Fribourg, Fribourg, Switzerland.
[h]Also at Physics Dept, University of South Africa, Pretoria, South Africa.
[i]Also at Departament de Fisica de la Universitat Autonoma de Barcelona, Barcelona, Spain.
[j]Also at Tomsk State University, Tomsk, and Moscow Institute of Physics and Technology State University, Dolgoprudny, Russia.
[k]Also at Department of Physics, Ben Gurion University of the Negev, Beer Sheva, Israel.
[l]Also at Universita di Napoli Parthenope, Napoli, Italy.
[m]Also at Institute of Particle Physics (IPP), Vancouver, Canada.
[n]Also at Department of Physics, University of Adelaide, Adelaide, Australia.
[o]Also at Dipartimento di Matematica, Informatica e Fisica, Università di Udine, Udine, Italy.
[p]Also at Department of Physics, St. Petersburg State Polytechnical University, St. Petersburg, Russia.
[q]Also at Borough of Manhattan Community College, City University of New York, New York, New York, USA.
[r]Also at Department of Physics, California State University, Fresno, USA.
[s]Also at Department of Financial and Management Engineering, University of the Aegean, Chios, Greece.
[t]Also at Department of Physics, California State University, East Bay, USA.
[u]Also at Institucio Catalana de Recerca i Estudis Avancats, ICREA, Barcelona, Spain.
[v]Also at Université Paris-Saclay, CNRS/IN2P3, IJCLab, 91405, Orsay, France.
[w]Also at Graduate School of Science, Osaka University, Osaka, Japan.
[x]Also at Physikalisches Institut, Albert-Ludwigs-Universität Freiburg, Freiburg, Germany.
[y]Also at Institute of Physics, Azerbaijan Academy of Sciences, Baku, Azerbaijan.
[z]Also at Institute for Mathematics, Astrophysics and Particle Physics, Radboud University Nijmegen/Nikhef, Nijmegen, Netherlands.
[aa]Also at CERN, Geneva, Switzerland.
[bb]Also at Department of Physics, Stanford University, Stanford, California, USA.
[cc]Also at Joint Institute for Nuclear Research, Dubna, Russia.
[dd]Also at Hellenic Open University, Patras, Greece.
[ee]Also at The City College of New York, New York, New York, USA.
[ff]Also at Department of Physics, California State University, Sacramento, USA.
[gg]Also at Moscow Institute of Physics and Technology State University, Dolgoprudny, Russia.
[hh]Also at Département de Physique Nucléaire et Corpusculaire, Université de Genève, Genève, Switzerland.
[ii]Also at Louisiana Tech University, Ruston, Louisiana, USA.
[jj]Also at Institute for Nuclear Research and Nuclear Energy (INRNE) of the Bulgarian Academy of Sciences, Sofia, Bulgaria.
[kk]Also at Faculty of Physics, M.V. Lomonosov Moscow State University, Moscow, Russia.
[ll]Also at Department of Applied Physics and Astronomy, University of Sharjah, Sharjah, United Arab Emirates.
[mm]Also at Institut für Experimentalphysik, Universität Hamburg, Hamburg, Germany.
[nn]Also at CPPM, Aix-Marseille Université, CNRS/IN2P3, Marseille, France.

[oo]Also at National Research Nuclear University MEPhI, Moscow, Russia.
[pp]Also at Institute for Particle and Nuclear Physics, Wigner Research Centre for Physics, Budapest, Hungary.
[qq]Also at Giresun University, Faculty of Engineering, Giresun, Turkey.
[rr]Also at Department of Physics and Astronomy, Michigan State University, East Lansing, Michigan, USA.